Title

Diagnosis of dental caries with Short Wave Infrared (SWIR) light

Author

Zhu, Yihua

Publication Date

2024

Peer reviewed|Thesis/dissertation

Diagnosis of dental caries with Short-Wave Infrared (SWIR) light

by
Yihua Zhu

DISSERTATION
Submitted in partial satisfaction of the requirements for degree of
DOCTOR OF PHILOSOPHY

in

Oral and Craniofacial Sciences

in the

GRADUATE DIVISION
of the
UNIVERSITY OF CALIFORNIA, SAN FRANCISCO

Approved:

DocuSigned by:
Nathan Young
8A2E719BA22D404...

Nathan Young
Chair

DocuSigned by:
Daniel Fried
[illegible]

Daniel Fried

DocuSigned by:
Cynthia Darling
[illegible]

Cynthia Darling

DocuSigned by:
OANH T LE
19F40BB62FC0481...

OANH T LE

Committee Members

DEDICATION

This dissertation is dedicated to my family and friends.

ACKNOWLEDGEMENTS

At the forefront of these invaluable contributions is Dr. Daniel Fried, whose faith in my potential back in 2019 has been a cornerstone of my academic and personal growth. When I found myself at a critical crossroads, with my visa nearing expiration and the looming possibility of having to leave behind my aspirations and return to China, it was Dr. Fried who extended a lifeline. His decision to offer me a position as a staff research associate, at a time when options seemed bleak, was not just a job opportunity; it was a beacon of hope. Dr. Fried's unwavering support did not merely secure my stay but also ignited a passion within me for the groundbreaking field of optical dental research. The opportunity to delve into this research under his mentorship transformed my professional trajectory, leading me to embrace the challenging yet rewarding path of pursuing my PhD. I cannot appreciate enough the versatile skillset and scientific knowledge you helped me to develop over the past five years.

I would like to acknowledge the members of my Thesis and Qualifying Exam committees: Drs. Cynthia Darling, Nathan Young, Donald Curtis, Michal Staninec, and Oanh Le. I am grateful for their invaluable feedback throughout my research journey.

I also would like to thank the current and past members of the Fried Lab who contributed to my academic achievements: Dr. Jacob Simon, Dr. Nai-yuan “Nick” Chang, William Fried, Vincent Yang, Dr. Marwa Abdelaziz, Dr. Chung “Wilson” Ng, Dr. Jungsoo Kim, Dr. Jing “Jane” Wang, John Tressel, Filipp Kashirtsev, Joany Xue, Morgan Ng, Dr. Yi-Ching Ho, Tina Dillas, Spencer Wycoff, Kevin Cheung, Minyoung “Lily” Kim and Hannah Takasuka. My work could not have been completed without their help.

This work was supported by the NIDCR/NIH grants R01-DE028295 and R01-DE027335.

CONTRIBUTIONS

CHAPTER II

Used with permission from Journal of Biomedical Optics:

Zhu, Y., et al. (2021). "Dual short wavelength infrared transillumination/reflectance mode imaging for caries detection." J Biomed Opt **26**(4): 043004.

CHAPTER III

Used with permission from Diagnostics:

Zhu, Y. and D. Fried (2022). "Measurement of the Depth of Lesions on Proximal Surfaces with SWIR Multispectral Transillumination and Reflectance Imaging." Diagnostics (Basel) **12**(3): 597.

CHAPTER IV

Used with permission from Diagnostics:

Zhu, Y., et al. (2023). "Diagnostic Performance of Multispectral SWIR Transillumination and Reflectance Imaging for Caries Detection." Diagnostics (Basel) **13**(17): 2824.

CHAPTER V

Used with permission from Lasers in Surgery and Medicine:

Zhu, Y., et al. (2023). "Monitoring lesion activity on primary teeth with CP-OCT and SWIR reflectance imaging." Lasers Surg Med **55**(6): 601-609.

CHAPTER VI

Used with permission from Diagnostics:

Zhu, Y., et al. (2023). "Active surveillance of root caries in vivo with CP-OCT." Diagnostics (Basel) **13**(3): 465.

Diagnosis of Dental Caries with Short-Wave Infrared (SWIR) Light

Yihua Zhu

ABSTRACT

This dissertation presents a comprehensive investigation into the application of Short-Wave Infrared (SWIR) imaging and Optical Coherence Tomography (OCT) for the enhanced detection and assessment of dental caries. Traditional diagnostic methods, such as radiographs, are limited by their inability to detect and diagnose early-stage, less severe carious lesions, often leading to delayed treatment and unnecessary restorations [1, 2]. SWIR imaging is highly promising to detect early caries with enhanced contrast due to the high transparency of dental enamel at longer wavelengths and its high sensitivity to demineralization [3-5]. SWIR imaging has been mostly limited to either transillumination or reflectance imaging at specific SWIR wavelengths. While promising, it suffers from limitations in specificity due to the complex structure of teeth and the interference of specular reflection that can obscure accurate lesion detection, especially during clinical imaging [6]. We hypothesize that dual-mode, multi-wavelength SWIR imaging combined with automated methods of image processing will increase diagnostic accuracy by providing semi-automatic detection of early demineralization and precise assessment of lesion severity *in vivo*. In addition, we postulate that integration of OCT will enable non-invasive analysis of lesion activity, facilitating timely preventive treatments [7-9]. We anticipate that this combination of various diagnostic modalities will significantly improve the clinical detection and management of dental caries and lead to better preservation of natural tooth structure. Moreover, such methods do not require the use of ionizing radiation and can be used for more frequent monitoring of lesion severity reducing the need for surgical intervention.

Table of Contents

List of Figures

CHAPTER I: Introduction

CHAPTER II: Dual short wavelength infrared (SWIR) transillumination/reflectance mode imaging for caries detection

CHAPTER III: Measurement of the depth of lesions on proximal surfaces with dual SWIR transillumination and reflectance imaging

CHAPTER IV: Clinical diagnostic performance of multispectral SWIR transillumination and reflectance imaging for caries detection

CHAPTER V: Monitoring lesion activity on primary teeth with CP-OCT and SWIR reflectance imaging

CHAPTER VI: Active Surveillance of Root Caries *in Vivo* with CP-OCT

CHAPTER VII: Clinical SWIR and CP-OCT Imaging of Interproximal Lesions

List of Tables

CHAPTER II: Dual short wavelength infrared (SWIR) transillumination/reflectance mode imaging for caries detection

CHAPTER III: Measurement of the depth of lesions on proximal surfaces with dual SWIR transillumination and reflectance imaging

CHAPTER IV: Clinical diagnostic performance of multispectral SWIR transillumination and reflectance imaging for caries detection

CHAPTER I

Introduction: Diagnosis of Dental Caries with Short-Wave Infrared (SWIR) Light

1.1 Dissertation Overview

Dental caries remains one of the most prevalent chronic diseases worldwide, affecting individuals across all age groups [10-12]. Despite advancements in dental care and hygiene, the early detection and accurate diagnosis of carious lesions poses significant challenges. Traditional diagnostic methods, including visual inspection and radiographs, are limited by their inability to detect early-stage lesions and their reliance on subjective interpretation [13-15]. This often leads to delayed treatment, invasive interventions, and unnecessary tooth restorations [1, 2]. The significance of developing more precise, non-invasive diagnostic tools is paramount in shifting the paradigm towards preventive dentistry and minimally invasive treatments. New innovative imaging technologies that can overcome the limitations of conventional diagnostics are needed such as Short-Wave Infrared (SWIR) imaging and Optical Coherence Tomography (OCT) for the early detection and accurate assessment of dental caries. In addition to the challenges addressed by traditional and single-mode SWIR imaging in early caries detection, this research emphasizes a multispectral and multimodal imaging approach. While predecessors laid the foundation with single-mode SWIR methods, this thesis introduces an innovative combination of two or more imaging modalities to enhance the adaptability of SWIR imaging for various lesion types [3-5]. We hypothesize that the simultaneous acquisition of multispectral transillumination and reflectance images will significantly improve diagnostic performance, reduce the potential for false positives and provide a more comprehensive analysis of lesion severity. This advancement supports a more conservative approach towards the management of dental caries with more monitoring and less invasive intervention.

1.2 Significance

Current clinical methods are unreliable for identifying the early stages of dental caries. For example, the convenstional diagnosis of early caries is based on visual and tactile evaluations [16-18]. The lack of diagnostic tools to distinguish early caries likely leads to false-positives and overtreatment [18, 19]. If carious lesions are detected early enough it is likely that they can be arrested by non-surgical means such as fluoride therapy, anti-bacterial therapy, dietary changes or by low power laser irradiation [20, 21]. In the past 20 years, SWIR imaging technologies have been developed and shown promising results for imaging early dental caries. Specifically, transillumination at 1300-nm and reflectance at >1450-nm can be used to detect both proximal lesions and occlusal lesions with high contrast [6]. The scattering coefficient of demineralized enamel is markedly higher than sound enamel beyond 1300-nm, making SWIR imaging an effective technique for detecting dental caries [22]. For example, occlusal transillumination is a novel imaging technique in which the tooth can be imaged from the occlusal surface after shining light at and below the gun line [23, 24]. Previous studies have shown that this method is able to detect both occlusal and approximal lesions with high contrast especially at 1300-nm, where enamel has very low attenuation coefficient and displays high transparency [24]. Besides occlusal transillumination, SWIR reflectance imaging shows even higher lesion contrast at > 1400-nm, due to the increase in water absorption at higher SWIR wavelengths, thanks to the significant amount of water composition in the enamel matrix [25, 26]. The increase in water absorption darkens the reflectance intensity in the sound enamel, creating the highest contrast with highly scattering demineralization in the longer wavelength. The imaging geometries of transillumination and reflectance are shown in **Fig.1.4.3** [27]. These novel imaging techniques exploit the unique optical properties of sound and demineralized dental hard tissues at higher SWIR wavelengths. It is shown

that light scattering in enamel decreases as the wavelength increases ($1/\lambda^3$), where λ is the wavelength, because of the size of principal light scatters (**Fig. 1.4.1**) [28-30]. At 1300-nm, both enamel and water have very low attenuation coefficients, enabling the high-penetrating performance of SWIR transillumination and Optical Coherence Tomography (OCT). At higher wavelengths (>1400-nm), the absorption coefficient (μ_a) of water increases and this enhances high-contrast reflectance imaging of lesions. In addition to the high sensitivity to demineralization, stains do not interfere. **Fig. 1.4.2** shows that stains that completely mask demineralization in the pits and fissures at visible and NIR wavelengths do not interfere in the SWIR spectrum [31]. Pigmented molecules are highly conjugated molecules such as melanin and porphyrins produced by bacteria, such molecules do not manifest electronic absorption bands beyond 1200-nm [32-34]. Moreover, recent studies have shown that there's an association between diagnostic x-rays and risk of cancer development due to ionizing radiation [35, 36]. SWIR imaging using non-ionizing radiation and has been shown to have the potential to replace dental radiographs for caries screening [5, 6, 27, 37]. The use of non-ionizing radiation allows more frequent monitoring of lesion activity and severity, reducing the need of surgical intervention. Without weighing the health risk of ionizing radiation, the major diagnostic limitation of diagnostic x-rays is that they are unable to detect early occlusal carious lesions because of the overlapping features of the crowns and the low radio-sensitivity to demineralization in dental enamel [17, 38, 39]. It is unlikely that improvements in radiographic sensitivity will enable detection of early enamel lesions because of this problem. In a study conducted in 2021, clinicians who were trained to interpret SWIR images were asked to visually score 3 Regions of Interest (ROI) (mesial proximal, distal proximal, occlusal) on 120 teeth by looking at radiographs, occlusal SWIR transillumination, and reflectance images individually in random order. Reflectance imaging at 1600-nm yielded much higher

diagnostic accuracy for lesions on both occlusal and proximal surfaces than radiographs (occlusal: 0.81 vs 0.36, proximal: 0.59 vs 0.49) [40]. However, the markedly higher sensitivity of SWIR imaging to early demineralization also increases the potential for false positives [41, 42]. This can be compounded by interference from specular reflection and multiple scattering from tooth structure [40, 43]. The first goal of this project is to develop methods to improve the diagnostic performance of SWIR imaging for caries detection and diagnosis, by combining multiple wavelengths and imaging geometries and modalities to strengthen the inclusion criteria for positive lesion detection.

Accurate caries diagnosis also requires the assessment of lesion activity to determine if the detected lesions require intervention [44, 45]. The lack of reliable diagnostic tools is a major challenge for assessing lesion activity and new tools are needed [46]. It has been demonstrated that SWIR imaging has the potential to differentiate developmental defects and arrested lesions from active lesions [47-50]. Arrested and non-carious developmental defects such as fluorosis do not require further intervention [51, 52]. Conventional criteria for lesion activity assessments (i.e. ICDAS II) such as color, texture and hardness assessments are subjective and unreliable [53, 54]. Previous studies have shown that the optical changes due to the loss of water from porous lesions can be exploited to assess lesion severity with SWIR reflectance imaging [25, 55, 56]. Arrested lesions have a highly mineralized surface zone which is formed during remineralization that reduces the permeability to water and plaque generated acids [25, 56]. Chang et al. [57] has shown that the remineralized transparent surface zone thickness is inversely related to the rate of water evaporation during air dehydration by using SWIR reflectance imaging. In addition, optical coherence tomography (OCT) is capable of imaging cross-sections in teeth to a depth of 4 mm in enamel and 2 mm in dentin with an axial resolution of less than 10-μm [58-60]. **Fig. 1.4.4**

demonstrates that OCT is able to detect the presence of a remineralized surface zone that arrests lesion development [61]. Apart from the visualization of the remineralized surface zone, OCT also allows the quantification of lesion severity by relating the lesion's integrated reflectivity to integrated mineral loss, due to the increased scattering coefficient of demineralization at 1300-nm [62]. Furthermore, both OCT and SWIR reflectance imaging can be utilized to quantify lesion activity with dehydration [57, 63]. In addition, in a recent clinical study published in 2020, CP-OCT was first utilized to assess root caries lesion severity and activity *in vivo* [64]. Despite the success at displaying the surface zone and measuring integrated reflectivity, the clinical translation of OCT and SWIR dehydration imaging still faces challenges. For example, the intensity of OCT scans can vary markedly from scan to scan due to changes in local environmental conditions induced by breathing or by artifacts caused by infection control coverings, making it difficult to compare integrated reflectivity across different images. Movement artifacts may cause distortion in OCT images, introducing challenges in measuring accurate lesion depth and the acquisition of dehydration rate data. An excess of saliva may also increase specular reflection shielding the lesions in the occlusal pits, disrupting the accurate plot of dehydration curves. A second goal of this research is to develop both hardware and software solutions to resolve the clinical challenges of OCT and SWIR imaging for lesion activity assessment.

1.3 Dissertation Aims

The overall objective of this proposed research is to develop improved methods and devices for the detection and diagnosis of dental caries. Conventional methods of caries detection such as radiographs cannot detect less severe, hidden, and early lesions [6, 65-69]. Typically more than 30% of the mineral content must be lost in lesion areas before being radiographically captured [1,

2]. Radiographs have poor sensitivity for occlusal lesions and lesions are typically not detected until restoration is needed [70]. Due to the low radiographic sensitivity, the early diagnosis of occlusal lesions is often based on visual and tactile evaluations that may lead to false positives and overtreatment [18, 19, 71]. Surgical intervention can be avoided with early detection, enabling non-invasive therapies such as fluoride treatment, anti-bacterial treatment, or low intensity laser irradiation [20, 21]. The unique differences in optical properties of dental enamel, dentin, and caries at >1200-nm established the foundation of SWIR dental imaging. Multiple imaging techniques such as SWIR reflectance, SWIR occlusal transillumination, and Optical Coherence Tomography (OCT) have been developed and shown promising results to detect early demineralization and assess lesion severity. ***The central hypothesis is that the clinical diagnostic performance of SWIR imaging can be significantly improved by incorporating multiple wavelengths and imaging geometries and advanced image post-processing strategies.***

AIM 1: To test the hypothesis that multi-wavelength dual-mode SWIR imaging can significantly improve the diagnostic performance of caries detection on tooth proximal and occlusal surfaces. Individual SWIR probes for occlusal transillumination, approximal transillumination at 1300-nm and reflectance at >1450-nm have been utilized to detect both occlusal and proximal *in vivo* lesions [27]. The probes were utilized to scan teeth that were scheduled for extraction and achieved high lesion contrast and significantly higher sensitivity than radiography for the detection of both occlusal and proximal lesions. However, while individual SWIR probes achieved high sensitivity, the specificity was lower than that of radiography, increasing the potential of false positives and probability of overtreatment. In addition, the use of three separate probes is impractical and it is difficult to use images from the separate probes in a combined analysis due to challenges in image registration. To address these concerns, benchtop

dual-mode SWIR occlusal transillumination and cross-polarized reflectance imaging systems to detect occlusal caries and assess lesion severity were investigated [5, 72]. Positive relationships between imaged lesion contrast/width and true lesion depth were discovered [5]. These multispectral experiments revealed that even though individual SWIR imaging modalities performed well achieving high lesion contrast, it would be more beneficial to combine both techniques into a single probe since both imaging techniques require the sensor to be positioned on the occlusal surface, thus allowing accurate image registration for lesion severity analysis and a significantly reduced image acquisition time. However, the size and complexity of the bench top dual-wavelength system makes it difficult to translate into a practical clinical setup [5]. Given the rapid development of modern material engineering such as CAD design and stereolithography 3D printing, clinical dual-SWIR probes are proposed that are capable of achieving simultaneous reflectance at > 1450-nm and occlusal transillumination at 1300-nm for clinical dental caries screening. In addition, simultaneous transillumination and reflectance image acquisition at two wavelengths allows highly accurate image registration, and reduces false positives. In addition, it is proposed that the lesion depth can be estimated with information extracted from registered images, due to the transparent nature of dental enamel at SWIR wavelengths [28]. The dual-SWIR probes will be able to incorporate multiple imaging geometries, combining occlusal transillumination and reflectance with the imaging sensor positioned above the occlusal surface, and combining proximal transillumination and reflectance with the sensor placed at the lingual/facial surfaces.

AIM 2: To test the hypothesis that Optical Coherence Tomography (OCT) and SWIR reflectance imaging can be used to assess clinical lesion activity over time. Several *in vitro* studies have shown that OCT can accurately assess the severity and activity of caries lesions

through measurement of the lesion depth and thickness of the remineralized surface zone [9, 73, 74]. In addition, the integrated reflectivity of lesion measured with OCT has been shown to be a reliable indicator of lesion severity *ex vivo* [62, 75]. Even though OCT was able to detect occlusal and root caries clinically with high contrast by scanning above occlusal and smooth surfaces [7, 51], clinical translation of OCT still faces challenges, namely monitoring lesion severity and activity over time due to inconsistency in clinical image quality. Clinical studies have shown that the remineralized surface zones of root caries can be acquired using CP-OCT [64]. However, clinical conditions introduce new challenges affecting quantitative analysis of lesion severity and activity. The inconsistency in motion, condensation, and other artifacts limit the clinical performance of OCT. This inconsistency in image quality makes it difficult to compare crucial quantitative metrics such as integrated reflectivity and lesion depth across different samples and over time. In this aim advanced computer vision techniques are proposed to improve the diagnostic performance of OCT for clinical caries activity assessment. In addition to OCT, several studies have shown that SWIR imaging at wavelengths from 1450-nm to 2350-nm can be used to assess lesion activity on coronal surfaces due to large increases in lesion contrast during dehydration [49, 76]. This technique is based on the contrast between water's high absorption coefficient and demineralization's high scattering coefficient at SWIR wavelengths, and arrested lesions with a remineralized surface zone inhibit the diffusion and evaporation of water during dehydration [49, 56, 57, 77]. SWIR reflectance encountered challenges during its initial clinical use, including motion instability during the long time required for dehydration and suboptimal air delivery to targeted lesion areas [64]. In addition, excess saliva present during *in vivo* imaging complicates the accurate acquisition of dehydration curves due to water's high SWIR absorption that introduces strong specular reflection and masks the lesion. Movement during the 30-second imaging also

affects the accuracy due to change in polarization. To address those issues, a revised clinical imaging protocol paired with a redesigned dehydration device is proposed in this aim to improve the efficacy of the application of SWIR imaging in lesion activity assessment.

1.4 Figures

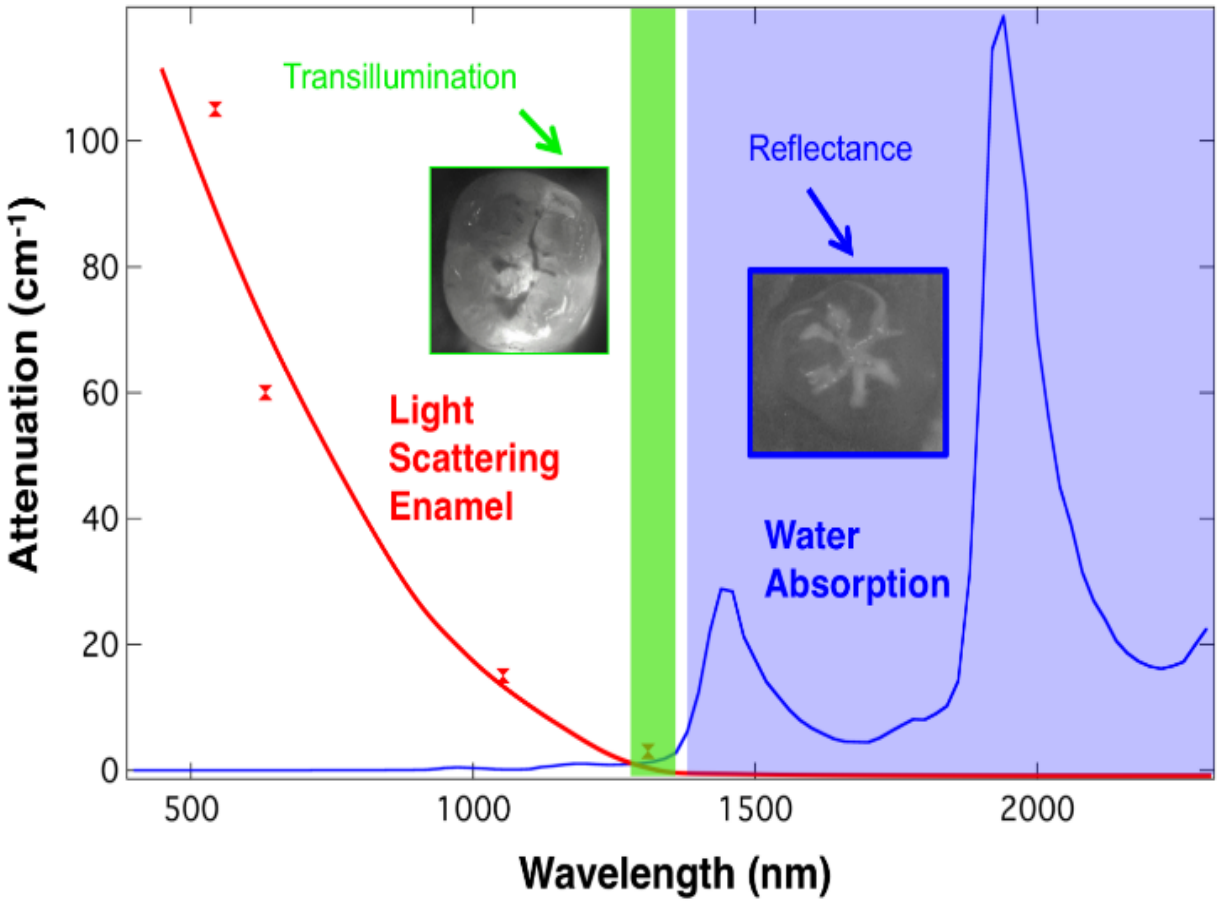

Figure. 1.4.1. The attenuation coefficient (extinction) for dental enamel (red line) and the absorption coefficient of water (blue line) from visible to SWIR wavelengths [28]. The combination of low attenuation of both enamel and water at 1300-nm (green region) allows transillumination imaging of dental caries. The increase in water absorption at higher wavelength (blue region) gives the highest contrast of dental demineralization with reflectance imaging.

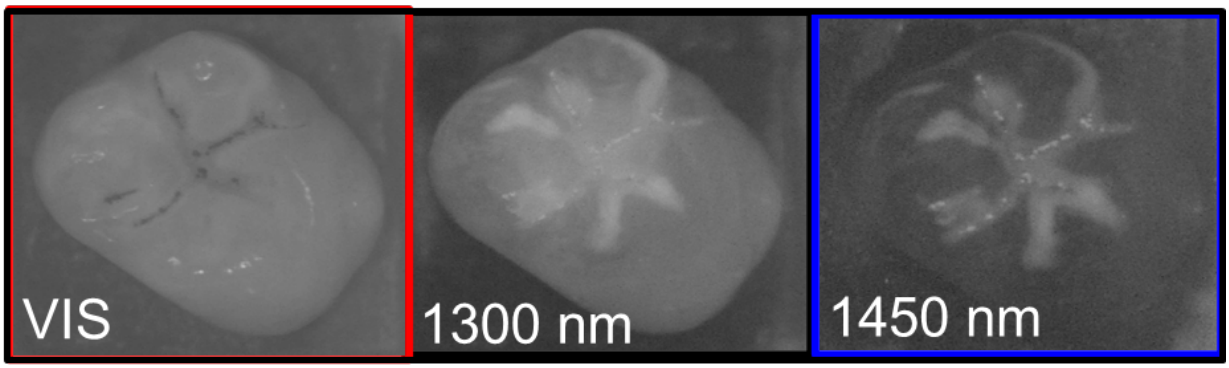

Figure. 1.4.2. Occlusal surface of a tooth [31]. (A)Visible image; (B) Reflectance at 1300-nm; (C) Reflectance at 1450-nm. Stains that cover up the occlusal lesion don't show up in SWIR reflectance images due to its SWIR transparency.

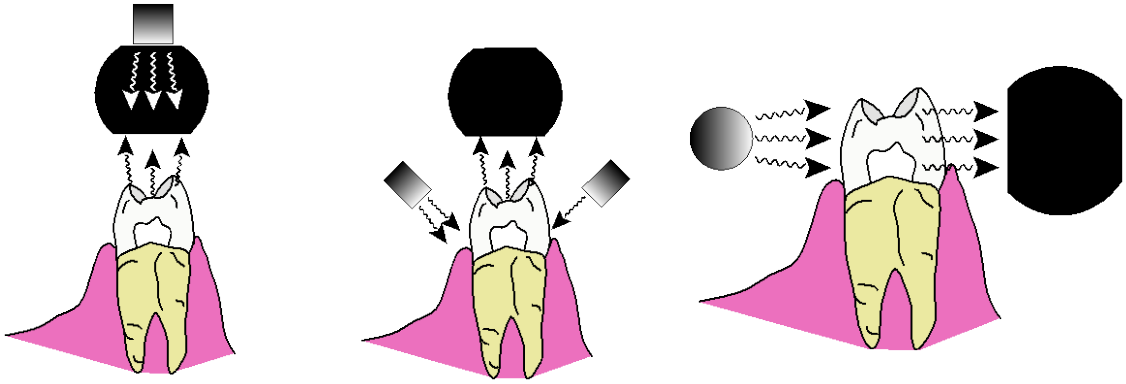

Figure. 1.4.3. SWIR imaging geometries [27]. Camera (black), Light source (gradient), light path (arrows). (A) Reflectance (SWIR-R); (B) Occlusal transillumination (SWIR-OT); (C) Approximal transillumination (SWIR-PT).

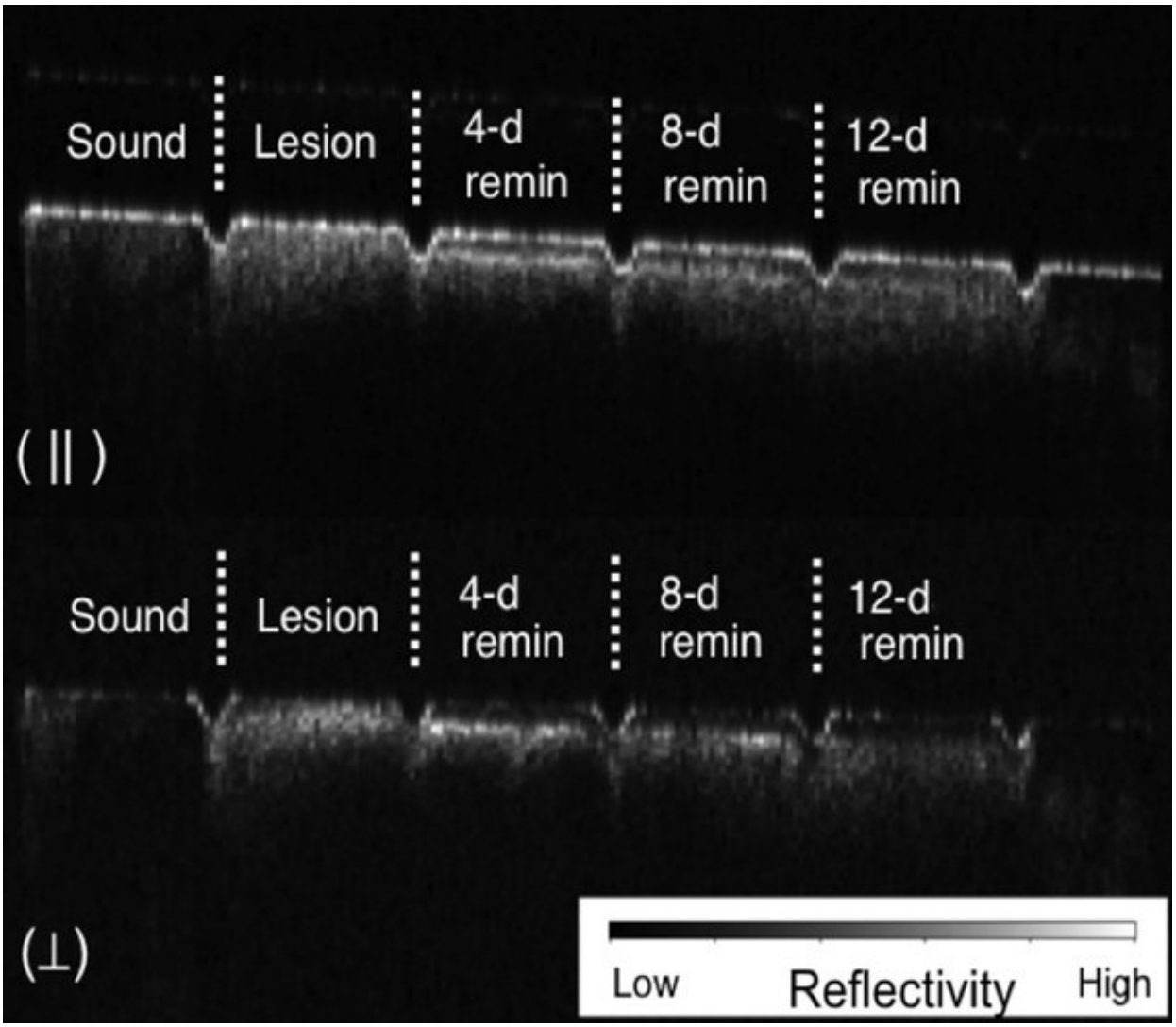

Figure. 1.4.4. PS-OCT b-scan images of a sample showing the sound (protected) regions located on the extreme left and right side of the sample, the lesion area (0-days exposed to remin. soln) and the areas exposed for increasing periods of time to the remineralization solution, 4, 8, and 12-days [61]. The (||) image represents the light reflected in the original polarization while the (⊥) image is the orthogonal polarization or cross polarization image which was used for analysis in these studies.

CHAPTER II

Dual short wavelength infrared (SWIR) transillumination/reflectance mode imaging for caries detection

2.1 Summary

We have developed a clinical probe capable of acquiring near simultaneous short wavelength infrared (SWIR) reflectance and occlusal transillumination images of lesions on tooth proximal and occlusal surfaces. We hypothesize that dual images will aid in differentiating between shallow and deep occlusal lesions and reduce the potential of false positives. Aim: The aim of this study was to test the performance of the dual reflectance and occlusal transillumination probe on extracted teeth prior to commencing clinical studies. Approach: The dual probe was 3D printed and the imaging system uses an InGaAs camera and broadband superluminescent diode light sources that emit broadband light at 1300-nm for occlusal transillumination and 1600-nm light for cross-polarization reflectance. The diagnostic performance of the dual probe was assessed using 120 extracted teeth with approximal and occlusal lesions. Reflectance and transillumination images were fused into single images to enhance the contrast between sound and lesion areas. The lesion contrast in both modes did not increase significantly with either the lesion depth or the distance from the occlusal surface for approximal lesions. In addition, the diagnostic performance of radiography, the individual reflectance and transillumination images, dual images and fused images were compared using micro computed tomography (microCT) as the gold standard. Results: Reflectance imaging at 1600-nm yielded the highest diagnostic accuracy for lesions on both occlusal and proximal surfaces while radiography yielded the lowest number of false positives. Conclusion: This study demonstrates that simultaneous acquisition of both reflectance and transillumination SWIR images is possible with a single clinical device.

2.2 Introduction

Short wavelength infrared (SWIR) and near-IR imaging (NIR) methods have been under development for almost 20 years for use in dentistry and several NIR clinical devices are now available commercially. Due to the high transparency of enamel at longer wavelengths, novel imaging configurations are feasible in which the tooth can be imaged from the occlusal surface after shining light at and below the gum line, which we call occlusal transillumination [23, 24]. Approximal lesions, the lesions located at the proximal contact points in between teeth, can be imaged via occlusal transillumination of the proximal contact points between teeth and by directing SWIR light below the crown while imaging the occlusal surface [24, 78, 79]. The latter approach is capable of imaging occlusal lesions as well with high contrast [23, 24, 47, 80-82]. In 2010, it was demonstrated that approximal lesions that appeared on radiographs could be detected *in vivo* with SWIR imaging at 1310-nm with similar sensitivity [24] and that occlusal transillumination could be employed clinically. This was the first step in demonstrating the clinical potential of NIR and SWIR imaging for approximal caries detection. In the most recent clinical study in 2016 [6], SWIR transillumination and SWIR reflectance imaging probes were used to screen premolar teeth scheduled for extraction for caries lesions at wavelengths greater than 1300-nm. The teeth were collected and sectioned into 200-µm slices and examined with polarized light microscopy and transverse microradiography which served as the gold standard. In addition, extra-oral radiographs were taken of teeth and the diagnostic performance of SWIR imaging was compared with radiography. The sensitivity of the combined SWIR imaging probes was significantly higher ($P < 0.05$) than radiographs for both occlusal and approximal lesions *in vivo*. It was anticipated that SWIR methods would be more sensitive than radiographs for occlusal lesions since the radiographic sensitivity for occlusal lesions is extremely poor, however, the sensitivity was also

much higher for approximal lesions than radiography, 0.53 vs 0.23. In addition, the sensitivity of each individual SWIR method was either individually equal to or higher than radiography.

Several shorter wavelength NIR devices that utilize either reflectance and transillumination imaging have been introduced commercially operating at 830 and 780-nm [83-87]. The shorter wavelength allows the use of less expensive, silicon-based detectors. However, longer wavelength SWIR light has significant advantages. The use of shorter wavelength 830-nm NIR light was first investigated almost 20 years ago [78]. The contrast was significantly lower than at 1300-nm and simulated lesions could not be imaged through the full thickness of enamel [78]. It is also important to point out that stains interfere significantly at 780-nm [88] and the contrast between sound and demineralized enamel is markedly higher at wavelengths beyond 1400-nm in reflectance measurements [70, 88, 89].

Epidemiological data gathered from the National Health and Nutritional Survey (NHANES) [90, 91] and Dental Practice-Based Research Network (DPBRN) [92-94] indicates that nearly one third of all patients have a questionable occlusal carious lesion (QOC) located on a posterior tooth. QOC's are given the name "questionable" because clinicians' lack instrumentation capable of measuring the depth of pit and fissure lesions and determining if the dental decay has reached the underlying dentin. Bitewing radiographs are not sensitive enough to detect most occlusal lesions, and visible diagnosis is confounded by stain trapped in the occlusal anatomy [88]. Prior *in vitro* studies attempted to combine SWIR reflectance and transillumination measurements in order to estimate QOC depth and severity [5, 82, 95]. Zakian et al. [96, 97] used multiple wavelengths of SWIR hyperspectral reflectance images to estimate the severity of occlusal lesions. Since, multispectral SWIR reflectance and transillumination experiments have demonstrated that the

tooth appears darker at wavelengths coincident with increased water absorption, multispectral images can be used to produce increased contrast between different tooth structures such as sound enamel and dentin, dental decay and composite restorative materials [97-99]. Combining measurements from different SWIR imaging wavelengths and comparing them with concurrent measurements acquired by complementary imaging modalities should provide improved assessment of lesion depth and severity.

Both the reflectance and the occlusal transillumination probes sample light that is emitted from tooth occlusal surfaces, therefore it is feasible to combine both methods into a single probe that can be positioned above the tooth for rapid clinical screening. Different illumination wavelengths can be used that are optimized for each imaging mode, namely SWIR wavelengths greater than 1400-nm for reflectance and 1300-nm for transillumination. Simon et al. [27] built a benchtop simultaneous SWIR reflectance and transillumination system with tunable filters that ranged from 830-1700-nm and showed that the combined images have potential for the diagnosis of QOC's. In a study the following year using the same benchtop system and simulated approximal lesions it was shown that multispectral combined images can potentially be used to improve the differentiation of cavitated and noncavitated approximal lesions [100]. In a third study carried out in 2018, Simon et al. [5] used the same benchtop system to image 37 extracted teeth with occlusal caries lesions and sectioned the teeth and measured the lesion depth with polarized light microscopy (PLM). This 2018 study showed that the contrast of reflectance at 1500-1700-nm correlated with the lesion depth while the transillumination at 1200-1700-nm showed no correlation. The lesion width, the lesions' buccal-lingual dimension along the fissure, showed a positive correlation with lesion depth for reflectance and transillumination. These initial investigations demonstrated the potential of acquiring simultaneous multiwavelength SWIR

reflection and transillumination images to improve the detection of caries lesions on both occlusal and proximal surfaces. We hypothesize that the greatest utility of a combined SWIR reflectance and transillumination clinical probe will be to reduce false positives since it is unlikely that confounding structural features or specular reflection are going to be present in both reflectance and transillumination images. In addition, the dual probe will provide complementary diagnostic information about lesion severity to help discriminate early superficial lesions on tooth surfaces from deeply penetrating lesions.

In this study, a system for the acquisition of simultaneous SWIR reflectance and transillumination system suitable for clinical use was developed and tested on 120 teeth extracted teeth with occlusal and approximal lesions using microCT as a gold standard.

2.3 Materials and Methods

2.3.1 Sample Preparation

Teeth with no identifiers were collected from patients in the San Francisco Bay area and Geneva Switzerland with approval from the UCSF Committee on Human Research. Extracted teeth (n=120) were selected with occlusal and approximal lesions for this study. Teeth were sterilized using gamma radiation and stored in 0.1% thymol solution to maintain tissue hydration and prevent bacterial growth. Then, samples were mounted in black orthodontic acrylic blocks from Great Lakes Orthodontics (Tonawanda, NY) and imaged with digital radiographs using a CareStream 2200 System from Kodak (Rochester, NY) operating at 60 kV.

2.3.2 Design and Fabrication of the Dual SWIR Probe

The dual probe was designed in Fusion 360 from Autodesk (San Francisco, CA). The dual probe design consists of a handpiece with reflectance and a transillumination attachment, shown in **Figs. 2.7.1A-C.** The handpiece incorporated an insert (**Fig. 2.7.1D**) to attach the optical fiber for reflectance along with a 5-mm Thorlabs (Newton, NJ) polarizing beam splitter cube. The insert utilized black resin to reduce artifacts from unwanted scattering in the handpiece. A cross-sectional view of the reflectance probe body is shown in **Fig. 2.7.1C**. Light from a fiber optic cable travels from the back of the handpiece to the insert (**Fig. 2.7.1D**) and is directed at a right angle by the polarizing beam splitter cube (6) towards the tooth surface as shown by the path of the red arrow in **Fig. 2.7.1C**. Reflected and transmitted light from the tooth is reflected off a polished aluminum surface (7) attached at a 45-degree angle at the distal end of the handpiece. There is an air nozzle positioned on the bottom of the probe (3) directed towards the aluminum reflector to prevent fogging of the aluminum surface. The air nozzle can also be used to dry the tooth surface to increase lesion contrast and potentially assess lesion activity [9, 49, 101].

The transillumination attachment (**Fig. 2.7.1E**) attaches to the distal end of the handpiece as shown in **Fig. 2.7.1B**. It was fabricated with Formlabs (Boston, MA) Flexible Resin. The flexible resin can tolerate moderate stretch and compression, making it an ideal choice for imaging teeth with different shapes and sizes. The transillumination optical fibers enter each arm of the attachment and are inserted into the two ports at the rear of the appliance (8) as shown in **Figs.2.7.1B & E** and into Teflon plugs (9). The Teflon plugs diffusely spread the light from the optical fiber into the tooth on the buccal and lingual surfaces below the dentinal enamel junction and into the gingival tissues when used clinically. They were fabricated from 1/8” diameter Teflon rod cut to a length

of 3 mm. The separation of each arm is 1-cm and they are flexible and can stretch to almost 2-cm to accommodate larger teeth.

The handpiece was fabricated using a Formlabs Form 3 Low Force Stereolithography 3D printer. The final design is exported as a STL file and transferred to Formlabs PreForm to generate supports for a final 3D printing scheme. A spatial resolution of 100-µm was used for all prints. Formlabs Dental SG Resin was used for printing the reflectance probe to provide biocompatibility and autoclavability. After 3D printing, handpiece was transferred to Formlabs Form Wash to rinse off the resin residue with isopropyl alcohol for 5 minutes and cure for 30 minutes at 60°C in the Form Cure. The attachment (Fig. 2.7.1D) housing the 5-mm polarization beam splitting (PBS) cube was printed using Formlabs black resin. After curing, supports are removed with a clip and surfaces are trimmed with water sanding technique to remove sharp edges and achieve smooth finishing.

To assemble the dual SWIR probe, the insert with the PBS cube (Fig. 2.7.1D) is attached to the top of the handpiece. The aluminium reflector (7) is attached to the distal end of the handpiece and held in place with a set screw. The transillumination attachment (Fig. 2.7.1E) slides on top of the handpiece and securely locks the insert with the beamsplitter cube (6) in place.

2.3.3 Image Acquisition and Analysis

The SWIR reflectance images were captured using a Model GA1280J (Sensors Unlimited, Princeton, NK) camera with a 1280 x 1024 pixel format, a 15-µm pixel pitch and a bit depth of 12-bit. Two 1-in diameter planoconvex antireflection coated lenses of 60-mm and 100-mm focal length along with an adjustable aperture were placed between the handpiece and the InGaAs camera to provide a field of view of 11-mm x 11-mm at the focus plane. A low-OH optical fiber of 1-mm diameter was used to deliver light from a 1604-nm superluminescent diode (SLD), Model

ESL 1620-2111 from Exalos (Schlieren, Switzerland) with an output of 17-mW and a bandwidth of 46-nm. The intensity delivered to the tooth was 5-mW. The transillumination light is delivered through two 0.4-mm diameter low-OH optical fibers. A 1314-nm (BW) SLD, Model DL-CS3452A-FP 1620-2111 from Denselight (Singapore) with an output of 48-mW and a bandwidth of 33-nm was used as the source for transillumination. A 50/50 beamsplitter was used to deliver light to each arm for transillumination. The output intensity of each arm was set at 10-mw before entering the Teflon plugs. The reflectance and transillumination light sources output were controlled via two OSW12(22) MEMS fiber optic switches from Thorlabs. The camera and the optic switch were controlled in custom authored programs in LabView (Austin, TX). The two optical switches alternate between the 1300-nm light source for transillumination and the 1600-nm source for reflectance allowing near simultaneous acquisition at a rate of 30 Hz. A diagram of the setup along with an image of the with imaging optics and the assembled dual probe is shown in **Fig. 2.7.2A**. **Figure 2.7.2A** shows the larger Model GA1280J InGaAs camera that was used to acquire the *in vitro* images used in this study. The probe can also be used with the smaller 640 x 480 pixel micro-SWIR camera (SU640CSX) measuring only 32-mm x 32-mm x 28-mm from Sensors Unlimited (Princeton, NJ) that is better suited for clinical imaging and it is shown in **Fig. 2.7.2B** with the assembled probe.

The samples were dried of excess water with an air nozzle before imaging due to the strong water absorption at 1600-nm [79]. Image processing of the images was performed by custom scripts written using MATLAB from Mathworks (Natick, MA). The acquired 12-bit images (4096) were converted to 16-bit (65535) by multiplying by 16 and subtracting 1 to facilitate processing using MATLAB. Lesion ROIs were identified from the transillumination/reflectance images. Co-registration was unnecessary since they were acquired near simultaneously by the same imaging

optics. Sound areas for comparison were chosen from areas surrounding the lesion. This better represents the contrast between the lesion and sound tissues that would be viewed by the clinician. The contrast was calculated for each lesion using the formula $(I_L - I_S)/I_L$ for reflectance images and $(I_S - I_L)/I_S$ for transillumination images, where I_L is the average intensity in the lesion area ROI, and I_S is the average intensity in the sound ROI [80]. Lesion areas were confirmed using the microCT images.

In addition to calculating the lesion contrast in transillumination and reflectance images, a dual fusion mode combining the two images was created in MATLAB and included in the analysis utilizing the weight, or fraction of the intensity applied from each image. The dual fusion mode is a weighted linear combination of the intensities of the inverted transillumination ($I_{Tinv} = 65535 - I_T$) and the reflectance (I_R) 16-bit images. The lesion contrast in fusion mode was calculated using $aI_{Tinv} + bI_R$, with alpha (a) ranging from 0 to 1, where a = 1-b.

2.3.4 Scoring of Digital Radiographs and SWIR Images by Clinicians

Three DDS examiners participated in the study, two examiners had several years of research experience with SWIR imaging and one examiner had no prior experience with SWIR imaging. A training set was used to standardize the knowledge of the three examiners prior to the study. All examiners were presented with radiographs and SWIR images of 120 teeth and asked to score the occlusal, mesial approximal and distal approximal surfaces of each tooth. At least one of the examiners indicated that at least one of the images for 14 of the teeth was unreadable. Therefore 106 sets of images with 4 different imaging methods (transillumination, reflectance, dual, both) were evaluated. The order of the images was randomized for each of the 4 testing sets among the 3 examiners. The examiners were asked to provide a binary score (lesion or no lesion) for each of

the 3 surfaces. Diagnostic accuracy was calculated using (TP+TN)/(TP+TN+FP+FN) where TP, TN, FP and FN are true positives, true negatives, false positives and false negative, respectively. MicroCT was used as the gold standard. The percent agreement for each tooth was calculated, and then the average % agreement was calculated for all the samples to represent the study interrater reliability. Clinician scores of interrater reliability (percent agreement), accuracy and false positives were calculated for the four SWIR image types and the radiographs and the values are tabulated in **Table 2.7.2**.

2.4 Results

Several images from a tooth with an occlusal lesion in a fissure that penetrates almost to the underlying dentin are shown in **Fig. 2.7.3**. The visible image of the occlusal surface (**Fig. 2.7.3V**) displays a mandibular premolar with red/brown staining in the central fissure and mesial pit, however there is no evidence of increased white (value) areas that are indicative of visible demineralization on the tooth surface. The SWIR reflectance image (**Fig. 2.7.3R**) displays with high contrast increased light scattering from the stained fissure and pit indicating that the enamel is demineralized in these areas. There are also some other areas of high intensity, particularly on the buccal cusp tip. that may be due to demineralization but is more likely specular reflection from the surface. There is no decay visible in the radiograph (**Fig. 2.7.3X**) while the microCT slice clearly shows that the v-shaped lesion in the fissure has penetrated almost through the enamel. The decay in the fissure and the pit is also detectable in the transillumination image (**Fig. 2.7.3T**) increasing the probability that those areas are actually demineralized and not due to an optical anomaly. The bright spot originating from the buccal cusp tip in the reflectance image is not visible in the transillumination image and is likely an area of specular reflection. The fusion image (**Fig.**

2.7.3a) shows the lesion areas with high contrast, however it also highlights areas of suspected specular reflection.

Several images of another tooth with approximal lesions at both proximal contact points are shown in **Fig. 2.7.4.** The visible image of the occlusal surface shows nearly no evidence of approximal lesions (**Fig. 2.7.4V**) and only one of the lesions is visible in the radiograph (**Fig. 2.7.4X**) and it appears to penetrate less than halfway through the enamel. The SWIR reflectance, transillumination and microCT images agree quite well all showing that both lesions penetrate almost to the dentinal enamel junction (DEJ). The fusion image (**Fig. 2.7.4a**) shows the lesions with high contrast and the surrounding sound enamel areas appear more uniform in intensity.

Fig. 2.7.5 demonstrates the effect of varying alpha ($aI_{Tinv} + bI_R$) in the dual fusion images. Images with alpha values varying from 0.0 to 0.9 are shown of a tooth with an approximal lesion. For this particularly tooth the contrast of the lesion increased with increasing alpha. The contrast did not increase with increasing alpha for all of the teeth, some exhibited a decrease with increasing alpha. The mean lesion contrast from all samples is plotted as a function of the alpha coefficient in **Fig. 2.7.6** for occlusal lesions (circles, n=120) and approximal lesions (triangles, n=120). The approximal lesion depth was measured from the proximal surface contact point to deepest lesion point in the pulpal direction while the lesion depth for occlusal lesions was measured from the occlusal surface to deepest lesion point in the pulpal direction.

The mean lesion contrast is plotted versus lesion depth for occlusal lesions in **Fig. 2.7.7** for reflectance, transillumination and the fusion mode images. The reflectance and transillumination measurements were all from the occlusal surface. There was no significant dependence on the lesion contrast with lesion depth. For approximal lesions the lesion contrast was determined versus

the distance of the lesion from the occlusal surface. This comparison is shown in **Fig. 2.7.8** for the reflectance and transillumination images along with the fusion images and there was also no significant dependence on the lesion contrast with distance from the occlusal surface.

The effect of α on the mean lesion contrast is tabulated in **Table 2.7.1** for occlusal and approximal lesions. For occlusal lesions, the reflectance mode alone performs exceptionally as it shows a mean lesion contrast of 0.65 versus 0.57 from transillumination mode. Dual fusion mode negatively impacts the mean occlusal lesion contrast, and as α gets higher the mean lesion contrast decreases. For approximal lesions, $\alpha = 0.4$ shows a mean lesion contrast of 0.615, improving the contrast of 49.4% of the approximal lesions and showing contrast enhancement of 8.2% from the reflectance mode and 22.8% from the transillumination mode.

The examiner agreement (percent agreement), accuracy and false positive rate are listed in **Table 2.7.2** for the three clinician assessments of the SWIR images and the radiographs. The mesial and distal proximal surfaces were combined for the table. The examiner agreement was highest for the radiographs. The examiner agreement was moderate for transillumination, reflectance, merged images and side by side images for both occlusal and proximal surfaces. Reflectance yielded the highest accuracy and lowest false positive rate while transillumination yielded the lowest accuracy and the highest false positive rate among SWIR imaging. The use of dual mode yielded a slight improvement in accuracy, percent agreement, and false positive rate over transillumination alone but was inferior to reflectance. The use of side by side reflectance and transillumination images did not appear to improve diagnostic performance or reduce the false positive rate. Both the false positive rate and the accuracy of radiographs were lower than the SWIR methods.

2.5 Discussion

In this study a compact dual reflectance and transillumination SWIR imaging device was employed to acquire images of 120 extracted teeth with caries lesions. Near simultaneous reflectance and occlusal transillumination images are collected from the tooth occlusal surface which facilitates registration and integration. The reflectance probe delivers 1600-nm light to the tooth occlusal surface while the occlusal transillumination probe delivers 1300-nm light cervically at the lingual and buccal sides of the tooth allowing it to propagate into the tooth diffuse in the cervical-coronal direction interacting with approximal and occlusal lesions and exiting the occlusal surface. The transillumination probe utilizes light at 1300-nm where the enamel is most transparent. Scattering in enamel continues to decrease with increasing wavelength beyond 1300-nm, however water absorption increases markedly beyond 1400-nm greatly increasing attenuation [22]. The dual SWIR probe can capture high definition *in-vitro* transillumination and reflectance SWIR images of extracted teeth. The probe was fabricated using a 3D printer and utilized two broadband fiber-optic superluminescent diode (SLD) light sources. Previous studies have investigated the contrast of caries lesions using both reflectance and transmitted light. This was the first study demonstrating the performance of an imaging system that simultaneously acquires cross polarized reflectance and occlusal transillumination images at multiple SWIR wavelengths using a single compact handpiece suitable for clinical use. In addition, it was the first study to compare the SWIR lesion contrast with microCT images as the gold standard for lesion depth.

The primary motivation for acquiring dual mode images is to reduce the probability of false positives and remove the need to switch between transillumination and reflectance probes during screening. In SWIR occlusal transillumination, cracks and structural features in the tooth can

block light propagation through the tooth producing features that resemble lesions, greatly increasing the potential for false positives. Specular reflection interferes with SWIR reflectance measurements and even when high extinction ratio polarizers are employed, there is still substantial specular reflection present in cross polarization images that has the potential to generate additional false positives. Even though studies are lacking indicating that NIR imaging leads to an increased number of false positives, clinicians using this new technology have voiced concern regarding false positives. Moreover, the markedly higher sensitivity of NIR and SWIR imaging compared to radiography is likely to lead to an increase in false positives simply on the basis of the higher sensitivity. In our most recent clinical study involving SWIR imaging of teeth scheduled to be extracted with unknown caries status, the specificity of SWIR imaging was lower than for radiography, although the difference was not statistically significant [6]. In that study images of the teeth were acquired using three separate imaging probes: SWIR reflectance (1600-nm), SWIR occlusal transillumination (1300-nm) and SWIR proximal transillumination (1300-nm), combining multiple images for diagnostic performance improved both the sensitivity and the specificity.

Another important advantage of imaging in the SWIR beyond 1150-nm is that the chromophores responsible for stains on teeth do not absorb light at longer wavelengths since there is not sufficient energy for electronic excitation [97, 102]. This is of particular importance in the stained pits and fissures of tooth occlusal surface. Ng et al. [88] demonstrated that it is necessary to use SWIR wavelengths greater than 1150-nm to avoid significant interference from stains when measuring lesion contrast in reflectance and transillumination modalities. Therefore, stains can be easily differentiated from actual demineralization in the SWIR range, which is not possible at visible wavelengths or at NIR/SWIR wavelengths of less than 1150-nm. Chung et al. [70] showed that

absorption due to stains contributed more to the lesion contrast than increased scattering due to demineralization at visible wavelengths and that is clearly demonstrated in **Fig 2.7.3.** Since it is impractical and unnecessary to remove stains from the deep grooves and fissures on tooth occlusal surfaces, lack of interference from stains at longer SWIR wavelengths is a significant advantage.

Dental radiographs suffer from very low contrast and it takes considerable experience and expertise to accurately read such images. The principal advantage of radiographs is the very high specificity, i.e. if a lesion is visible in a radiograph it is most likely a true positive, therefore overtreatment is less likely. In addition to the low sensitivity, radiographs typically underestimate the penetration depth of approximal lesions and dentists typically have to estimate that the lesions penetrate much deeper than they appear based on subjective factors involving caries risk status. Images acquired in this study suggest that SWIR images better represent the true depth of the approximal lesions and better match the depth indicated in microCT images than radiographs. SWIR images are also quantifiable and provide measurements that can be utilized for non-bias assessment of lesion depth and severity.

Both reflectance and occlusal transillumination imaging modes yield high contrast for approximal lesions. Since more light propagates through the transparent outer enamel than through the highly scattering dentin core, cracks, fractures and other defects in the tooth can markedly influence light propagation in the tooth and can produce false positives. For example, two small fractures a few millimeters apart can produce a dark area on the outer ring of enamel that closely resembles an approximal lesion and this is the most common location for cracks in posterior teeth. The same cracks do not interfere with reflectance imaging since the light paths are directly above the lesion. Therefore, access to both reflectance and occlusal transillumination has the potential to increase

the sensitivity and specificity of caries detection by optically sampling the entire external surface of existing lesions.

Reflectance imaging is more sensitive than occlusal transillumination for the detection of occlusal lesions. Even shallow demineralization confined to the outer half of the enamel can appear with high contrast in reflectance images. The challenge with SWIR imaging of occlusal lesions is differentiating the very shallow and superficial lesions from the lesions that penetrate through the enamel and into the underlying dentin. It is these deeper penetrating lesions that require removal and restoration. Remineralization therapy is a more appropriate treatment approach for shallow lesions. Previous studies have shown that the contrast increases significantly with increasing depth for SWIR reflectance imaging, however the magnitude of the change is not sufficient to warrant the use of contrast thresholds to define lesion severity [4]. Multiple studies including this one show that there is no dependence of the lesion contrast on depth for occlusal transillumination. A more reliable indicator of lesion depth and severity high lesion contrast and the lesion size or width in the dimension perpendicular to the fissure or radial to a pit [4, 70]. Severe occlusal lesions typically arise in the plaque collection sites in the pits and fissures and grow from the base of the fissure to the underlying dentin. Upon reaching the dentin the lesion can spread more rapidly laterally along the dentinal-enamel junction. That lateral spread can be easily seen through the transparent sound enamel above the lesion, particularly at SWIR wavelengths and this approach of detecting these hidden occlusal lesions has been demonstrated *in vivo* using SWIR imaging and optical coherence tomography in two clinical studies [103, 104]. If the lesion becomes severe enough the lesion can become visible to the naked eye as a dark shadow. In this study, there was no significant correlation of the lesion depth and the lesion contrast for either occlusal or approximal lesions for SWIR reflectance or transillumination. This contrasts with our earlier study utilizing SWIR reflectance

[4] where a significant correlation was observed between the lesion contrast and lesion depth for occlusal lesions. That prior study used optical coherence tomography to identify the occlusal lesions while this study used microCT, therefore many of the lesions in the prior study were much shallower than the lesions identified in this study. This is one disadvantage of using microCT over optical coherence tomography, microCT is insensitive to the very shallow lesions that are commonly found on occlusal surfaces. The shallowest lesions imaged in this study were all greater than 0.5-mm in depth. In reflectance, the reflected intensity is expected to saturate above a given thickness/depth where it no longer increases with increasing depth [105]. The thickness at which saturation occurs depends on the wavelength and the degree of demineralization. For greater lesion depths additional metrics are required for extrapolating potential lesion depth.

In addition to measurements of the lesion contrast, the SWIR images and radiographs were scored by three clinicians and microCT was used as a gold standard. Assessments of diagnostic performance should be carried out *in vivo* with a selection of teeth with a similar caries incidence expected for that population. That was certainly not the case in this study where all the teeth had lesions, however the objective of this study was to show that the use of near simultaneous SWIR reflectance and occlusal transillumination images has the potential for removing false positives and increasing diagnostic performance. Another concern with an *in vitro* study of this nature is that we have observed that *in vivo* transillumination images are typically better than *in vitro* images of lesions on extracted teeth due to the better internal hydration of vital teeth. The loss of internal water from extracted teeth markedly increases the scattering of sound dental tissues and reduces the lesion contrast [70]. In addition, there were no overlapping or adjoining teeth, such teeth are expected to reduce the performance of radiographs and SWIR transillumination for imaging approximal lesions and would not be expected to influence the imaging of occlusal lesions or

influence reflectance imaging. SWIR reflectance alone yielded the highest examiner agreement, highest accuracy and lowest false positive rate among the four image types. The SWIR reflectance alone had a higher accuracy than radiographs for approximal lesions (0.59 vs 0.49) and markedly higher accuracy for occlusal lesions (0.81 vs 0.36). The examiner agreement was highest for radiography and lowest for SWIR transillumination. This suggests that more training is required to read the SWIR images particularly the SWIR transillumination images. It was anticipated that either the dual mode or side by side SWIR images would yield the highest performance. However, the diagnostic performance for SWIR transillumination was quite low and that low performance most likely adversely influenced the dual mode and side by side images. It is likely that the performance of SWIR transillumination is most dramatically reduced in *in vitro* measurements due to the influence of the gingival tissues and the internal hydration of the tooth. The performance of this handpiece shown in **Fig. 2.7.2B** will be assessed *in vivo* over the next year and we will be able to confirm this hypothesis.

2.6 Conclusions

In summary, we have developed a clinical probe capable of acquiring near simultaneous short wavelength infrared (SWIR) reflectance and occlusal transillumination images of approximal and occlusal lesions. The performance of the probe *in vitro* was assessed by imaging 120 extracted teeth with lesions on the occlusal and proximal surfaces. The next step will be to image teeth *in vivo* of unknown caries status scheduled for extraction for orthodontic reasons in order to assess the diagnostic performance of this dual probe *in vivo*.

2.7 Tables and Figures

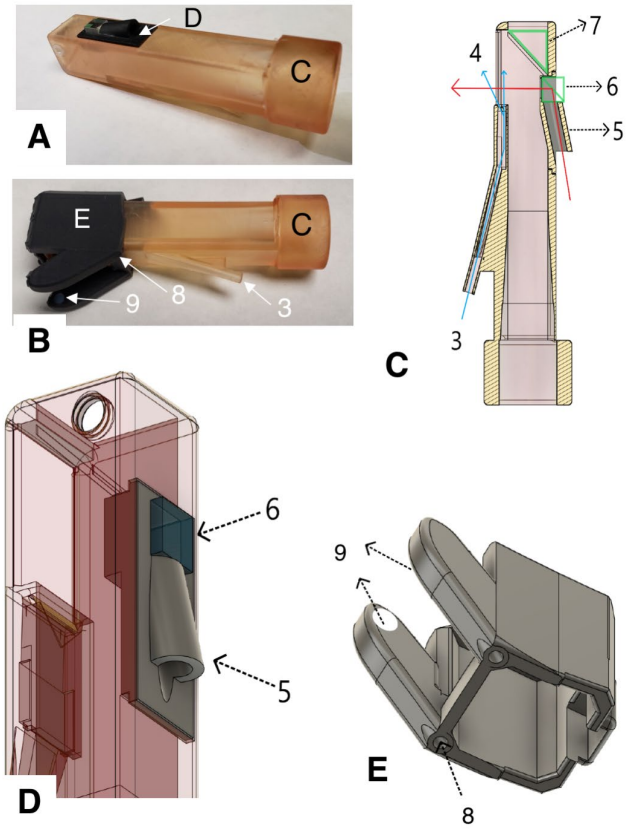

Figure 2.7.1. (A) 3D printed handpiece for reflectance with insert (D) made of black resin with a polarizing beamsplitter cube (6), (B) Handpiece with attachment for transillumination (E). (C) Handpiece cross-sectional view; the reflectance fiber is inserted through the port at (5) from the back of the polarization chamber, and light is polarized (6) and delivered to the tooth occlusal surface as shown by the red arrow. Air enters the nozzle at (3) and is directed towards the tooth surface at (4) as shown by the blue arrows. Reflected and transmitted light from the tooth is directed to the camera by a right-angle polished surface (7). The insert for the polarizing beamsplitter cube (D) is snapped to the back of the handpiece. Transillumination fibers are inserted into the two ports (8) at the rear of the transillumination appliance (E) and into the Teflon plugs (9) at the end of each probe arm. The transillumination appliance (E) is placed over the end of the reflectance attachment as shown in (B) and **Fig. 2.**

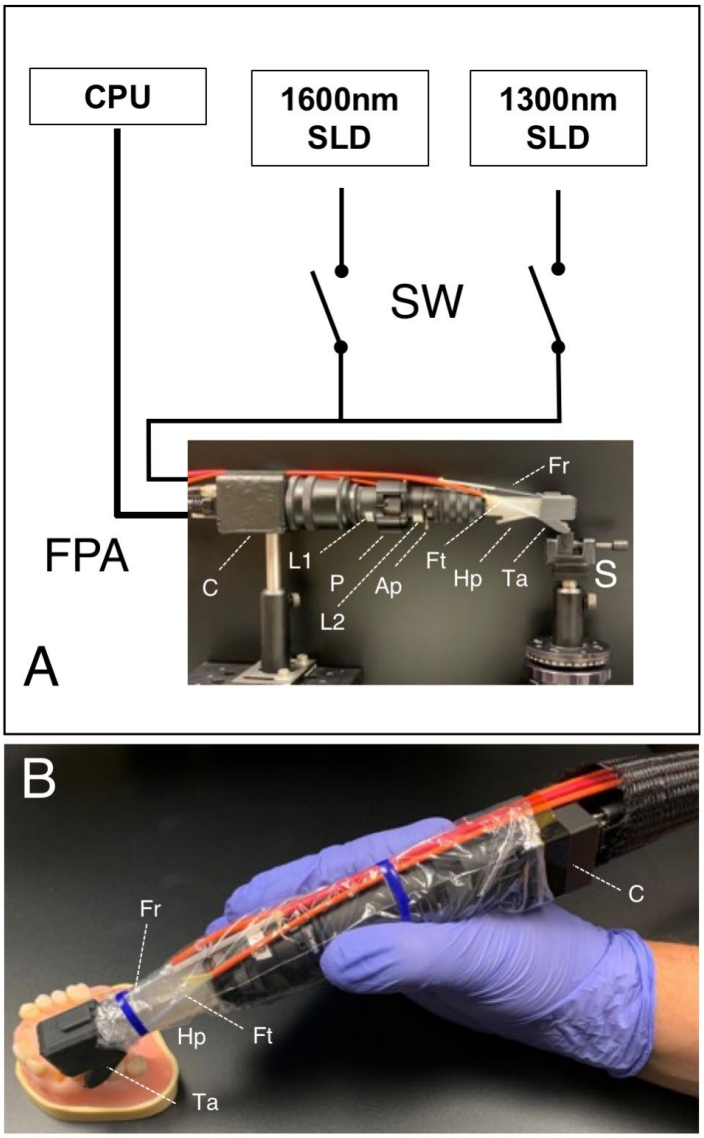

Figure 2.7.2. (A) Diagram of dual imaging system which employs a computer, two SLDs, two fiber optic switches (SW) and an InGaAs FPA with external optics and handpiece which is position over a sample tooth (S). The camera (C), 100 mm lens (L1), polarizer (P), 60 mm lens (L2), adjustable aperture (Ap), reflectance handpiece (Hp) and transillumination attachment (Ta) are shown along with the orange optical fibers for reflectance (Fr) and transillumination (Ft). (B) The handheld dual imaging handpiece equipped with the smaller InGaAs camera that will be used for clinical imaging.

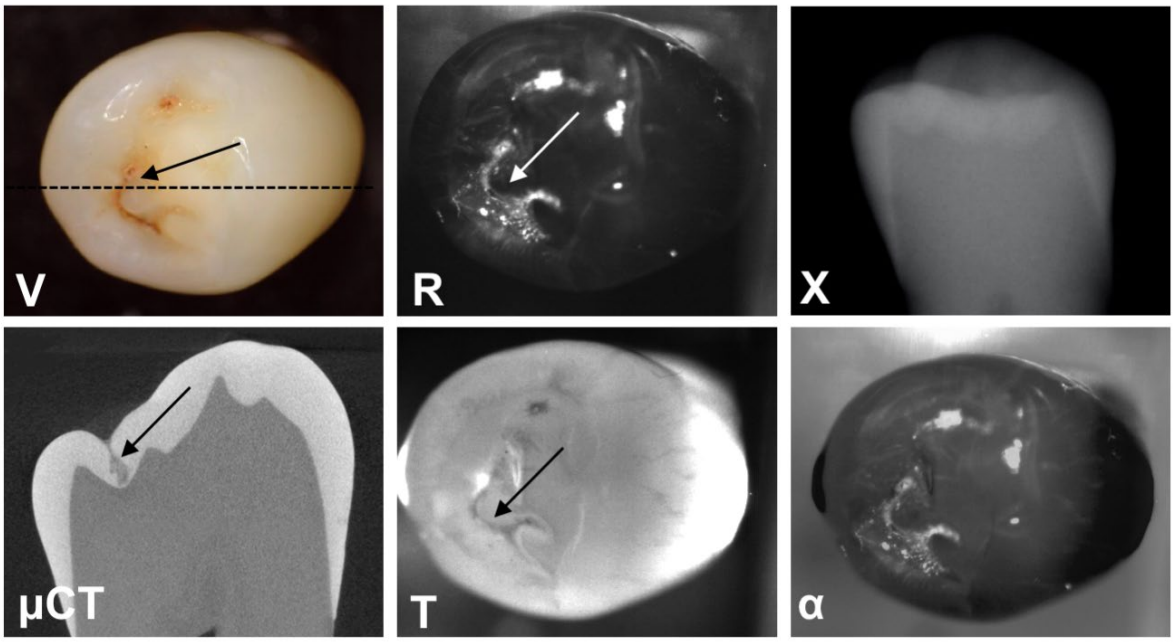

Figure 2.7.3. (V) Visible, (R) SWIR reflectance at 1600-nm, (X) dental radiographic, (µCT) micro-CT, (T) SWIR transillumination at 1300-nm and (a) combined R+T fusion (a=0.4) images of a tooth with an occlusal lesion. Arrows point to the occlusal lesion and the dotted line in (V) shows the orientation of the slice in the µCT image.

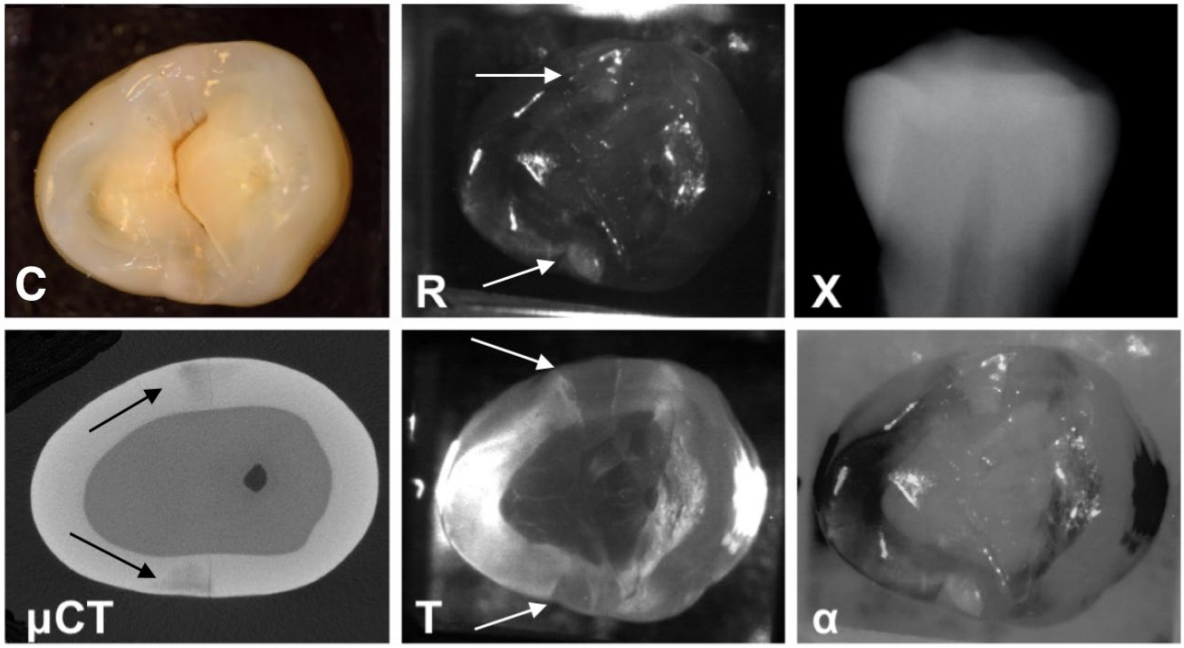

Figure 2.7.4. (C) Color, (R) SWIR reflectance at 1600-nm, (X) dental radiographic, (μCT) micro-CT, (T) SWIR transillumination at 1300-nm and (a) combined R+T fusion (a=0.4) images of a tooth with two approximal lesions. Arrows point to lesions.

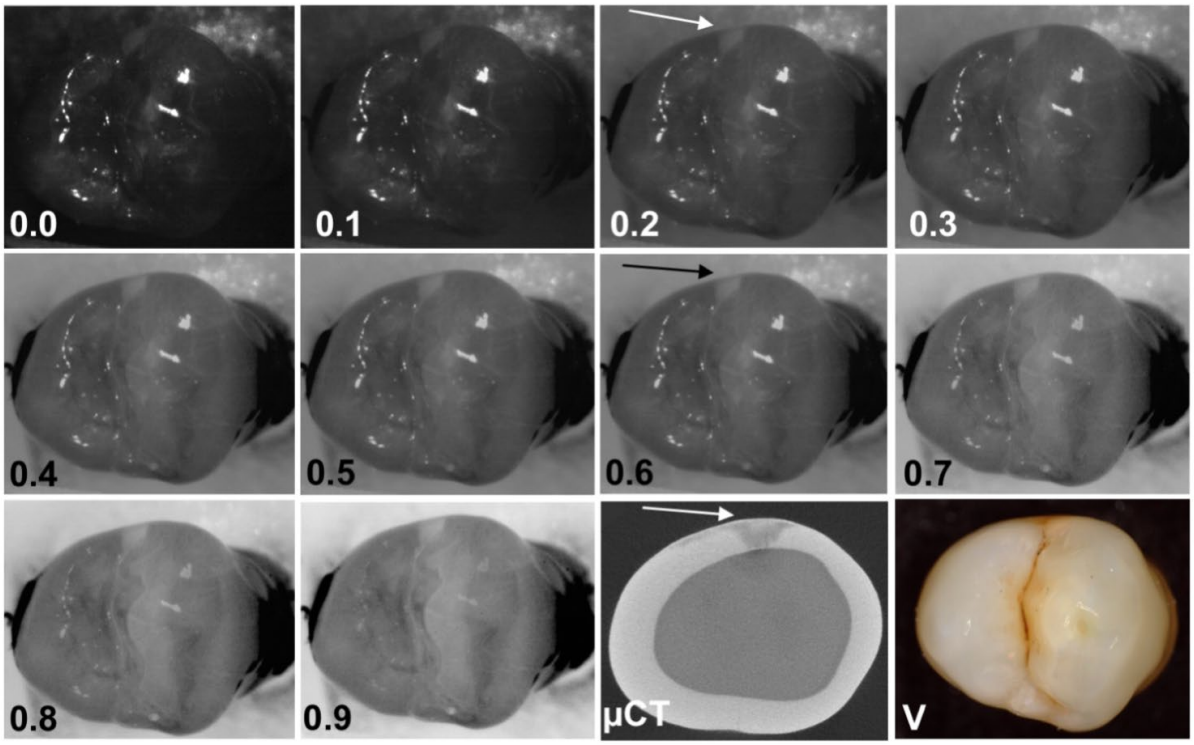

Figure 2.7.5. Combined transillumination and reflectance images with a varying from 0 to 0.9 along with visible (V) and an occlusal (µCT) micro-CT image of a tooth with occlusal decay. For this particular tooth the contrast increased with increasing a.

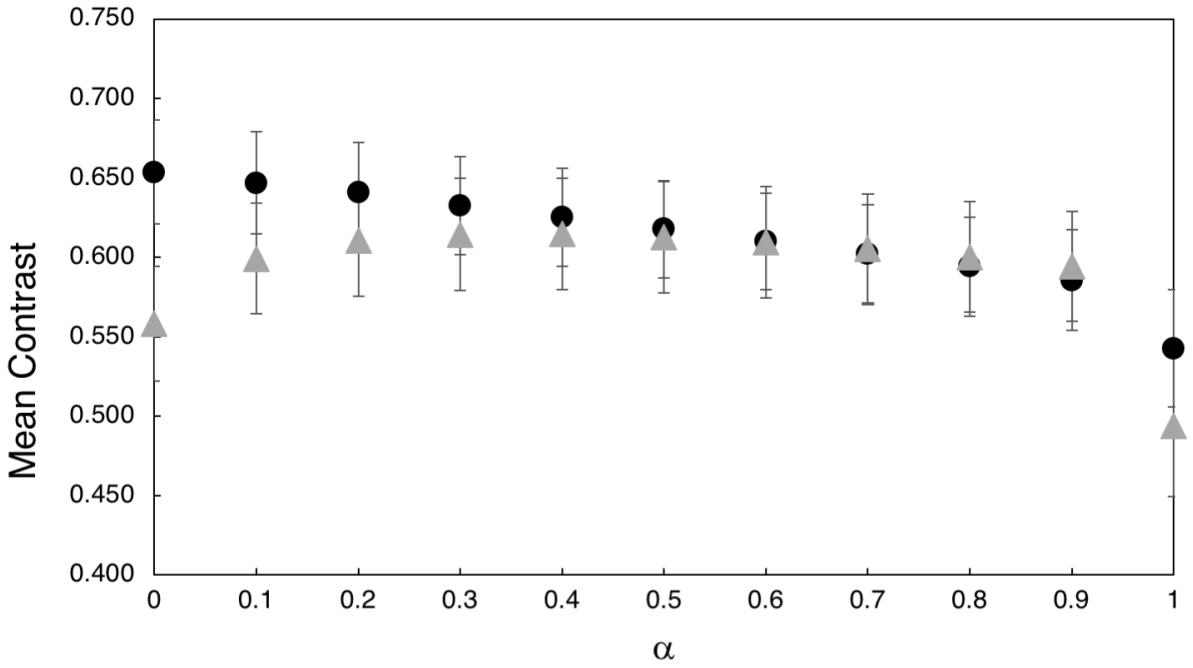

Figure 2.7.6. Plot of mean ± sd of lesion contrast vs alpha for dual probe fusion mode images for occlusal lesions (circles, n=120) and approximal lesions (triangles, n=120).

Table 2.7.1. Effect of alpha (α) on the mean lesion contrast for occlusal and approximal lesions.

Alpha (α)	**(α = 0) R**	**0.1**	**0.2**	**0.3**	**0.4**	**0.5**	**0.6**	**0.7**	**0.8**	**0.9**	**(α = 1) (T)**
Occlusal Lesion Contrast	0.651	0.641	0.631	0.621	0.612	0.602	0.594	0.584	0.575	0.566	0.533
Approximal Lesion Contrast	0.558	0.599	0.611	0.614	0.615	0.613	0.610	0.605	0.6	0.595	0.494

Table 2.7.2. Clinician Scores for the occlusal and proximal surfaces of 106 teeth for percent agreement, accuracy and false positive rate for SWIR imaging methods and radiography.

Examiners	Method	Occlusal	Proximal
Percent Agreement	Transillumination	0.75	0.76
	Reflectance	0.87	0.84
	Dual	0.80	0.79
	Side by Side	0.82	0.80
	Radiography	0.88	0.91
Accuracy	Transillumination	0.54	0.45
	Reflectance	0.81	0.59
	Dual	0.71	0.53
	Side by Side	0.70	0.55
	Radiography	0.36	0.49
False Positive rate	Transillumination	0.50	0.55
	Reflectance	0.31	0.36
	Dual	0.47	0.39
	Side by Side	0.36	0.36
	Radiography	0.08	0.16

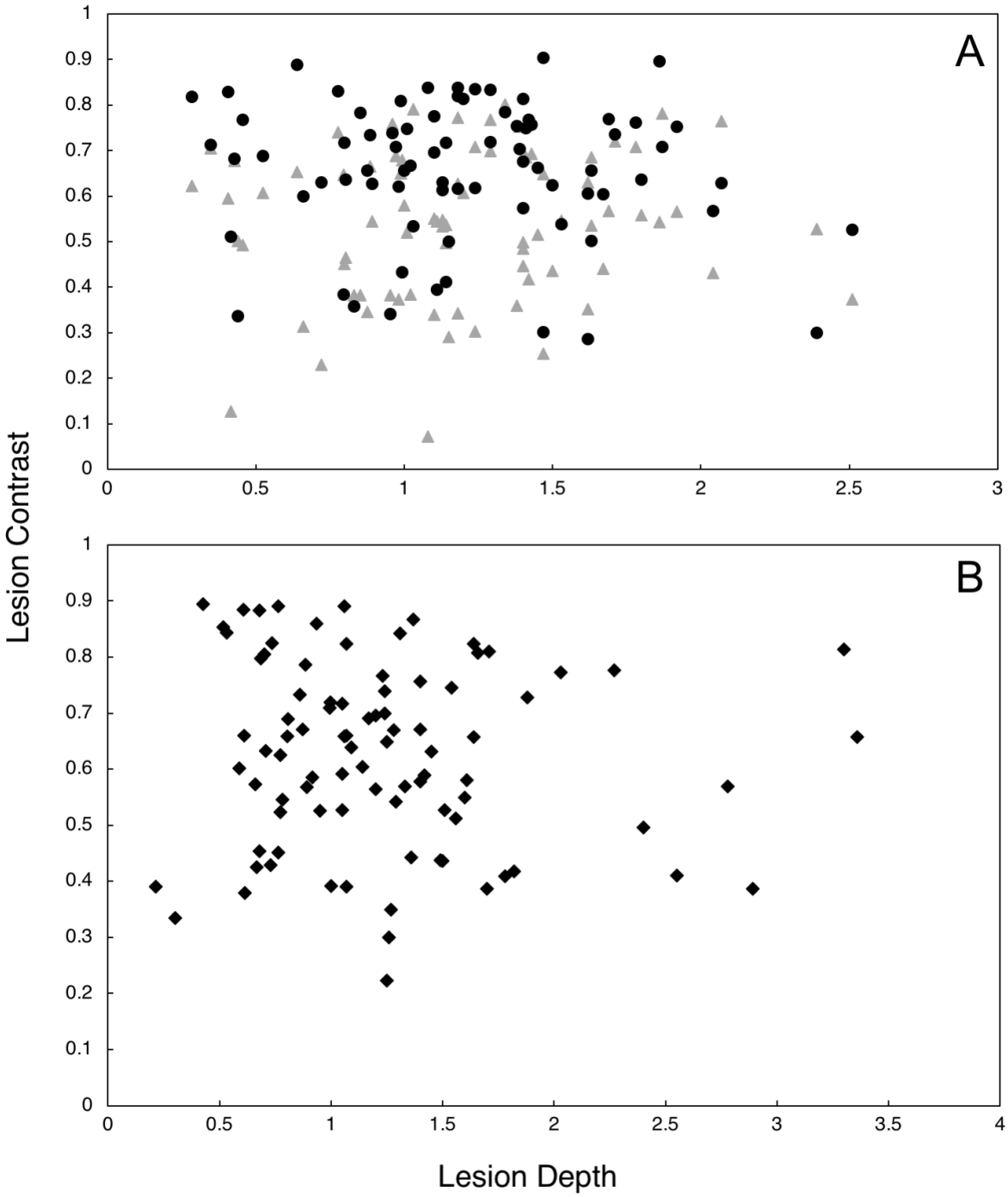

Figure 2.7.7. Occlusal lesion contrast vs lesion depth measured with microCT. (A) Reflectance (circles) and transillumination (triangles). (B) fusion mode images (a=0.4).

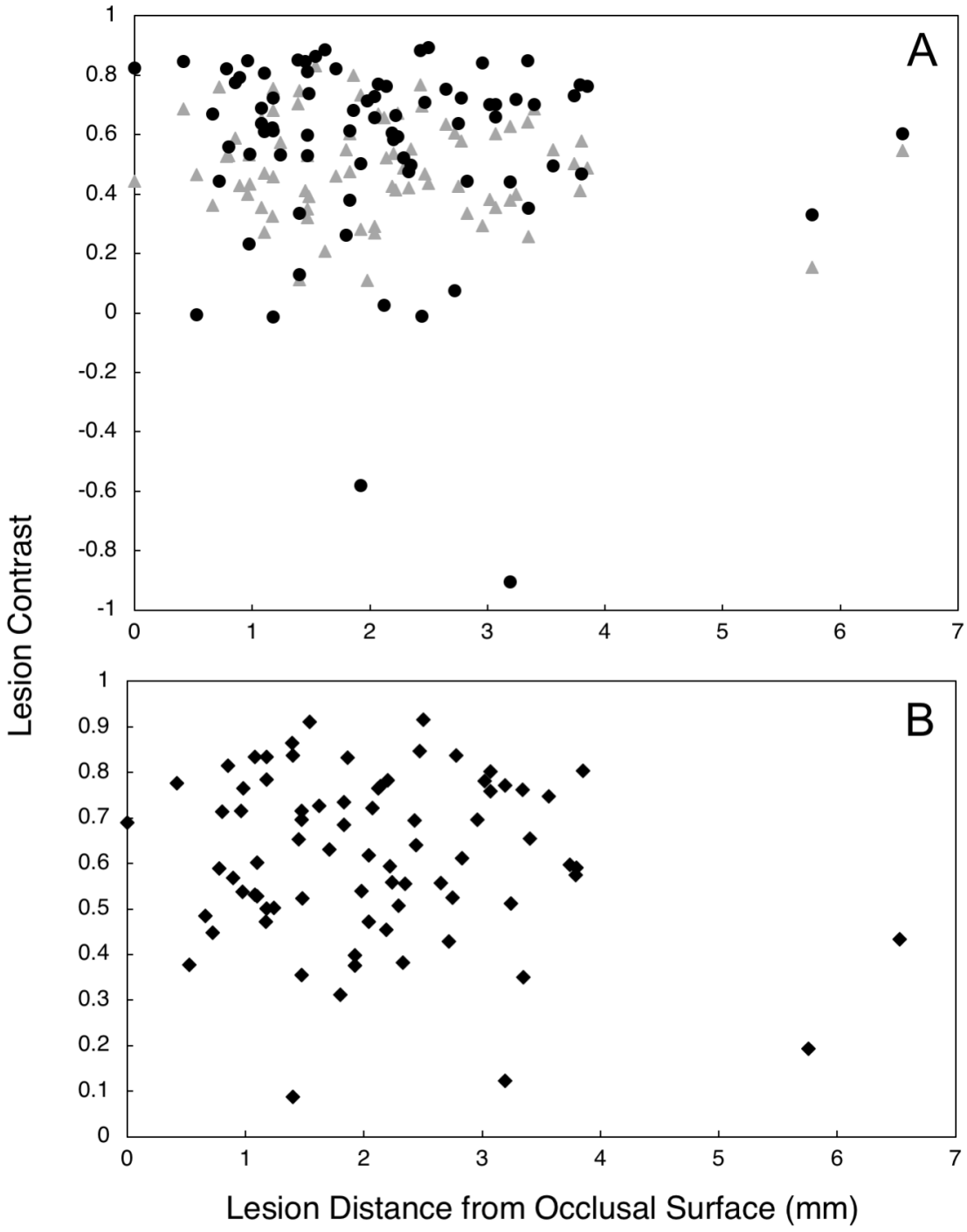

Figure 2.7.8. Approximal lesion contrast vs lesion distance from the occlusal surface measured with microCT. (A) Reflectance (circles) and transillumination (triangles). (B) fusion mode (a=0.4) images.

CHAPTER III

Measurement of the depth of lesions on proximal surfaces with dual SWIR transillumination and reflectance imaging

3.1 Summary

The aim of this study was to compare the diagnostic performance of dual SWIR transillumination and reflectance multispectral imaging devices for imaging interproximal lesions with radiography using extracted teeth that had been imaged with micro-computed tomography (microCT). Thirty six extracted teeth with 67 lesions on the proximal surfaces were imaged using a newly fabricated SWIR multispectral proximal transillumination and reflectance imaging device along with an existing SWIR multispectral occlusal transillumination and reflectance device. The ability of SWIR imaging and radiography to detect lesions and accurately assess lesion dimensions were compared using microCT as a standard. Occlusal and proximal transillumination and occlusal reflectance performed best for imaging interproximal lesions while proximal reflectance was not useful for imaging interproximal lesions from tooth buccal and lingual surfaces. There was high correlation of the lesion dimensions measured in occlusal and proximal transillumination images compared to microCT and moderate correlation in occlusal reflectance images. The correlation between the lesion depth measured in radiographs and the lesion depth measured with microCT was not significant. This study demonstrates that SWIR occlusal and proximal transillumination and SWIR occlusal reflectance images are useful for imaging interproximal lesions and they provide more accurate measurements of lesion severity.

3.2 Introduction

Short wavelength infrared (SWIR) and near-IR imaging (NIR) methods have been under development for almost 20 years for use in dentistry and several NIR clinical devices are now available commercially. Due to the high transparency of enamel at longer wavelengths, multiple imaging configurations are feasible, caries lesions can be imaged using transillumination and reflectance from tooth occlusal, buccal and lingual surfaces [24, 102]. In proximal

transillumination the light source and detector are placed on the buccal and lingual sides of the tooth (see **Fig. 3.7.1**). The positions can be alternated to get images of each surface since this method will have greater sensitivity for those lesions located closer to the detector. This is the same imaging geometry used to acquire bitewing radiographs. Interproximal lesions, the lesions located at the proximal contact points in between teeth, can be imaged via all three imaging geometries. Transillumination of the proximal contact points between teeth can also be accomplished via occlusal transillumination by directing SWIR light below the crown while imaging the occlusal surface [24, 78, 79] (see **Fig. 3.7.1**). The latter approach is capable of imaging occlusal lesions as well with high contrast [24, 47, 80-82, 102]. In 2010, it was demonstrated that interproximal lesions that appeared on radiographs could be detected *in vivo* using proximal and occlusal transillumination imaging at 1310-nm with similar sensitivity [24]. This was the first step in demonstrating the clinical potential of NIR and SWIR imaging for interproximal caries detection. A later clinical study employing SWIR transillumination and SWIR reflectance imaging probes to screen premolar teeth that were scheduled for extraction, established that the sensitivity of SWIR imaging was significantly higher ($P < 0.05$) than radiographs for both occlusal and interproximal lesions [6]. The sensitivity of each individual SWIR method was either individually equal to or higher than radiography.

Several shorter wavelength NIR devices that utilize either reflectance and transillumination imaging have been introduced commercially operating at 830 and 780-nm [83-87]. The use of shorter wavelength 830-nm NIR light was first investigated almost 20 years ago [78]. Shorter wavelengths allow the use of less expensive silicon based detectors. However, longer wavelength SWIR light has significant advantages. The contrast of simulated lesions in enamel at 830-nm was significantly lower than at 1300-nm and they could not be imaged through the maximum thickness

of enamel [78]. It is also important to point out that stains interfere significantly at wavelengths less than 1100-nm [88] and the contrast between sound and demineralized enamel is markedly higher at wavelengths beyond 1400-nm in reflectance measurements [70, 88, 89].

Several studies over the past decade have indicated that transillumination performs best at 1300-nm where the transparency of enamel is highest while the contrast of lesions on tooth surfaces imaged using reflectance continues to increase with increasing wavelength and is highest at 1950-nm [70, 88, 89]. Several studies have investigated multispectral measurements using either one modality or combining transillumination and reflectance measurements. Zakian et al. [96, 97] used multiple wavelengths of SWIR hyperspectral reflectance images to estimate the severity of occlusal lesions. Since, multispectral SWIR reflectance and transillumination experiments have demonstrated that the tooth appears darker at wavelengths coincident with increased water absorption, multispectral images can be used to produce increased contrast between different tooth structures such as sound enamel and dentin, dental decay and composite restorative materials [97-99]. Combining measurements from different SWIR imaging wavelengths and comparing them with concurrent measurements acquired by complementary imaging modalities should provide improved assessment of lesion depth and severity. Radiographs markedly underestimate the depth and severity of interproximal lesions and clinicians are forced to assume that lesions penetrate much deeper than indicated in radiographs [13-15]. If lesions are noncavitated and limited in penetration to only the enamel they can often be arrested by chemical intervention without the need to remove the decay with the drill. Therefore, a more accurate imaging system for assessing the depth of penetration of interproximal lesions would be a significant step forward and enable clinicians to make more informed decisions regarding treatment. Moreover, a combined SWIR reflectance and transillumination clinical probe will likely reduce false positives since it is

improbable that confounding structural features or specular reflection will be present in both reflectance and transillumination images. Reflectance and occlusal transillumination probes have been combined into a single probe since light is collected from tooth occlusal surfaces for both methods. Different illumination wavelengths have been used optimized for each imaging mode, namely SWIR wavelengths greater than 1400-nm for reflectance and 1300-nm for transillumination. Simon et al. [27] built a benchtop simultaneous SWIR reflectance and transillumination system with tunable filters that ranged from 830-1700-nm and showed that the combined images have potential for the diagnosis of occlusal lesions [5] and simulated cavitated and noncavitated interproximal lesions [100]. A compact system that is capable of simultaneous acquisition of SWIR reflectance and occlusal transillumination images suitable for clinical use was developed and tested on 120 teeth extracted teeth with occlusal and interproximal lesions using microCT as a gold standard [43, 106, 107]. That system is currently being used for clinical studies. The purpose of this study is to develop a second dual SWIR transillumination and reflectance probe designed to image from tooth buccal and lingual surfaces and assess the performance of this new dual probe and the existing occlusal transillumination and reflectance probe for imaging interproximal lesions on extracted teeth.

3.3 Materials and Methods

3.3.1 Sample Preparation

Teeth with no identifiers were collected from patients in the San Francisco Bay area and Geneva Switzerland with approval from the UCSF Committee on Human Research. Extracted teeth (n=36) were selected with 67 interproximal lesions for this study. Teeth were sterilized using gamma radiation and stored in 0.1% thymol solution to maintain tissue hydration and prevent bacterial growth. Then, samples were mounted in black orthodontic acrylic blocks from Great Lakes

Orthodontics (Tonawanda, NY) and imaged with digital radiographs using a CareStream 2200 System from Kodak (Rochester, NY) operating at 60 kV.

All teeth were imaged using Microcomputed X-ray tomography (μCT) with a 10-μm resolution. A Scanco μCT 50 from Scanco USA (Wayne, PA) located at the UCSF Bone Imaging Core Facility was used to acquire the images. Visible color images of the samples were acquired using a USB microscope, Model AM7915MZT from AnMO Electronics Corp. (New Taipei City, Taiwan) with extended depth of field and cross polarization. The digital microscope captures 5 mega-pixel (2,952 x 1,944) color images.

3.3.2 Design and Fabrication of the Dual Proximal Reflectance and Transillumination SWIR probe

The dual proximal reflectance and transillumination SWIR probe was designed in Fusion 360 from Autodesk (San Francisco, CA). The dual probe design consists of a handpiece with a reflectance and a transillumination attachment, shown in **Figs. 3.7.2A-E**. The handpiece was fabricated using a Formlabs Form 3 Low Force Stereolithography 3D printer. The final design was exported as a STL file and transferred to Formlabs PreForm to generate supports for a final 3D printing scheme. A spatial resolution of 100 μm was used for all prints. The probe consists of two components, a main body containing the light source for reflectance and the light collection optics and a second attachment containing the transillumination light source. The main body of the probe is very similar to the main body of our occlusal reflectance and transillumination probe with the exception that unpolarized light is used for reflectance [106]. The proximal transillumination attachment shown in **Fig. 3.7.2A** consists of the main body of the probe containing the light source for reflectance and the light collection optics, a 3D-printed sliding frame (3), a black Delrin tube enclosing the transillumination light source (5), a rod holder (4) that connects (3) and (5), shown

in **Figure 3.7.2A.** Broadband light from a tungsten halogen lamp with a bandpass filter at 1450 (with a bandwidth of 80-nm) is transmitted through a 1 mm diameter optical fiber (10) inserted into a 2 mm in diameter Teflon tube (8) enclosed in the probe's backpiece (2). There is an air nozzle positioned on the bottom of the probe opposite the light source for reflectance (2) directed towards the aluminum reflector to prevent fogging of the aluminum surface. The air nozzle can also be used to dry the tooth surface to increase lesion contrast and potentially assess lesion activity [9, 49, 101].

More details about the probe's main body and reflectance backpiece (2) are described in Zhu et al. [106]. For proximal transillumination, the transillumination light source shown in **Fig. 3.7.2C** is placed on the side of the tooth opposite to the main body of the probe as shown in **Fig. 3.7.2B.** Several different proximal transillumination light diffusers were tested to determine which yields the highest contrast of interproximal lesions. Three different diffusing materials were tested: Teflon, Delrin and Formlabs white resin and several different diffuser geometries were investigated. The highest contrast was achieved using a 2 mm in diameter Teflon rod with a 400 μm optical fiber inserted in the center with 1300-nm light. The Teflon diffuser is shown in **Fig. 3.7.2B**, and consists of a 400 μm optical fiber (11) connected to a superluminescent diode (SLD) enclosed inside the Teflon tube (9) that is placed inside a black Delrin tube (5). For maximum transillumination light intensity, a right-angled aluminum reflector (7) is fitted at the end of the Delrin rod to direct the diffuse light from the Teflon tube to the proximal contact between the teeth. The proximal transillumination attachment allows horizontal and vertical adjustments during sample screening so teeth with various shapes and sizes can be imaged with optimum light illumination, as shown by the black arrows in **Fig. 3.7.2A.** The fully assembled *in vitro* imaging system is shown in **Fig. 3.7.2D.** A version more suitable for clinical imaging was also designed

utilizing Formlabs Flexible resin to connect the Delrin rod holder and the probe's main body, and this is shown in **Fig. 3.7.2E.** The flexible frame is composed of soft and flexible material allowing clinicians to apply squeezing force with thumb to adjust light placement during clinical imaging.

3.3.3 Image Acquisition and Analysis

The SWIR reflectance images were captured using a Model GA1280J (Sensors Unlimited, Princeton, NK) camera with a 1280 x 1024 pixel format, a 15 μm pixel pitch and a bit depth of 12 bit. Two 1 inch in diameter planoconvex antireflection coated lenses of 60 mm and 100 mm focal length along with an adjustable aperture were placed between the handpiece and the InGaAs camera to provide a field of view of 11 mm x 11 mm at the focus plane. The transillumination light was delivered through a 0.4 mm diameter low-OH optical fiber. A 1312-nm superluminescent diode (SLD) from Covega (Jessip, MD) with an output of 22 mW and a bandwidth of 50-nm was used as the light source for transillumination. The output intensity was set at 10 mw before entering the Teflon scattering rod. The reflectance and transillumination light sources were manually shut on and off and were not simultaneously acquired. The probe can also be used with the smaller 640 x 480 pixel micro-SWIR camera (SU640CSX) measuring only 32 mm x 32 mm x 28 mm from Sensors Unlimited (Princeton, NJ) that is better suited for clinical imaging. The light for reflectance was delivered through a low-OH 1 mm optical fiber connected to a Model SLS202 extended wavelength tungsten-halogen light source from Thorlabs (Newton, NJ) with a bandpass filter centered at 1460-nm with a bandwidth of 85-nm.

Images of the interproximal lesions were also acquired using a multispectral, dual occlusal transillumination and reflectance imaging probe. A low-OH optical fiber of 1 mm diameter was used to deliver light from a 1604-nm superluminescent diode (SLD), Model ESL 1620-2111 from Exalos (Schlieren, Switzerland) with an output of 17 mW and a bandwidth of 46-nm. The intensity

delivered to the tooth was 5 mW. The transillumination light was delivered through two 0.4 mm diameter low-OH optical fibers. A 1314-nm (BW) SLD, Model DL-CS3452A-FP 1620-2111 from Denselight (Singapore) with an output of 48 mW and a bandwidth of 33-nm was used as the source for transillumination. A 50/50 beamsplitter was used to deliver light to each arm for transillumination. The output intensity of each arm was set at 10 mw before entering the Teflon plugs. Details regarding the fabrication of the dual occlusal transillumination and reflectance imaging probe system and optical probe have been previously described in [106].

The samples were dried of excess water with an air nozzle before imaging due to the strong water absorption at 1450 and 1600-nm [4]. Image processing of the images was performed by custom scripts written using MATLAB from Mathworks (Natick, MA). The acquired 12-bit images (4096) were converted to 16-bit (65535) by multiplying by 16 and subtracting 1 to facilitate processing using MATLAB. Lesion areas were identified from the transillumination/reflectance images. Sound areas or regions of interest (ROI) for comparison were chosen from areas surrounding the lesion. This better represents the contrast between the lesion and sound tissues that would be viewed by the clinician. The contrast was calculated for each lesion using the formula $(I_L - I_S)/I_L$ for reflectance images and $(I_S - I_L)/I_S$ for transillumination images, where I_L is the average intensity in the lesion area, and I_S is the average intensity in the sound ROI [5]. Lesion areas were confirmed using the microCT images.

The lesion depth and width in the XY plane and the distance to the occlusal surface (Z) were measured as shown in **Figure 3.7.1** as appropriate for each imaging device. The lesion geometric information was measured in pixels first and then converted to micrometers imaging a reference ruler at the focal length for the SWIR images. It was not possible to perform a similar calibration

for the radiographs. The linear correlation between the lesion dimensions measured with SWIR imaging methods and radiography with microCT was determined and correlation coefficients (R^2) are reported if the correlation is significant ($P<0.05$).

3.4 Results

MicroCT was used to image the 36 extracted teeth used for this study. There were 67 lesions visible on microCT images indicating that most of the teeth had lesions at both contact points (mesial and distal sides), i.e., 67 out of a possible 72 if lesions were present at all contact points, two per tooth. Out of the 67 lesions, 16 of the lesions were very small and were only visible with microCT. Only 22 of the 67 lesions had measurable contrast on dental radiographs for a detection rate of only 33%. Proximal transillumination at 1300-nm performed well showing measurable contrast for 40 out of 67 lesions, giving a 60% lesion detection rate. The lesion contrast was high for most proximal transillumination images, however only seven of the lesions were visible in the proximal reflectance images of the buccal and lingual surfaces. There are two interproximal lesions on the tooth shown in **Fig. 3.7.3**, one is deep and penetrates into the dentin while the second lesion is shallow and only penetrates halfway through the enamel. Both lesions are visible in the radiograph. Both lesions show significant contrast in the proximal transillumination mode. When imaged from the lingual side, **Fig. 3.7.3C**, both lesions are visible, however only one of the lesions is visible when the imager was positioned on the buccal side of the tooth, **Fig. 3.7.3A**. However, the two lesions are not visible in the corresponding reflectance images shown in Figures 3.7.3B&D, neither from the lingual or from the buccal surface. Both lesions are clearly visible in the microCT image shown in **Fig. 3.7.3E**.

Another tooth with two interproximal lesions is shown in **Fig. 3.7.4**. One lesion penetrates almost to the dentin in the microCT image. The other lesion is very small and is barely visible in the microCT images. Occlusal transillumination and occlusal reflectance images are shown, and the larger lesion is visible in both the transillumination and reflectance images.

A major concern regarding the diagnosis of lesions on proximal surfaces is that radiographs markedly underestimate the depth of penetration [13-15]. The lesion penetration from the proximal surface (X_{pt}) and distance to the occlusal surface (Z_{pt}) were measured for the 40 lesions that were visible in the proximal transillumination mode images and compared with similar dimensions measured with microCT (X_{μ}, Z_{μ}) as shown in **Fig. 3.7.2**. Similar measurements were not carried out for the proximal reflectance measurements since only seven of the lesions were visible in the proximal reflectance images. The lesion depth measured with proximal transillumination (X_{pt}) and with microCT (X_{μ}) is plotted in **Fig. 3.7.5** for the 40 lesions that were visible. There was significant ($P<0.05$) and moderate correlation between the two measurements with R^2 equal to 0.40. There was also significant correlation of the distance to the occlusal surface (Z_{pt}) measured with proximal transillumination and with microCT (Z_{μ}) but it was lower with R^2 equal to 0.33, as shown in **Fig. 3.7.6**. The teeth were also imaged using the other dual probe, the occlusal transillumination and reflectance probe and the sensitivity was higher, 51 out 67 of the lesions had measurable contrast in occlusal transillumination mode and 45/67 had contrast in occlusal reflectance mode for detection rates of 76 and 67% respectively. The depth of the interproximal lesions was also measured using occlusal transillumination (X_{ot}) and reflectance (X_{or}). Those measurements are plotted in **Fig. 3.7.7** against the depths measured with microCT (X_{μ}). There was significant ($P<0.05$) and even higher correlation for occlusal transillumination (X_{ot}) with R^2 equal to 0.80. Lesion depth measurements with occlusal reflectance (X_{or}) also correlated with

microCT depth measurements ($P< 0.05$) but the correlation was not as high as for occlusal transillumination with R^2 equal to 0.38. The lesion width was also measured with occlusal transillumination (Y_{ot}) and occlusal reflectance (Y_{or}). The lesion width measured with occlusal transillumination (Y_{ot}) correlated with the lesion width measured with microCT (Y_{μ}) with an R^2 equal to 0.33. There was no correlation of the lesion width with microCT for the occlusal reflectance (Y_{or}) images.

Lesion depths were also measured for radiography (X_r) in pixels and those values are plotted against the microCT (X_{μ}) measurements in **Fig. 3.7.8**. There was no significant correlation ($P>0.05$) of the measured lesion depths between radiography and microCT. The mean lesion contrast ± standard deviation, the correlation of the lesion depth with microCT and the number of lesions that were visible in each SWIR imaging modality is tabulated in **Table 1**.

3.5 Discussion

In this study, a dual proximal transillumination and reflectance imaging device was fabricated and assessed for imaging interproximal lesions from the buccal/lingual tooth surfaces. The motivation for this device is to increase diagnostic performance by reducing false positives and providing more accurate measurements of lesion severity. The performance of proximal reflectance imaging from the buccal/lingual surface was disappointing, only 7 of the 67 interproximal lesions were visible from tooth proximal surfaces. This result was not anticipated, prior clinical studies with occlusal reflectance measurements indicated that occlusal reflectance had a higher sensitivity than proximal and occlusal transillumination for the detection of caries lesions on both occlusal and proximal surfaces [6]. In this study 45 of the 67 interproximal lesions were visible in occlusal reflectance images and the mean contrast of those lesions was higher than for the other SWIR

imaging modes. Therefore, it appears that reflectance imaging is only effective for imaging interproximal lesions from the occlusal surface. The thickness of enamel between the tooth surface and interproximal lesions is similar for imaging from the tooth buccal/lingual and the occlusal surface. Therefore, the thickness of sound enamel between the tooth surface and the lesion does not explain the difference in performance. The most likely explanation is that the higher tooth curvature when imaging from tooth buccal and lingual surfaces increases refraction and total internal reflection and markedly reduces lesion contrast.

According to this study and three other studies, proximal and occlusal transillumination imaging and occlusal reflectance imaging performed as well or significantly better than radiography for the detection of lesions on proximal surfaces [6, 24, 106]. This study has also shown that proximal and occlusal transillumination imaging and occlusal reflectance imaging provide more accurate measurements of the depth and severity of the lesions compared to radiography. Accurate measurements of lesion severity are required for clinicians to make informed decisions about treatment. If the lesions are shallow and confined to the enamel than chemical intervention with anti-caries and remineralization agents is warranted and the lesion can be followed overtime to see if it continues to progress. If the lesion has penetrated and spread well into the dentin than surgical intervention may be required. Since SWIR imaging methods do not involve exposure to ionizing radiation and they provide more accurate measurements of lesion depth penetration they are better suited for following the progression of lesions overtime.

Proximal reflectance measurements from tooth buccal and lingual surfaces did not prove to be particularly useful for imaging interproximal lesions on tooth proximal surfaces however, other types of lesions are often found on tooth buccal and lingual surfaces. Lesions are found in buccal

and lingual pits and demineralization is very common around orthodontic brackets. Moreover, root caries and dental calculus on buccal and lingual surfaces are an increasing problem and SWIR reflectance measurements at wavelengths greater than 1400-nm can image calculus and root caries with very high contrast [108]. Such surfaces are typically heavily stained and covered in plaque deposits, SWIR imaging is particularly valuable for differentiating demineralization and calcified plaque on those surfaces from stains and noncalcified plaque. SWIR reflectance imaging is also useful for assessing the severity of fluorosis on tooth buccal surfaces [109]. Therefore, even though the addition of proximal reflectance did not prove to be particularly valuable for imaging interproximal lesions on proximal surfaces, the dual proximal reflectance and transillumination device should be valuable for imaging other lesion types on tooth buccal and lingual surfaces.

Proximal transillumination was also useful for showing the distance of the lesion from the occlusal surface. That distance is also visible in radiographs although radiographs require exposure to ionizing radiation and the higher sensitivity of proximal transillumination indicates that many lesions will only be visible in proximal transillumination images and that the distance from the tooth surface will frequently not be accessible from a radiograph. In this study almost twice as many lesions were visible in proximal transillumination compared to radiography (40 vs 22). When clinicians restore teeth with interproximal lesions, they have to drill from the tooth occlusal surface, therefore knowledge of the depth of the lesion and its position is important.

Lesion widths in the XY plane were also examined and compared with microCT. The lesion width is not visible in radiographs however it can be measured from the occlusal surface using occlusal transillumination and reflectance. Lesion depths are of greater interest since they show the depth of penetration, however the lesion width is also useful because it can be used to estimate the overall

size of the lesion and is valuable for making a more informed decision on whether surgical intervention is recommended.

A major concern of SWIR/NIR imaging methods is the increased potential for false positives due to the higher sensitivity of these methods compared to radiography. A primary motivation for imaging the interproximal lesions using multiple SWIR imaging modalities is to reduce the potential for false positives. False positives may occur due to cracks, anatomical features in the tooth and optical effects such as specular reflection. It is unlikely such effects would appear similarly in different imaging geometries and modalities. In order to be useful in this regard the sensitivity needs to be high in multiple imaging modalities. We have shown that the sensitivity is high for proximal transillumination, occlusal transillumination and occlusal reflectance imaging. The dual proximal transillumination reflectance device is not useful in this regard due to the low sensitivity of proximal reflectance imaging for interproximal lesions, however the dual occlusal transillumination and reflectance device is well suited for reducing false positives due to the high sensitivity of both modes of imaging.

Different imaging appliances can be designed to attach to the SWIR imager and in a 2016 clinical study, three imaging probes were used to image premolar teeth scheduled for extraction; proximal transillumination and occlusal transillumination probes operating at 1300-nm and a reflectance probe at 1600-nm [6]. Another reason for the dual probe is to reduce the number of probes that have to be used and switched during clinical imaging. The two dual probes used in this study should be sufficient to image most of the lesions encountered and it is certainly feasible to design them so they can be rapidly switched in the clinic.

This study further demonstrates the value of multispectral transillumination and reflectance probes for imaging caries lesions. In this study, the first dual proximal transillumination and reflectance SWIR imaging device was assembled the performance for imaging interproximal lesions on extracted teeth was assessed. The performance was compared with a dual occlusal transillumination and reflectance SWIR imaging device, radiography and microCT. Proximal and occlusal transillumination at 1300-nm and occlusal reflectance measurements at 1600-nm provided significantly higher sensitivity than radiography for the detection of interproximal lesions and were more useful for measuring the lesion dimensions.

3.6 Conclusion

Occlusal and proximal transillumination and occlusal reflectance images were useful for imaging interproximal lesions and they provide more accurate measurements of lesion dimensions compared to radiography. Moreover, it has been shown that all SWIR imaging geometries relevant to imaging caries lesions can be implemented in two multispectral clinical probes, one that acquires occlusal transillumination and reflectance images and the other that acquires transillumination and reflectance images.

3.7 Tables and Figures

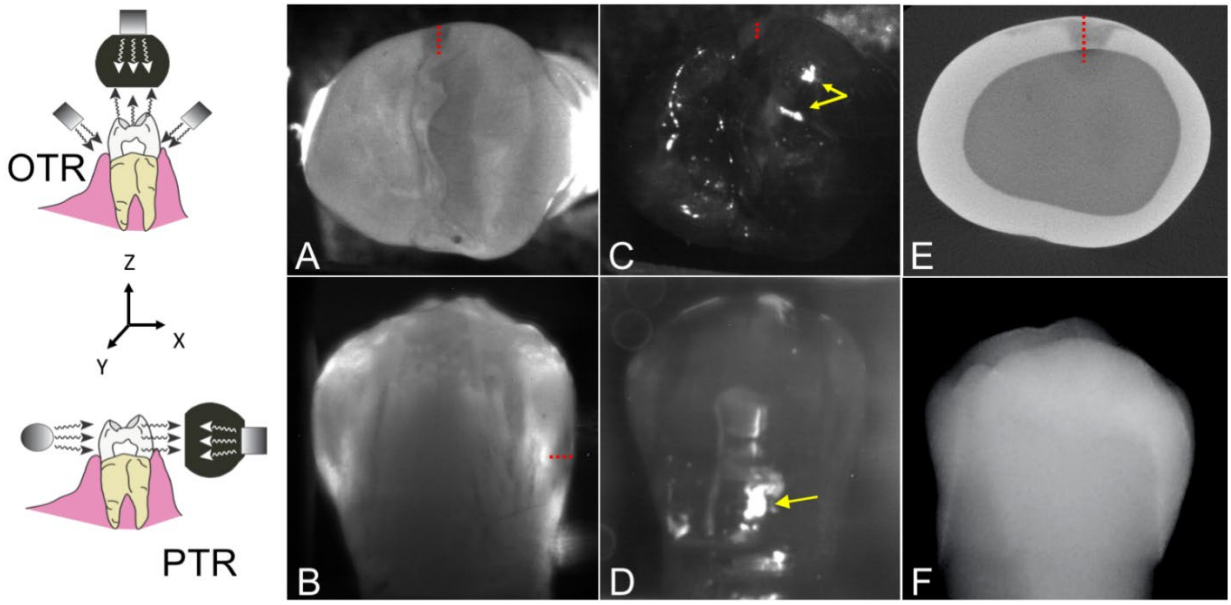

Figure 3.7.1. Diagrams of the occlusal (OTR) and proximal (PTR) dual SWIR transillumination and reflectance probes used in this study. The orientation of the XYZ axes with respect to the long axis of the tooth is shown. (A) Occlusal transillumination image, (B) proximal transillumination image (buccal surface), (C) occlusal reflectance image and (D) proximal reflectance (buccal surface) image, (E) transverse microCT slice in the XY plane of a tooth, and (F) dental radiograph of a tooth with an interproximal lesion are shown. The red dotted line represents the lesion depth from the proximal surface (X direction), the green dotted line represents the lesion width (Y direction) and the blue dotted line represents the vertical distance of the lesion to the tooth occlusal surface (Z direction). The yellow arrows in the reflectance images (C & D) are areas of specular reflection that can potential cause false positives.

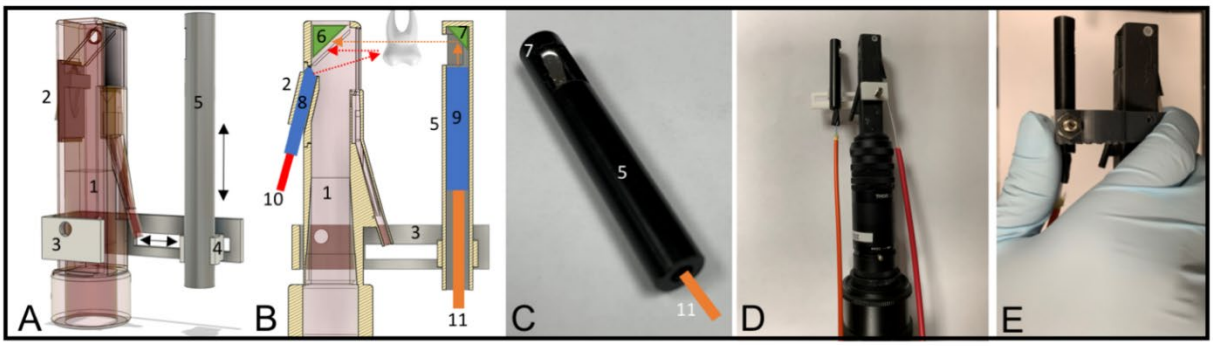

Figure 3.7.2. (A) 3D rendering and (B) cross section of the dual SWIR proximal probe is shown. Major parts include: (1) probe main body, (2) reflectance backpiece, (3) sliding frame, (4) Delrin rod holder, (5) Delrin tube, (6), right angled rectangular aluminum reflector, (7) right angle cylindrical aluminum reflector, (8) Teflon tube for reflectance light source, (9) Teflon tube for proximal transillumination light source, (10) optical fiber delivering 1450-nm light for reflectance, (11) optical fiber delivering 1300-nm light for proximal transillumination. Proximal transillumination light propagation is shown in orange dashed arrows. Reflectance light propagation is shown with red dashed arrows. (C) Proximal transillumination light source (11) is encased in a Teflon tube placed inside a Delrin tube (5). The cylindrical aluminum mirror (7) reflects anisotropically scattered light from the Teflon tube and directs it to the sample. (D) Fully assembled dual SWIR proximal probe for *in vitro* use. ® For *in vivo* use, the sliding frame (3) can be replaced with a soft/flexible holder.

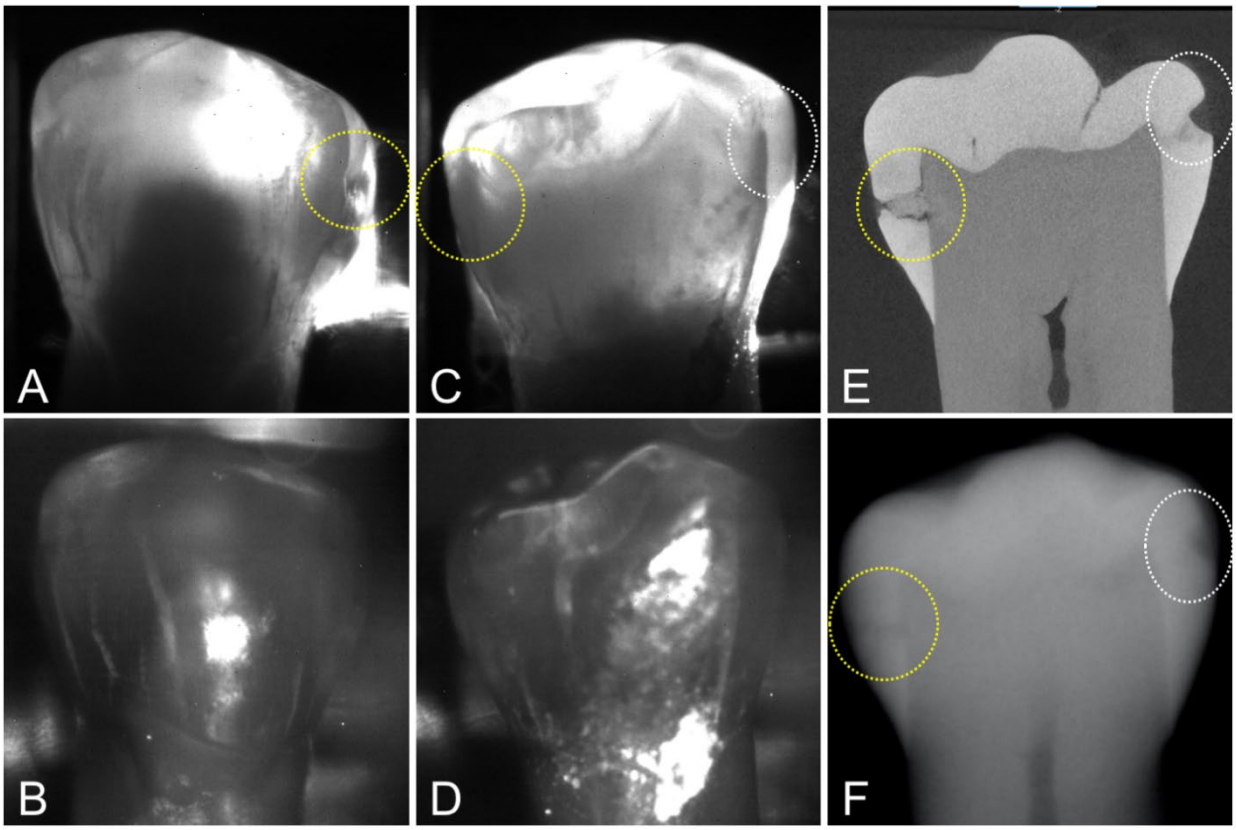

Figure 3.7.3. Proximal transillumination and reflectance images of a tooth with two interproximal lesions on opposing proximal surfaces. Lesion 1 (yellow circle) is more severe and penetrates to the dentin while lesion 2 (white circle) is limited to the enamel. (A) Transillumination and (B) Reflectance images with the imager on the buccal side of the tooth. (C) Transillumination and (D) Reflectance with the imager on the lingual side of the tooth. ® MicroCT slice (F) and Dental X-Radiograph are also shown. Neither lesion is visible in the proximal reflectance images.

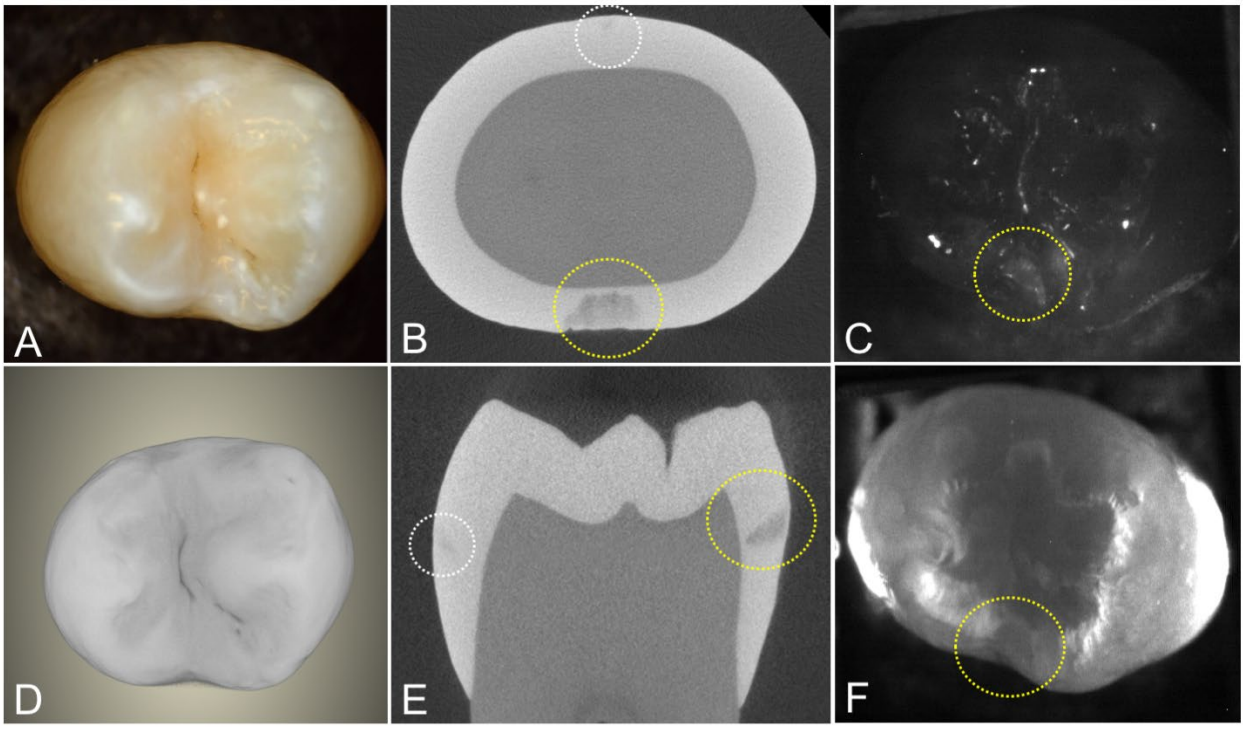

Figure 3.7.4. Images of a tooth with two interproximal lesions, one that is quite small and is only visible in the microCT images (white circle) and one much larger that was also visible in the SWIR images (yellow circle). (A) color and SWIR (C) occlual reflectance and (F) occlusal transillumination are shown along with a (D) microCT surface rendering of the tooth and extracted slices (B) transverse and parallel ® to the long axis of the tooth.

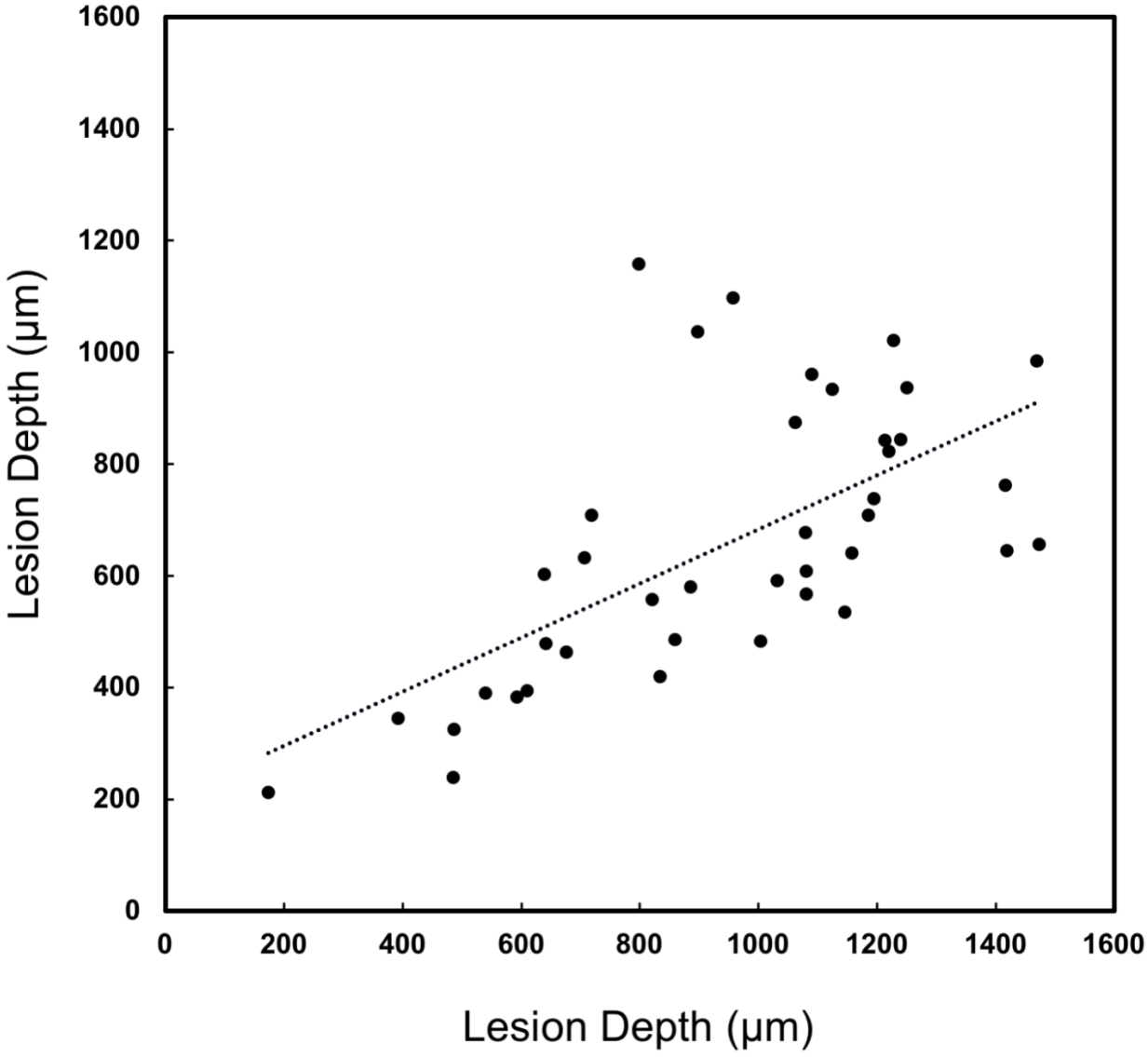

Figure 3.7.5. The lesion depth measured in proximal transillumination mode (X_{pt}) and microCT (X_{μ}). There was significant correlation between the two methods ($P<0.05$) with $R^2 = 0.40$ and 40 of the 67 lesions had sufficient contrast to perform the measurements.

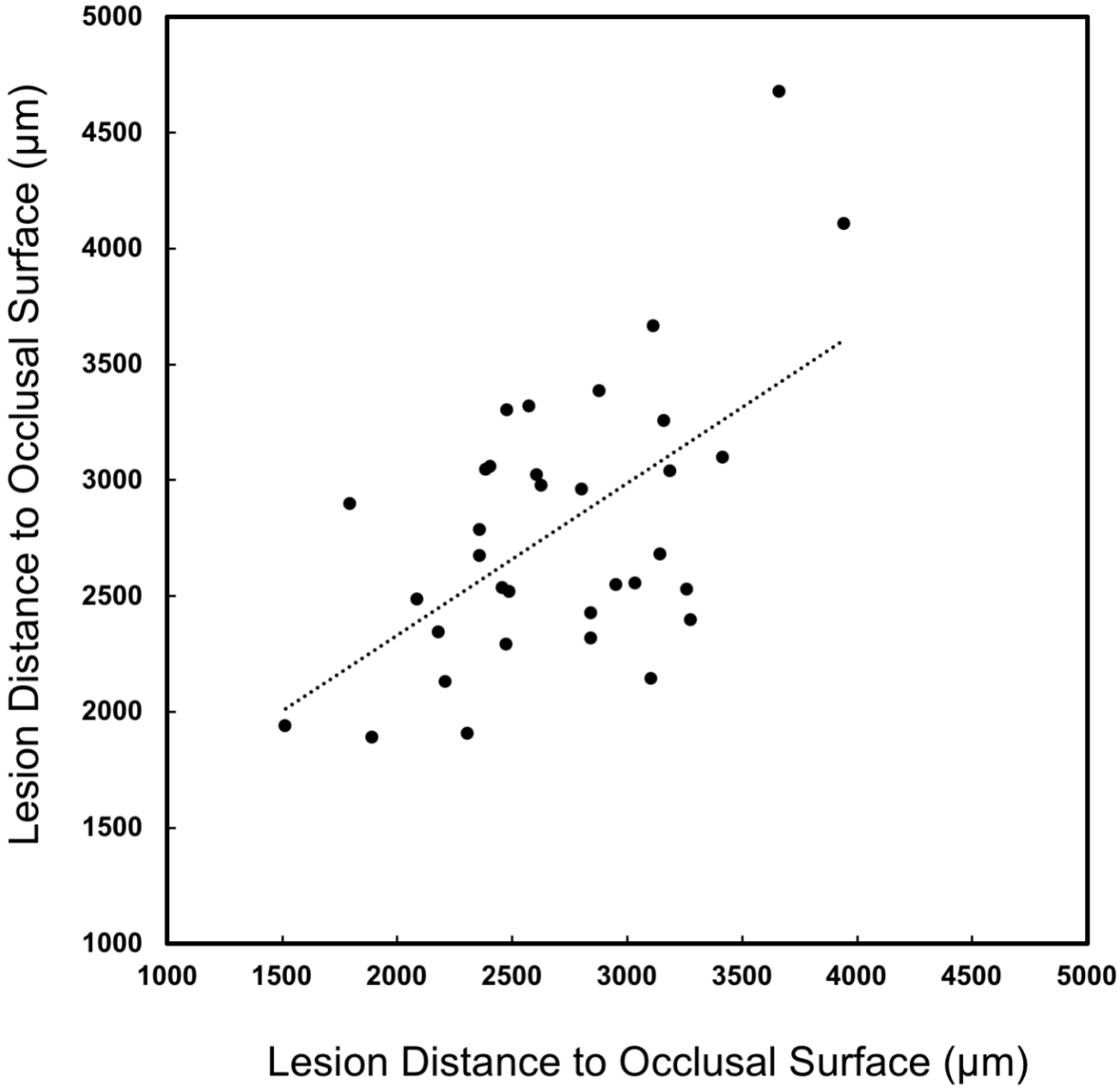

Figure 3.7.6. Depth below the occlusal surface measured in transillumination mode (Z_{ot}) and microCT (Z_{μ}). There was significant correlation between the two methods ($P<0.05$) with $R^2 = 0.33$ and 34 of the 67 lesions had sufficient contrast to perform the measurements.

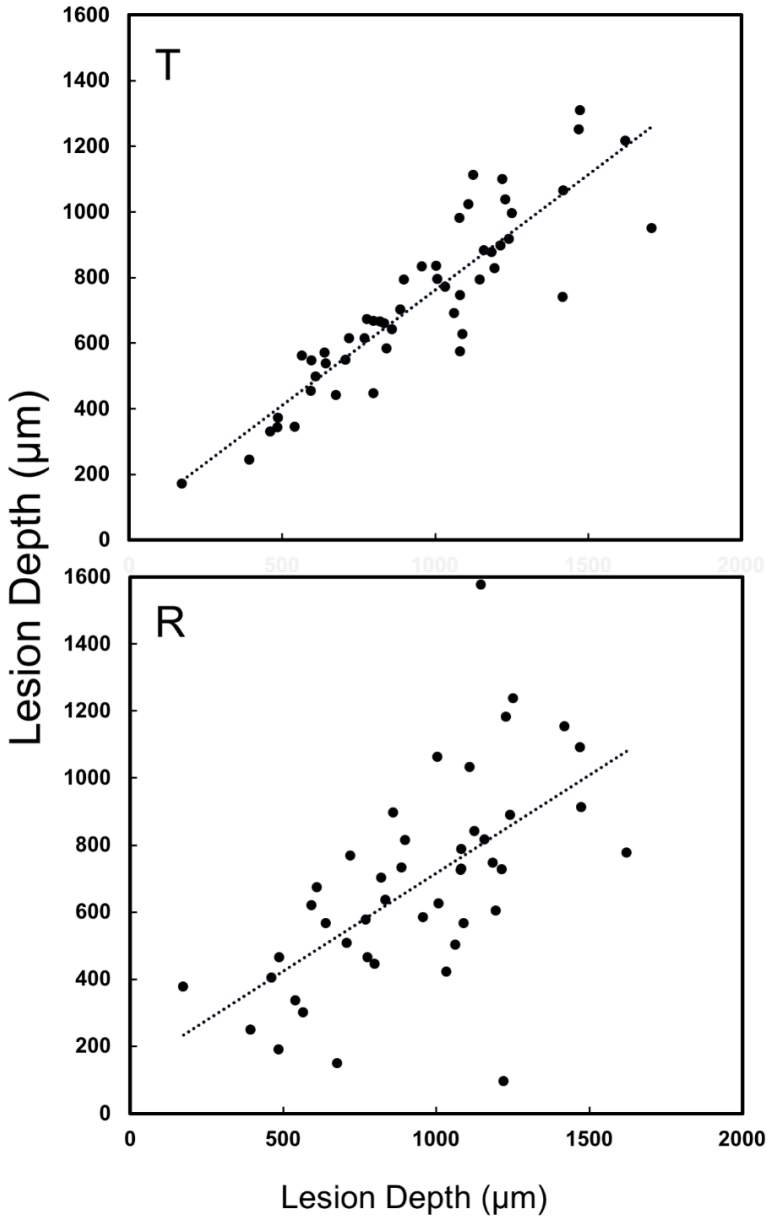

Figure 3.7.7. (T) Lesion depth measured in occlusal transillumination mode (X_{ot}) and microCT (X_{μ}). There was significant correlation between the two methods ($P<0.05$) with $R^2 = 0.80$ and 51 out of the 67 lesions had sufficient contrast to perform the measurements. ® Lesion depth measured in occlusal reflectance mode (X_{or}) and microCT (X_{μ}). There was significant correlation between the two methods ($P<0.05$) with $R^2 = 0.38$ and 45 of the 67 lesions had sufficient contrast to perform the measurements.

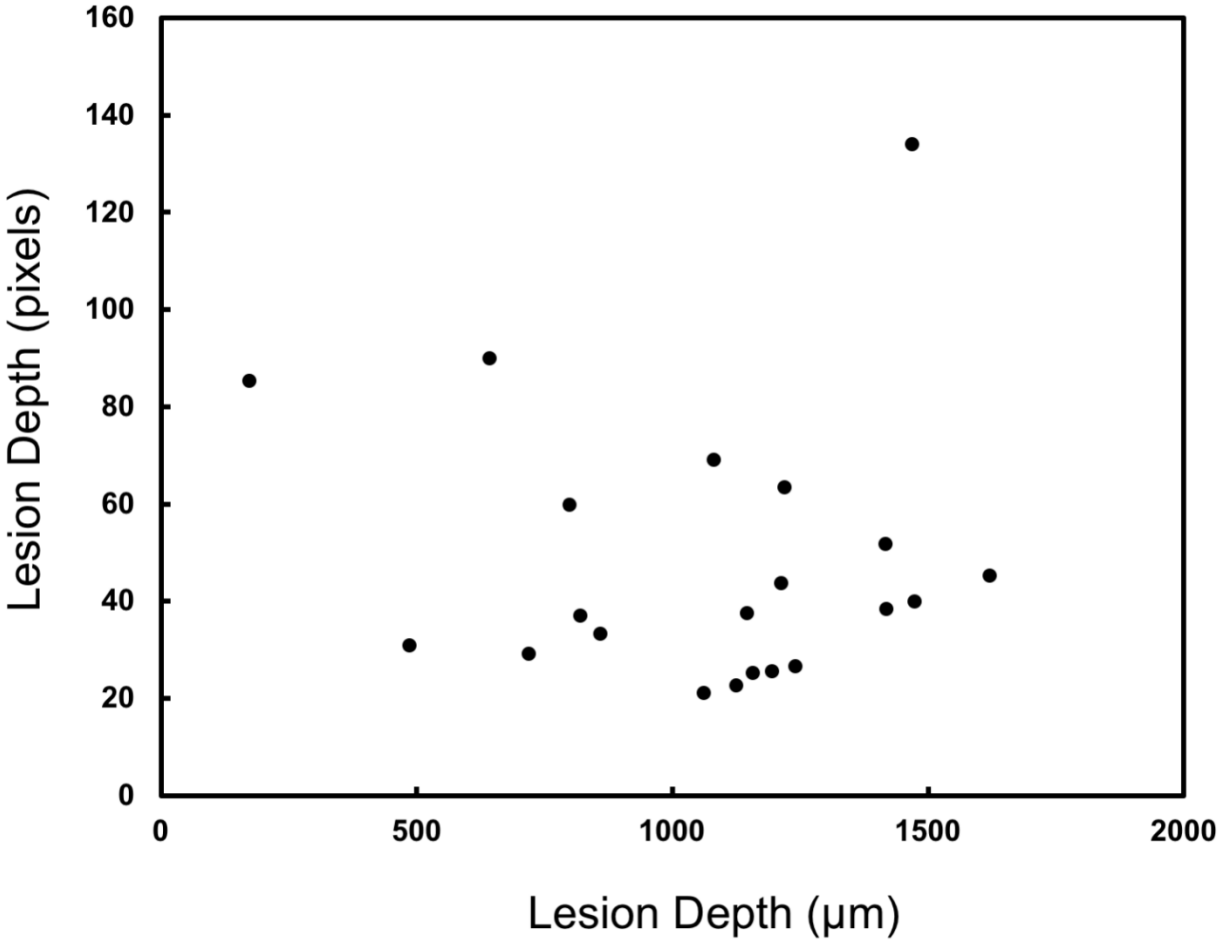

Figure 3.7.8. Lesion depth measured in radiography (X_r) and microCT (X_μ). There was no significant correlation between the two methods (P>0.05). Only 22 of the 67 lesions had sufficient contrast to perform the measurements.

Table 3.7.1. Mean lesion contrast ± s.d. for the SWIR methods and radiography and linear correlation coefficients (R2) for the lesion depth measured with those methods compared with microCT. The number of lesions that had measurable contrast in each imaging modality out of the 67 lesions identified with microCT is also listed.

	Proximal Transillumination	Occlusal Transillumination	Occlusal Reflectance	Radiograph
Mean Lesion Contrast ± s.d.	0.49 ± 0.11	0.45 ± 0.16	0.55 ± 0.21	0.26 ± 0.10
Lesion Depth Correlation (R^2)	0.40	0.80	0.38	N/A
Lesions Visible (N)	40	51	45	22

CHAPTER IV

Clinical diagnostic performance of multispectral SWIR transillumination and reflectance imaging for caries detection

4.1 Summary

The aim of this clinical study was to compare the diagnostic performance of dual short wavelength infrared (SWIR) occlusal transillumination and reflectance multispectral imaging with conventional visual assessment and radiography for caries detection on premolars scheduled for extraction for orthodontics reasons. Polarized light microscopy (PLM) and micro-computed tomography (microCT) performed after tooth extraction were used as gold standards. The custom fabricated imaging probe was 3D-printed and the imaging system employed a SWIR camera and fiber-optic light sources emitting light at 1300-nm for occlusal transillumination and 1600-nm for reflectance measurements. Teeth (n=135) on 40 test subjects were imaged *in vivo* using the SWIR imaging prototype in the study and teeth were extracted after imaging. Our study demonstrates for the first time that near simultaneous realtime transillumination and reflectance video can be successfully acquired for caries detection. Both SWIR imaging modalities had markedly higher sensitivity for lesions on proximal and occlusal surfaces compared to conventional methods (visual and radiographic). Reflectance imaging at 1600-nm had higher sensitivity and specificity than transillumination at 1300-nm. The combined SWIR methods yielded higher specificity but the combined sensitivity was lower than for each individual method.

4.2 Introduction

Despite the introduction of fluoridated drinking water, fluoride dentifrices and rinses, and improved dental hygiene in the US, dental decay continues to be the leading cause of tooth loss even though caries progression is potentially preventable and reversible if detected early [90, 91]. The locations of most newly discovered caries are on the occlusal pits/fissures of the posterior dentition and the interproximal contact sites between adjacent teeth where physical access is difficult. Radiographs have low diagnostic sensitivity due to overlapping enamel [1, 2]. Stains

interfere with visual diagnosis and other proposed imaging technologies such as fiber optic transillumination or fluorescence-based methods and may increase false positives [88]. Likewise, early lesions on proximal surfaces can also be difficult to detect due to lack of physical access and the challenge of radiographically identifying the initial, subtle mineral loss of these lesions [1, 2]. Radiographs are not effective for the early detection of occlusal caries lesions because of the overlapping features of the crowns [92, 94, 110]. Lesions are not typically visible on radiographs until decalcification has exceeded 30% [1, 2], while SWIR imaging methods are diagnostic with only 5% decalcification [111]. Moreover, the risk of exposure to ionizing radiation is poorly understood and even greatly reduced levels of radiation exposure may still pose a significant risk especially for children and pregnant women. It is unlikely that improvements in radiographic sensitivity will enable detection of hidden occlusal lesions or an improved diagnosis of suspicious occlusal caries lesions, those lesions with no cavitation and no radiographic radiolucency, but where caries is suspected due to surface roughness, opacities, or staining [92, 94, 110].

A highly sensitive and more reliable method for detecting demineralization during early lesion formation would be valuable for clinicians to monitor the activity of new caries and to assess the efficacy of non-surgical intervention. Short wavelength infrared (SWIR) and near-IR imaging (NIR) methods have been under development for almost 20 years for use in dentistry and several NIR clinical devices are now available commercially. Due to the high transparency of enamel at longer wavelengths, multiple imaging configurations are feasible. Lesions can be imaged using transillumination and reflectance from tooth occlusal, buccal and lingual surfaces [24, 102]. In proximal transillumination the light source and detector are placed on the buccal and lingual sides of the tooth. The positions can be alternated to get images of each surface since this method will have greater sensitivity for those lesions located closer to the detector [6]. This is the same

imaging geometry used to acquire bitewing radiographs. Interproximal lesions, the lesions located at the proximal contact points in between teeth, can be imaged via all three imaging geometries. Transillumination of the proximal contact points between teeth can also be accomplished via occlusal transillumination by directing SWIR light below the crown while imaging the occlusal surface [24, 78, 79] (see **Fig. 4.7.1**). The latter approach that was used in this study is capable of imaging occlusal lesions as well with high contrast [24, 47, 80-82, 102]. The first clinical SWIR/NIR study was carried out in 2010, it was demonstrated that interproximal lesions that appeared on radiographs could be detected *in vivo* using proximal and occlusal transillumination imaging at 1310-nm with similar sensitivity [24]. Currently the only clinical systems that are available operate at shorter NIR wavelengths at 830 and 780-nm [83-87]. The use of shorter wavelength 830-nm NIR light was first investigated more than 20 years ago when it was found that the contrast between sound and demineralized enamel was higher at longer SWIR wavelengths [78]. Shorter wavelengths allow the use of less expensive silicon based detectors. However, longer wavelength SWIR light has significant advantages, stains interfere significantly at wavelengths less than 1200-nm [88] and the contrast between sound and demineralized enamel is markedly higher at wavelengths beyond 1400-nm in reflectance measurements [70, 88, 89].

Studies over the past decade have indicated that transillumination performs best at 1300-nm where the transparency of enamel is highest while the contrast of lesions on tooth surfaces imaged using reflectance continues to increase with increasing wavelength and is highest at 1950-nm [70, 88, 89]. Several studies have investigated multispectral measurements using either one modality or combining transillumination and reflectance measurements. Zakian et al. [96, 97] used multiple wavelengths of SWIR hyperspectral reflectance images to estimate the severity of occlusal lesions. Since, multispectral SWIR reflectance and transillumination experiments have demonstrated that

the tooth appears darker at wavelengths coincident with increased water absorption, multispectral images can be used to produce increased contrast between different tooth structures such as sound enamel and dentin, dental decay and composite restorative materials [97-99]. Combining measurements from different SWIR imaging wavelengths and comparing them with concurrent measurements acquired by complementary imaging modalities should provide improved assessment of lesion depth and severity. Radiographs markedly underestimate the depth and severity of interproximal lesions and clinicians assume that lesions penetrate much deeper than indicated in radiographs [13-15]. SWIR occlusal transillumination and reflectance has been combined into a single probe and tested *in vitro* [43, 107, 112, 113]. Different illumination wavelengths have been used optimized for each imaging mode, namely SWIR wavelengths greater than 1400-nm for reflectance and 1300-nm for transillumination. Simon et al. [27] built a benchtop simultaneous SWIR reflectance and transillumination system with tunable filters that ranged from 830-1700-nm and showed that the combined images have potential for the diagnosis of occlusal lesions [5] and simulated cavitated and noncavitated interproximal lesions [100]. The purpose of this study was to evaluate the diagnostic performance of a dual SWIR occlusal transillumination and reflectance device *in vivo* on teeth scheduled for extraction for orthodontic reasons. This is the first clinical study to employ dual SWIR transillumination and reflectance integrated into a single imaging device. In a prior SWIR clinical imaging study, separate occlusal and proximal imaging devices operating at 1300-nm were used along with reflectance imaging at 1450-nm [6]. That study showed that occlusal transillumination and reflectance imaging both had higher performance than proximal transillumination. In addition to their higher performance, it is much easier to combine occlusal transillumination and reflectance imaging into a single device. That study also showed that each device performed as well as radiographs for proximal lesions

and if multiple devices were combined the sensitivity was much higher than for radiography [6]. Higher sensitivity may be of potential concern if it leads to over treatment due to a high number of false positives. We hypothesize that the use of a single SWIR occlusal transillumination and reflectance imaging will increase the specificity and reduce the potential for false positives.

4.3 Materials and Methods

4.3.1 Participant Recruitment and Procedures

Study participants (n=40 with 139 premolars) aged 12-60 with 2-4 premolars scheduled for extraction for orthodontic reasons were recruited from the UCSF Orthodontic Clinic by the study investigators (UCSF IRB 18-27656). One participant was lost to follow-up after the first visit and was excluded from the study. A total of 39 participants (n=39 with 135 premolars) completed the study. Color images of each tooth were acquired using a FocusDent MD740 (Vilnius, Lithuania) 1280x960 pixel intraoral camera and lesions were visually assessed [16]. After extraction and before sectioning teeth were mounted in black delrin blocks and imaged with digital radiographs using a CareStream 2200 System from Kodak (Rochester, NY) operating at 60 kV. Radiographical contrast was calculated using $(I_S-I_L)/I_S$ for each proximal contact. Where I_L is the lesion area and I_S is a sound control area. Areas for each I_L and I_S measurement were selected using PLM and microCT. I_L was measured as the mean intensity over the lesion area at each proximal contact and I_S was selected at a position either directly below or directly above I_L to ensure a similar enamel thickness. If no lesion was present the mean intensity was measured in an area of 20 x 20 pixels at the contact area to serve as I_L and an adjacent area was chosen for I_S.

4.3.2 Design and Fabrication of the Dual Reflectance and Occlusal Transillumination SWIR probe

The dual probe design consists of a reflectance probe body and an occlusal transillumination attachment, shown in **Fig. 4.7.1**. The reflectance probe body and the occlusal transillumination attachment were 3D printed and are autoclavable. There is an air nozzle near the mirror to prevent fogging of the mirror. The air nozzle can also be used to dry the lesion to increase lesion contrast and potentially assess lesion activity.

The dual reflectance and occlusal transillumination SWIR probe was designed in Fusion 360 from Autodesk (San Francisco, CA). The handpiece was fabricated using a Formlabs (Somerville, MA) Form 3 Low Force Stereolithography 3D printer. The probe consists of two components, a main body containing the light source for reflectance and the light collection optics and a second attachment containing the transillumination light source. Details regarding the fabrication of the dual occlusal transillumination and reflectance imaging probe system and optical probe have been previously described [40, 43, 107, 112, 113].

4.3.3 Image Acquisition and Analysis

The SWIR images were captured using a 640x480 pixel micro-SWIR camera (SU640CSX) measuring only 32x32x28 mm from Sensors Unlimited (Princeton, NJ). Two planoconvex antireflection coated lenses of 60 and 100 mm focal length along with an adjustable aperture were placed between the handpiece and the InGaAs camera to provide a field of view of 11 mm^2 at the focus plane. A low-OH optical fiber of 1 mm diameter was used to deliver light from a 1604-nm superluminescent diode (SLD), Model ESL 1620-2111 from Exalos (Schlieren, Switzerland) with an output of 17 mW and a bandwidth of 46-nm. The intensity delivered to the tooth was 5 mW.

The 1600-nm light passes through a polarizing beam splitting cube before incidence on the tooth and a linear polarizer was placed before the camera to achieve cross-polarization for glare reduction. The transillumination light was delivered through two 0.4 mm diameter low-OH optical fibers. A 1314-nm (BW) SLD, Model DL-CS3452A-FP 1620-2111 from Denselight (Singapore) with an output of 48 mW and a bandwidth of 33-nm was used as the source for transillumination. A 50/50 beamsplitter was used to deliver light to each arm for transillumination. The output intensity of each arm was set at 10 mw before entering the Teflon plugs located at the end of each arm.

Image processing of the images was performed by custom scripts written using MATLAB from Mathworks (Natick, MA). The acquired 12 bit images (4096) were converted to 16 bit (65535) by multiplying by 16 and subtracting 1 to facilitate processing using MATLAB. Contrast was calculated at 3 different lesion locations including occlusal grooves or fissures and the proximal mesial and distal contacts. The contrast was calculated for each location using the formula $(I_L - I_S)/I_L$ for reflectance images and $(I_S - I_L)/I_S$ for transillumination images. I_L was measured as the mean intensity over the lesion area. I_S was selected at adjacent confirmed sound locations [5]. I_L was also measured at the proximal contact or occlusal fissure even if no lesion was present in order to measure the contrast of sound areas for comparison. If no lesion was present the mean intensity was measured in an area of 20 x 20 pixels at the contact area to serve as I_L and an adjacent area was chosen for I_S. Lesion areas were confirmed using the PLM and microCT images.

4.3.4 Sectioning, polarized light microscopy (PLM) and microcomputed tomography (microCT)

The first 40 extracted teeth were sectioned and examined with polarized light microscopy (PLM). The remaining 95 teeth were examined intact using microcomputed x-ray tomography (microCT). The acquisition of an in house microCT system mid way through the study allowed us to switch to microCT. MicroCT does not require physical sectioning and avoids the risk of sample loss during sectioning. Samples (n=40) were serially sectioned into ~200 μm thick mesio-distal slices using a linear precision saw, Isomet 5000 (Buehler, Lake Buff, IL). PLM was used for histological examination of the thin sections using a Meiji Techno RZT microscope (Saitama, Japan) with an integrated digital camera, Canon EOS Digital Rebel XT (Tokyo, Japan). Sample sections were imbibed in deionized water and examined in the bright field mode with crossed-polarizers and a red I plate (550-nm retardation).

Whole teeth (n=95) were imaged using microCT with a 10 μm resolution. A Scanco MicroCT 50 from Scanco USA (Wayne, PA) was used to acquire the images. Acquisition parameters used for the microCT images were 90 kVP, 200 uA, 18 W, 20 FOV, 10 μm voxel size, 500 ms integration time, and an aluminium 0.5 mm filter.

4.4 Results

4.4.1 Imaged teeth and lesion statistics

A total of 40 patients were recruited from the UCSF Orthodontics clinic. A total number of 135 teeth were imaged with 135 occlusal surfaces and 270 proximal surfaces for a total of 405 surfaces. However, 51 surfaces were excluded from the final analysis for the following reasons: pre-existing

sealants, composite restorations, orthodontic bonding adhesive, tooth restored with composite after imaging, and tooth severely damaged during extraction. Hence, the total number of surfaces that were included for the final analysis totaled 354. The 354 surfaces were categorized based on surface type (sound tooth structure, enamel and dentinal lesions and surface location (occlusal or proximal)). PLM/ microCT identified 27 occlusal surfaces, 100 mesial proximal surfaces, and 86 distal proximal surfaces as sound tooth structure. Those surfaces are summarized in **Table 4.7.1**. There were 76 occlusal enamel lesions, 18 mesial enamel lesions, and 31 distal enamel lesions. Lesions penetrating into the underlining dentin (dentinal lesions) were found on 11 occlusal surfaces, 3 mesial surfaces, and 2 distal surfaces. Cracks were found on 1 occlusal surface, 6 mesial surfaces, and 4 distal surfaces. One single distal cavitation was discovered by the microCT analysis that was also classified as one of the five proximal dentinal lesions. Visual and radiographic assessment was carried out by three clinical examiners using the intraoral color images and radiographs taken of the extracted teeth. The diagnostic performance of these conventional methods is summarised in **Table 4.7.2**.

Images from one tooth from the study with two interproximal lesions are shown in **Fig. 4.7.2**. The color image in **Fig. 4.7.2A** shows a bicuspid with a sealant on the occlusal surface along with a visible lesion on the distal surface. Neither lesion is obvious in the radiograph in Figure 4.7.2B. Only one of the three clinical examiners detected the lesion on the distal surface in the radiograph and by visual examination and none identifed the lesion on the mesial surface by radiograph or visual examination. After tooth extraction and sectioning, PLM in **Fig. 4.7.2C** shows that lesions are present on the distal and mesial surfaces. The SWIR reflectance and occlusal transillumination images acquired with the dual probe are shown in **Figs. 4.7.2D&E** and both lesions are visible in the yellow circles.

Images from a second tooth from the study are shown in **Fig. 4.7.3**. The color image in **Fig. 4.7.3A** shows a bicuspid with hypomineralization and areas of high reflectivity near the mesial and distal surfaces indicated by the green arrows. No lesions are obvious in the radiograph in **Fig. 4.7.3B**. Only one of the three clinical examiners detected the proximal lesion on the distal surface in the radiograph and none identified it by visual assessment. The SWIR occlusal transillumination and reflectance images acquired with the dual probe are shown in **Figs. 4.7.3C&D** and both images show occlusal and proximal lesions in the positions of the yellow boxes.

MicroCT images in **Figs. 4.7.3E&F** show that lesions are present in the same areas of the yellow boxes. It is interesting that the bright areas in the color image of **Fig. 4.7.3A** do not correspond to lesion areas. It is likely they are due to hypomineralization. The SWIR reflectance image in **Fig. 4.7.3C** shows the triangular shaped lesion at the distal contact matching the microCT image and shows no increased reflectivity at the mesial contact.

There were 16 lesions that penetrated into dentin, 11 occlusal lesions and 5 lesions on proximal surfaces. None of the 11 occlusal dentinal lesions were detected by radiography. Radiography detected 3 out of 5 of the proximal lesions (mean of 3 examiners) and only 1 out of the 5 proximal lesions had a radiographic contrast greater than 0.1. Visual assessment (mean of 3 examiners) detected 1 out of 5 of the proximal lesions and 4 out of the 11 occlusal lesions. SWIR reflectance (contrast > 0.1) detected 6 of the 11 occlusal lesions and 5 out 5 of the proximal lesions while 8 of the 11 occlusal lesions and 3 out 5 of the proximal lesions were detected by SWIR occlusal transillumination (contrast > 0.1).

4.4.2 Diagnostic performance based on contrast thresholds

A total of 87 occlusal lesions (enamel and dentinal) were identified from PLM/MicroCT. Only one occlusal lesion was identified on radiographs by the three clinical examiners. The mean contrast of the occlusal lesions for SWIR reflectance was 0.18±0.14 and that for occlusal transillumination was 0.16±0.08. For both modalities the contrast was significantly higher in lesion areas.

There were 54 proximal lesions that were detected using PLM/microCT and the mean±(SD) of the radiographic contrast was 0.03±0.04. The radiographic contrast for all the proximal lesions that were detected by at least one of the three clinical examiners (n=23) was 0.07±0.08 and the radiographic contrast for the proximal lesions that were detected by all three of the clinical examiners was (n=3) 0.11±0.06. The mean contrast for SWIR reflectance was 0.19±0.15 and that for SWIR transillumination was 0.13±0.08. These values are tabulated in **Table 4.7.3**.

Sensitivity, specificity and accuracy were calculated for reflectance, transillumination and both combined for varying contrast thresholds from 0.02 to 0.2. If the contrast was higher than that particular threshold it was considered a detected lesion. Plots of the accuracy versus contrast threshold are shown in **Fig. 4.7.4**. An examination of **Fig. 4.7.4** shows that the accuracy reaches a plateau for lesions on proximal surfaces after a contrast threshold of 0.1 and drops of after 0.1 for occlusal lesions on occlusal surfaces. Therefore we chose a contrast threshold of 0.1 to calculate the diagnostic performance of reflectance, transillumination and both combined and the results are tabulated in **Table 4.7.4**.

4.5 Discussion

In this study, the diagnostic performance of a dual SWIR occlusal transillumination and reflectance imaging device was assessed *in vivo* on teeth scheduled for extraction based on orthodontic reasons. Caries status was unknown prior to imaging and PLM and microCT were used as gold standards. In this study, most of the 141 lesions were small and confined to the enamel. There were only 16 lesions that penetrated into dentin and there was only one severe lesion that was cavitated and penetrated into the inner half of the dentin. The diagnostic performance of the SWIR methods were compared with conventional visual and radiographic methods. The motivation for combining reflectance and transillumination was to increase diagnostic performance by reducing false positives and providing more accurate measurements of lesion severity. The specificity did increase to 0.93 for proximal surfaces and 0.96 for occlusal surfaces for combined SWIR imaging. However, the accuracy for the combined methods was lower than for SWIR reflectance alone.

The posterior occlusal surfaces and interproximal surfaces between adjacent posterior teeth are challenging areas to detect early demineralization using radiography, due to the overlapping topography of the occlusal surface and the low sensitivity for detection of early proximal lesions that extend only into enamel. Visual detection of early demineralization on occlusal surfaces may also be confounded by staining in the occlusal fissures that make it difficult for clinicians to accurately pinpoint the areas of demineralization [88]. Stains also tend to make early lesions appear more severe. A thorough and complete removal of all stain from the pits and fissures is not clinically feasible. Visual and radiographic assessment were performed on the teeth by three clinical examiners. Based on the poor agreement of conventional diagnosis for which the examiners have had many years of experience, we decided to measure and compare the

radiographic lesion contrast and the SWIR lesion contrast. In addition, in our prior dual transillumination and reflectance *in vitro* SWIR imaging study there was poor agreement among clinical examiners that can be attributed to limited experience with new technology [40].

Prior studies have demonstrated that occlusal transillumination and reflectance imaging modalities using longer wavelengths may offer higher sensitivity regarding early lesion detection [6, 83, 84, 86, 87], but each individual imaging modality on its own has lower specificity than radiography and may lead to more false positives. We demonstrated in this study that it is possible to capture near-simultaneous occlusal transillumination (1300-nm) and reflectance (1600-nm) videos of lesions successfully *in vivo*, that has not been done prior to this study. Both imaging modalities, whether considered separately or when combined, had markedly higher sensitivity for lesions on both proximal and occlusal surfaces compared to conventional visual assessment and radiography. It is important to note that the teeth utilized in this study were subject to crowding and were extracted for orthodontic reasons. SWIR imaging was performed *in vivo* while radiography was peformed on the teeth after extraction and did not suffer interference from crowding. Therefore, we suspect that the diagnostic performance of radiography would likely be even lower if it was performed *in vivo* with many overlapping teeth.

Higher sensitivity in detecting early lesions should be advantageous because clinicians can better assess the caries risk of the individual and intervene earlier with minimally invasive techniques to prevent such lesions from progressing further to avoid the need for surgical intervention. SWIR methods do not utilize ionizing radiation and are well suited for monitoring lesions over time to determine if they increase in severity.

The performance of reflectance imaging at 1600-nm was higher than for transillumination imaging at 1300-nm. One can argue that the performance of combined SWIR reflectance and transillumination was not any better than SWIR reflectance alone. Additional analysis needs to be performed to better assess the advantages of the combined imaging approach and fully evaluate the ability to assess lesion depth and severity. It was interesting that SWIR transillumination was most effective in detecting 8/11 of the deeper occlusal lesions that penetrated into dentin.

SWIR imaging is particularly well suited for use with artificial intelligence (AI). Casalegno et al. showed that AI could be used to analyze clinical near-IR transillumination images at 780-nm [114]. The much higher lesion contrast of SWIR methods compared to radiography and the lack of interference due to stains are major advantages that can likely be exploited using AI approaches to identify lesions.

This study suggests that SWIR Imaging methods offer high sensitivity for lesions on proximal and occlusal surfaces without the interference of stains that appear at wavelengths of less than 1200-nm. No SWIR methods are currently available in the commercial market due to high cost and security concerns, but we anticipate that this innovative technology will increasingly become more accessible for medical use. Commerical NIR imaging devices for caries detection operate at 780 and 850-nm, where studies show that there is still significant interference from stains [88]. In addition, the contrast between sound and demineralized tooth structure has previously been shown to be markedly higher at longer SWIR wavelengths than it is at 780 or 850-nm [88, 89]. The primary disadvantage of operating at longer SWIR wavelengths is that Si-based imaging technologies are only efficient at wavelengths under 1000-nm. Alterative imaging technologies such as InGaAs and Ge-enhanced Si are still expensive. The limited use of these more innovative

semiconductors technologies is a major reason for the high cost. However, with expanded use, those prices are expected to decrease. The cost has decreased significantly in the past 10 years and the performance has increased markedly.

4.6 Conclusion

Combined SWIR occlusal transillumination and reflectance images yielded an increase in specificity for lesions on both occlusal and proximal surfaces. The sensitivity of the SWIR imaging methods were markedly higher than for conventional methods. The contrast of lesions in the occlusal pits and fissures and the proximal contacts where most lesions are located was significantly higher ($p<0.05$) than sound areas for both SWIR occlusal transillumination and reflectance while there was no significant difference in contrast between lesion and sound areas for radiography.

4.7 Tables and Figures

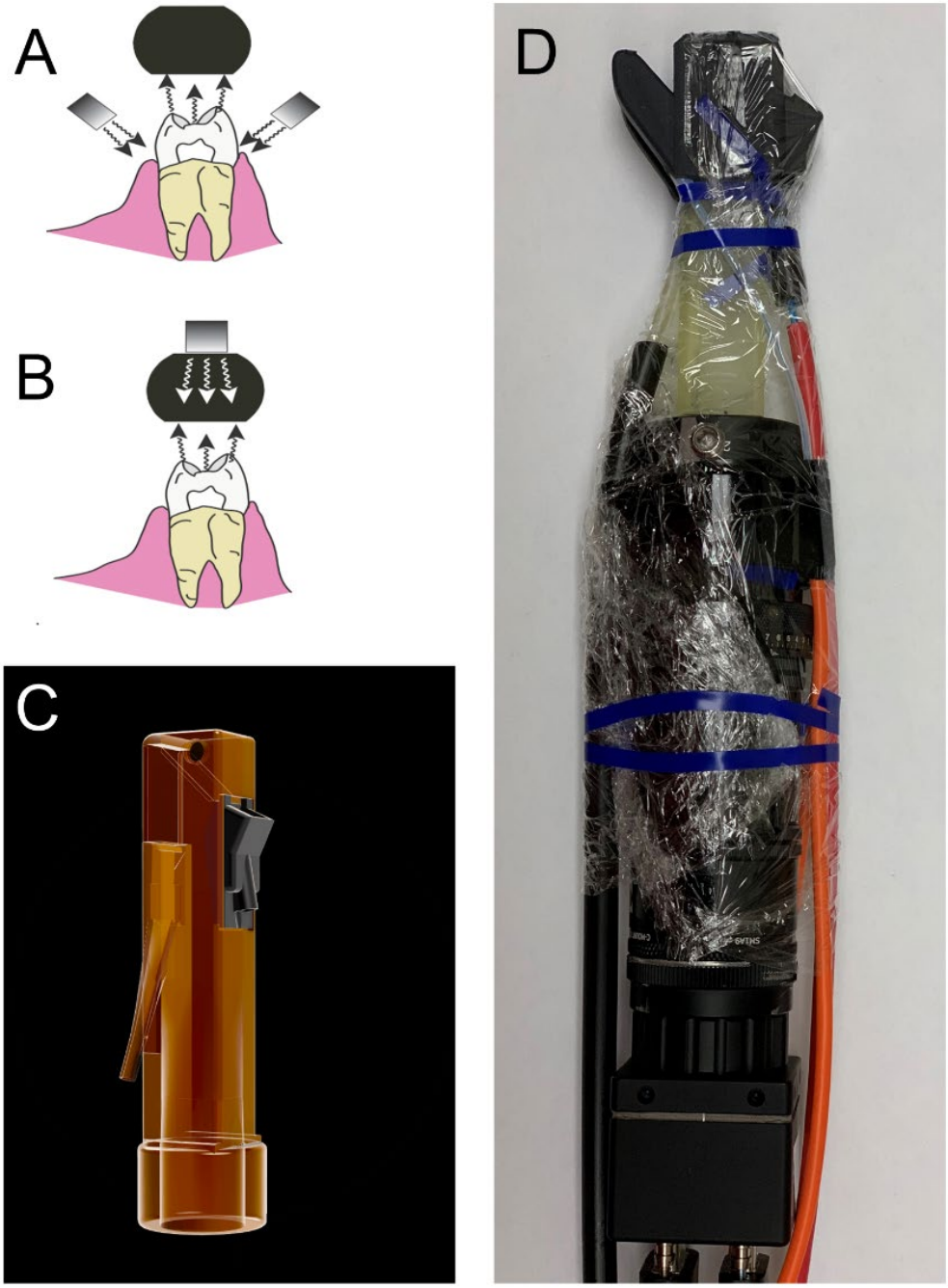

Figure 4.7.1. (A) Occlusal transillumination diagram, (B) reflectance diagram, (C) 3D printed handpiece attachment with insert (black) holding polarizing beam splitter cube. (D) Entire dual reflectance and transillumination wrapped for infection control and ready for clinical imaging

Table 4.7.1. Summary of proximal and occlusal surfaces based on PLM and microCT.

Surfaces	Occlusal	Proximal
Sound	27	186
Enamel Lesions	76	49
Dentinal Lesions	11	5
Total	114	240
Rejected	21	30

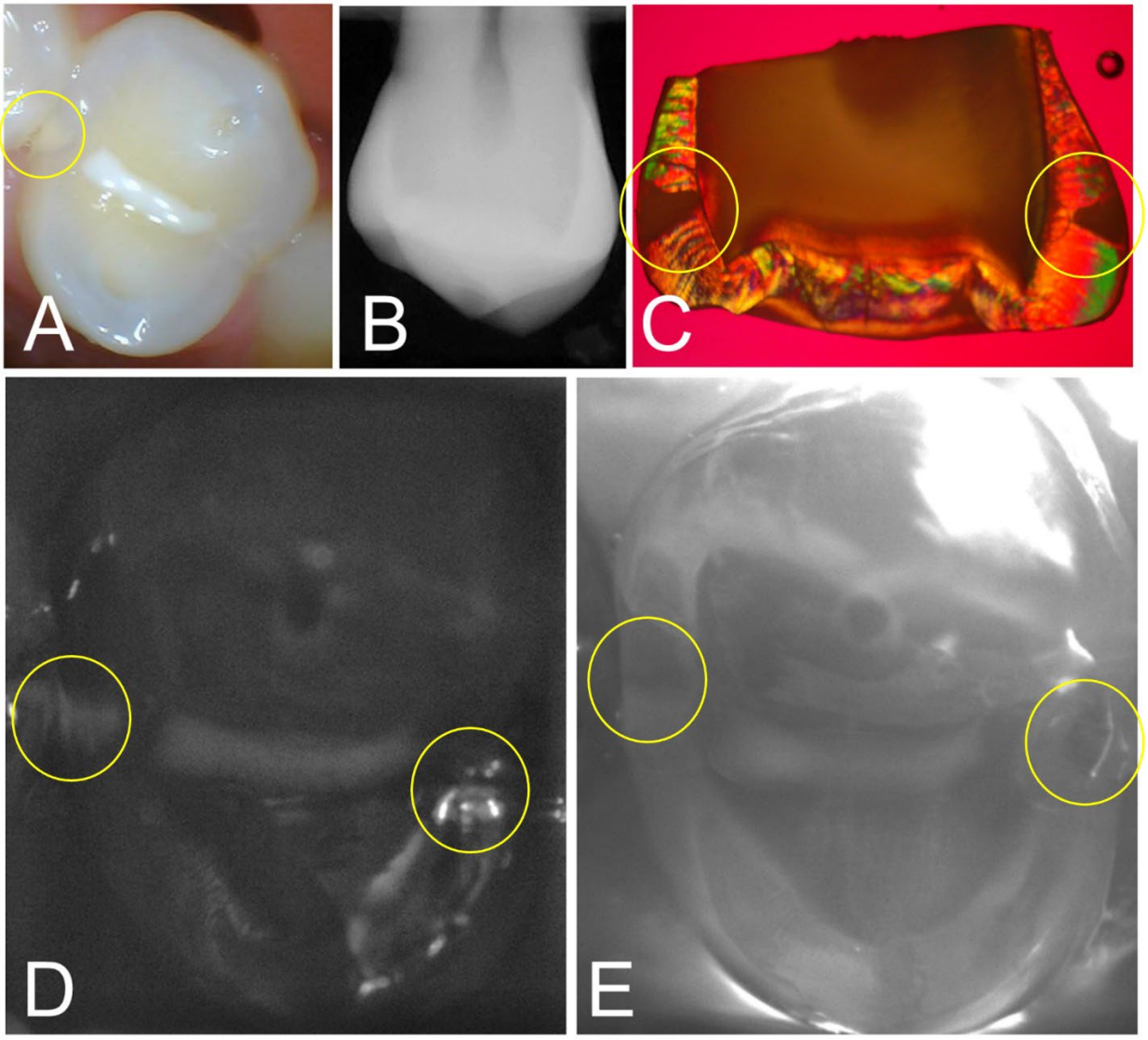

Figure 4.7.2. (A) Color image of a bicuspid with a sealant on the central fissure, a lesion is visible at the distal contact, while no lesion is visible on the mesial contact. (B) Radiograph shows no obvious lesions. (C) PLM image of a section cut from the tooth after extraction shows proximal lesions on both surfaces (yellow circles). (D) SWIR reflectance and (E) occlusal transillumination images show lesions on both surfaces.

Table 4.7.2. Conventional visual and radiographic assessment of the lesions on the occlusal and proximal surfaces with 3 clinical examiners.

	Proximal (n=54)	**Occlusal (n=87)**
Radiography		
Mean Number of Detected Lesions	12	1
Accuracy	0.79	0.24
Sensitivity	0.22	0.01
Specificity	0.95	0.99
Interexaminer Reliability	0.93	0.99
Visual Assessment		
Mean Number of Detected Lesions	1	25
Accuracy	0.78	0.41
Sensitivity	0.02	0.29
Specificity	1	0.81
Interexaminer Reliability	1	0.85

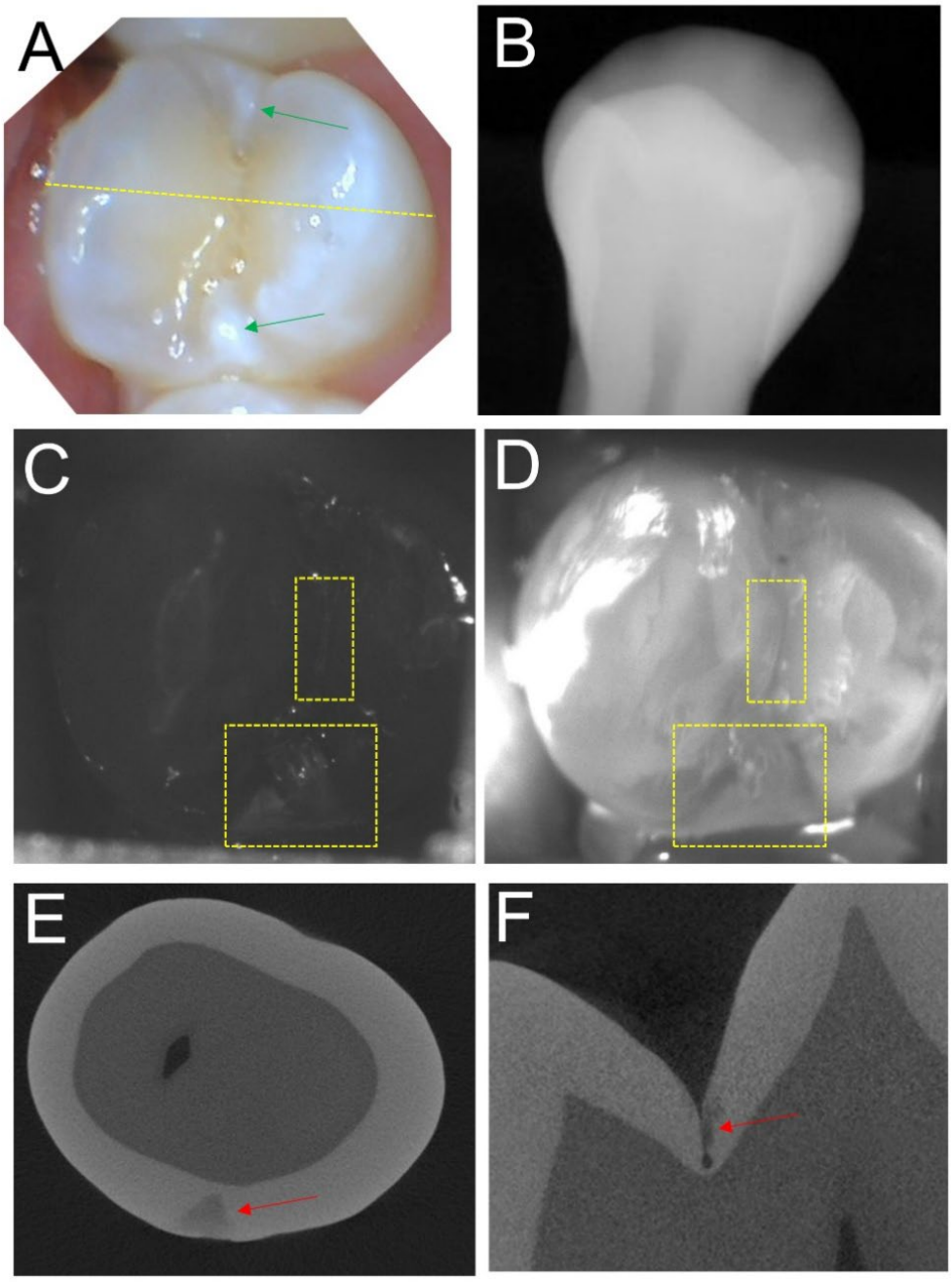

Figure 4.7.3. Images of a tooth with lesions on the occlusal and distal proximal surfaces. The color image in (A) shows several bright areas of high reflectivity near the mesial and distal surfaces indicated by the green arrows that may be due be due to proximal lesions or hypomineralization. No lesions are visible in the radiograph in (B). SWIR reflectance (C) and occlusal transillumination (D) images show occlusal and proximal lesions in the positions of the yellow boxes. MicroCT images show lesions on the distal proximal surface (E) and the occlusal (F) surface as indicated by the red arrows.

Table 4.7.3. Mean lesion contrast ± s.d. for radiography and SWIR occlusal transillumination and reflectance at the three potential lesion locations with and without lesions present. For columns with an asterisk the mean contrast was significantly higher for lesion areas (P< 0.05). For areas with no lesion present the contrast is the mean of the absolute value of the individual contrast values.

	Proximal			Occlusal	
	Radiography	**Reflectance**	**Transillumination**	**Reflectance**	**Transilluminatio**
No Lesion	0.021 ± 0.032	0.057 ± 0.075	0.10 ± 0.081	0.048 ± 0.045	0.088 ± 0.069
Lesion	0.030 ± 0.037	*0.19 ± 0.15	*0.13 ± 0.084	*0.18 ± 0.14	*0.16 ± 0.078

Table 4.7.4. Diagnostic performance of SWIR reflectance, occlusal transillumination and combined methods along with radiography using a diagnostic contrast threshold of 0.10.

	Accuracy	Sensitivity	Specificity
Proximal Surfaces			
Reflectance	0.83	0.72	0.86
Transillumination	0.63	0.63	0.62
Combined	0.81	0.44	0.93
Radiography	0.79	0.08	0.99
Occlusal Surfaces			
Reflectance	0.82	0.80	0.89
Transillumination	0.72	0.75	0.63
Combined	0.70	0.62	0.96

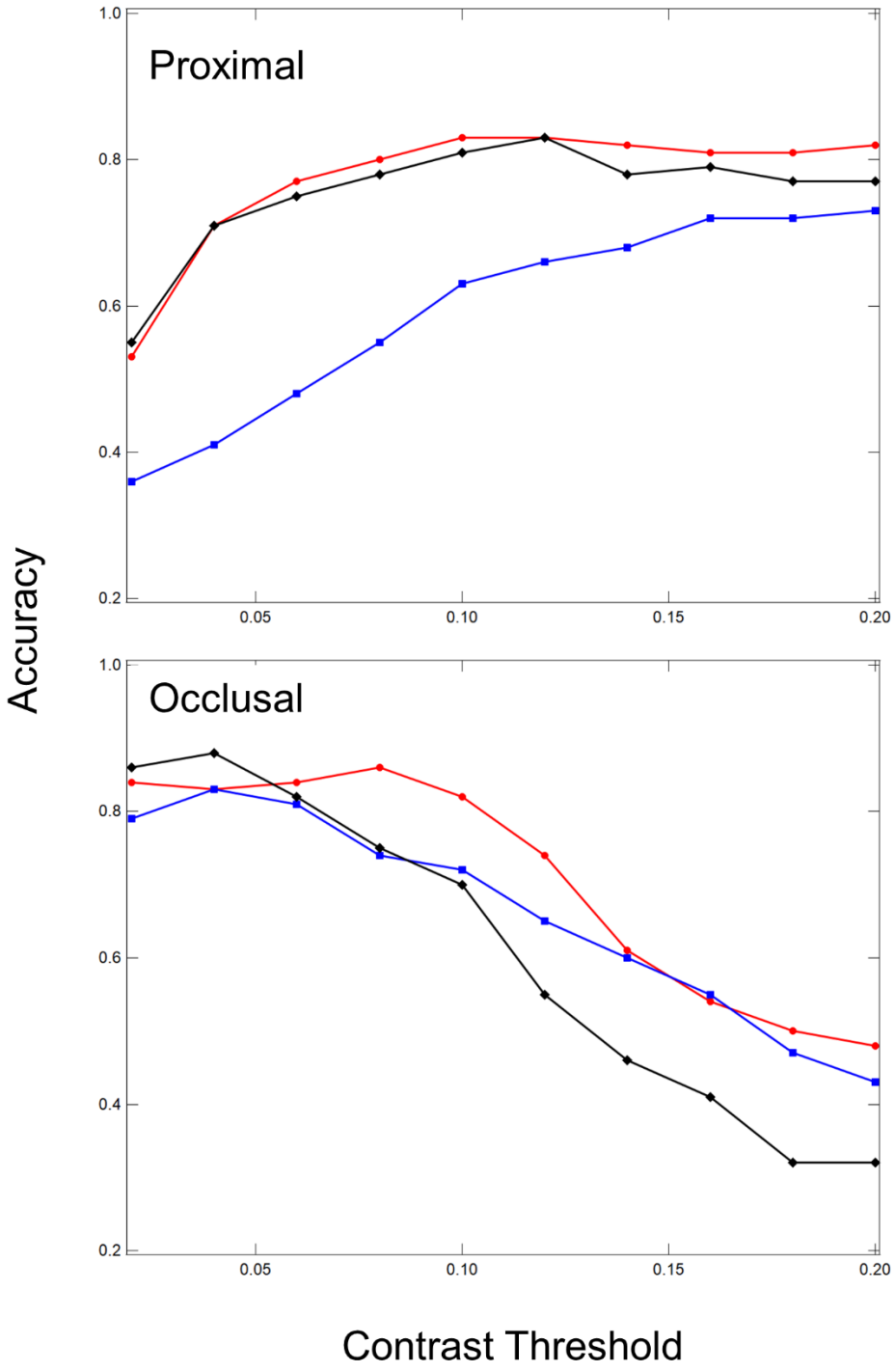

Figure 4.7.4. Plots of the accuracy calculated for SWIR reflectance (red), SWIR transillumination (blue) and the combined modalities (black) for the proximal (n=54) occlusal lesions (n=87) as a function of the lesion contrast threshold.

CHAPTER V

Monitoring lesion activity on primary teeth with CP-OCT and SWIR reflectance imaging

5.1 Summary

The purpose of this study was to use cross polarization optical coherence tomography (CP-OCT) and short wavelength infrared imaging (SWIR) reflectance imaging to monitor changes in the structure and activity of early occlusal caries on primary teeth over a period of six months during intervention with fluoride.

Participants (n=29) aged 6-10 each with two suspected active occlusal lesions on primary teeth completed the study. Fluoride varnish was applied to tooth surfaces every 3-months and participants were instructed to brush twice daily with a fluoride toothpaste. Images were acquired using CP-OCT every three months for 6 months. SWIR reflectance images were acquired during forced air-drying of the lesions for 30-seconds at 0 and 6-months.

Most of the 42 lesions appeared initially active at baseline. Only 6 lesions appeared arrested at baseline based on the presence of a highly mineralized transparent surface layer (TSL) in CP-OCT images. At 6 months, 14 of the lesions appeared arrested including the 6 initially arrested lesions and the TSL thickness increased significantly ($P<0.0001$). The mean lesion depth (Ld) and the integrated reflectivity over the lesion depth (DR) increased significantly ($P<0.05$) after 6 months for the 42 lesions analyzed. SWIR reflectance images showed that there was a significantly higher ($P<0.05$) delay before changes in intensity were measured for active lesions vs arrested lesions during lesion drying.

CP-OCT was able to monitor changes in lesion structure and activity including the formation of a highly mineralized TSL indicative of lesion arrest during nonsurgical intervention. Time-resolved SWIR reflectance imaging also shows that there are differences in the dehydration kinetics

between active and arrested lesions. This study demonstrates two independent imaging methods that can be used to monitor changes in lesion activity over time.

5.2 Introduction

The accurate assessment of lesion activity is essential for the effective clinical management of caries lesions. Caries lesions are arrested by the preferential deposition of mineral at the lesion surface that forms an outer layer of higher mineral content that serves as a barrier to the further diffusion of fluids into the body of the porous lesion [115-117]. The highly mineralized outer surface zone or transparent surface layer (TSL) can be detected using transverse microradiography (TMR) and polarized light microscopy (PLM) that require destruction of the tooth, or in the case of microcomputed tomography cannot be used *in-vivo*. Early occlusal caries is diagnosed by visual-tactile methods. Radiographs are not effective for early caries lesions that have not penetrated deep into the underlying dentin due to the overlapping topography of the crown. For pit and fissure caries, the tactile method via probing with an explorer showed low sensitivity and has been found to be unreliable in its diagnosis [118]. The occlusal pits and fissures are often heavily stained obscuring early demineralization and often leading to false positives via visual diagnosis [119-121].

New non-destructive diagnostic tools are needed that can assess lesion activity in a single visit and monitor changes in the activity of the lesions over time during nonsurgical intervention. Several studies have shown that short wavelength infrared (SWIR) imaging methods such as optical coherence tomography (OCT) at 1310-nm and time-resolved reflectance imaging at wavelengths greater than 1400-nm can be used to assess remineralization and lesion activity [49, 51, 61, 101,

122]. The purpose of this study is to test the hypothesis that both of these SWIR imaging methods can detect changes in lesion activity over time *in vivo*.

When lesions become arrested by mineral deposition in the outer layers of the lesion forming a highly mineralized surface zone, the diffusion of fluids into the lesion is inhibited. Therefore, the rate of water loss and the evaporation dynamics can be related to changes in lesion structure and porosity. Changes in fluorescence loss [123-125], thermal emission and SWIR reflectance [9, 49, 82, 101, 126-128] have been investigated as methods for assessing lesion severity and activity. Normal enamel is transparent at SWIR wavelengths, whereas early demineralization causes increased SWIR reflectance due to scattering [111]. Water in the pores at the surface of the lesion absorbs the incident SWIR light, particularly at wavelengths greater than 1400-nm, reducing surface scattering and lesion contrast [4, 70]. Loss of that water due to evaporation produces a marked increase in reflectivity and lesion contrast. *In-vivo* studies have been reported utilizing the fluorescence loss of white spot lesions on coronal surfaces [125] and thermal imaging to assess root caries during dehydration [129]. This study is the first clinical study to employ SWIR reflectance imaging during lesion dehydration to assess lesion activity.

Optical coherence tomography (OCT) can provide high resolution cross-sectional images of lesion structure non-invasively [59, 130]. Polarization-sensitive OCT (PS-OCT) and cross polarization OCT (CP-OCT) utilize the polarization properties of back-reflected light to obtain additional contrast in OCT images and reduce the interference of the strong reflections that occur at tooth surfaces [131-134]. *In vivo* studies using CP-OCT were able to accurately detect both early and severe occlusal lesions that were not visible on radiographs [7, 104].

Several studies have demonstrated that CP-OCT is able to monitor remineralization on tooth surfaces by detecting the formation of the highly mineralized transparent surface layer (TSL) on the lesion surface and a decrease in the integrated reflectivity over the lesion depth (DR) after exposure to a remineralization solution [61, 122, 135]. *In vitro* studies have shown that the presence of even a thin TSL of less than 20-µm in CP-OCT images reduces lesion activity significantly [56]. Removing the TSL on the lesions of extracted teeth in turn produces a corresponding rise in the permeability providing further confirmation of the role of the TSL in arresting lesions [136]. Methods have been developed to automatically measure the thickness of the TSL and DR from CP-OCT images [62, 75]. In a previous *in vivo* study, CP-OCT was used to monitor changes in the activity of smooth surface enamel lesions on permanent teeth [51]. Even though the test subjects recruited were required to have active lesions based on conventional visual/tactile assessment, CP-OCT imaging indicated that most of the lesions (62/63) had TSLs at baseline suggesting they were already arrested. CP-OCT images indicated there was no significant increase in lesion severity (DR) for those lesions measured after 30 weeks providing further confirmation they were indeed arrested. Primary teeth were chosen for this study to ensure that a higher percentage of the lesions would be initially active rather than arrested to demonstrate that changes in lesion severity and activity can be successfully monitored. In addition, lesions progress more rapidly in primary teeth than in permanent teeth due to the thinner layer of enamel requiring more frequent monitoring.

5.3 Materials and Methods

5.3.1 Participant Recruitment and Procedures

Study participants (n=30 with 60 primary molars) aged 6-10 were recruited from the UCSF Pediatric Dentistry clinic by the study investigators (UCSF IRB 18-25927). One participant was lost to follow-up after the first visit and was excluded from the study. A total of 29 participants (n=29 with 58 primary molars) completed the study. Participants were required to have at least two primary teeth with suspected pit and fissure caries. Lesions with obvious cavitation, existing restorations covering the pits and fissures or severe enough to require restorative treatment were rejected.

All 58 lesions were visually scored as a 1 in severity according to the International Caries Detection and Assessment System (ICDAS) [16]. CP-OCT and SWIR imaging showed that 6 of the lesions were likely false positives since no demineralization was observed in the images at any of the 3 time-points. Color images of each tooth were acquired at the initial visit and at month-6 using a FocusDent MD740 (Vilnius, Lithuania)1280x960-pixel intraoral camera. Fluoride varnish was applied to all lesions at 3-month intervals over a period of 6-months to promote remineralization. In addition, the participants were given a fluoride toothpaste with 0.76% monofluorophosphate and instructed to brush twice a day.

5.3.2 Time-Resolved SWIR Reflectance Imaging at 1400-1750-nm

An image of the fully assembled SWIR reflectance imaging device is shown in **Fig. 5.7.1A** along with diagrams of the 3D printed probe and it's components. The reflectance probe was designed in Fusion 360 from Autodesk (San Francisco, CA) and 3D printed using a Form 3 printer from

Formlabs (Boston, MA). The reflectance probe body consists of a right-angle aluminum mirror to collect light from the occlusal surface and an attachment for the reflectance fiber [137]. A low-OH optical fiber of 1-mm diameter fiber is inserted into a cylindrical Teflon plug (3.2x40-mm). Light exiting the plug is directed toward the tooth occlusal surface. There is an air nozzle attached to the reflectance body near the mirror to prevent fogging of the mirror and dehydrate the lesion surface to assess lesion activity [9, 49, 101]. The SWIR reflectance images were captured using a 640x480-pixel micro-SWIR camera (SU640CSX) measuring only 32x32x28-mm from Sensors Unlimited (Princeton, NJ). Two planoconvex antireflection coated lenses of 60 and 100-mm focal length along with an adjustable aperture were placed between the handpiece and the InGaAs camera to provide a field of view of 11-mm^2 at the focus plane. SWIR light from a compact tungsten halogen lamp Model SLS201 from Thorlabs (Newton, NJ) with a 1400-nm long-pass filter illuminated the occlusal surfaces.

Images were recorded at 4-Hz for the 30-second time window at 0 and 6-months and imported into MATLAB (Natick, MA) for further analysis. Profiles of intensity versus time were extracted from the mean intensity of a 5x5-pixel region of interest (ROI) that was manually selected. Lesions were designated as active or arrested based on the presence of a transparent surface zone (TSL) from the corresponding CP-OCT images. Unpaired t-tests were used to compare SWIR data between suspected arrested and active lesions.

5.3.3 Cross Polarization Optical Coherence Tomography (CP-OCT)

The cross-polarization OCT system used for this study was the Model IVS-3000-CP purchased from Santec (Komaki, Aichi, Japan). It operates at a wavelength of 1321-nm with a bandwidth of 111-nm (11.4-μm axial-resolution) and it is capable of acquiring complete tomographic images

6x6x7-mm in approximately 3-seconds. Images of the CP-OCT handpiece are shown in **Fig. 5.7.1B**. It has been used for multiple *in vivo* caries imaging studies [7, 51, 134].

An appliance made of autoclavable Dental SG resin printed using a 3D printer, Formlabs 2 (Somerville, MA) was placed on the distal end of the OCT scanning handpiece and the handpiece was covered with polyethylene film for infection control. Air at 10-psi was connected to the appliance to prevent fogging of the imaging window. Images were imported into Dragonfly from ORS software (Montreal, CA) for co-registration and analysis. A 3D Median filter was applied to reduce speckle noise in the images followed by 3D image registration to superimpose the lesion areas for all three visits. Images from the same sample at different visits also went through intensity normalization before quantitative measurement. The integrated reflectivity over the lesion depth (ΔR) which best represents the lesion severity was calculated by positioning a box within the lesion dimensions, calculating the mean pixel intensity in the box and multiplying by the lesion depth. Lesion depth (Ld) was measured on the registered lesion areas at the position of the maximum depth of the lesion. Lesion activity was evaluated as binary (arrested or active) based on detection of a TSL after image-processing. The TSL was measured along a ruler drawn at the center of the lesion orthogonal to the surface. All arrested lesions have TSLs measured as the distance between two adjacent intensity peaks (surface reflection from top of TSL to lesion underneath) measured after filtering. Statistical comparisons between suspected active and arrested lesion areas were performed in GraphPad Prism (San Diego, CA). RM-ANOVA with Tukey-Kramer multiple comparisons test was used to compare the CP-OCT data at 0, 3 & 6-months.

5.4 Results

Out of the 30 test subjects recruited, 29 test subjects completed the study. Suspected lesions on two teeth were monitored on each test subject. Six of the remaining 58 lesions were determined to be sound since no lesions were visible in the CP-OCT images at any time points. A further 10 lesions were disqualified due to the inability to co-register the CP-OCT lesions at all three time-points yielding an CP-OCT sample size of 42 lesions. Visual monitoring indicated no changes in ICDAS scores for any of the lesions after 6-months.

Color and CP-OCT images extracted from two suspected active lesions, one that remained active and progressed further in depth and severity and a second lesion that became arrested are shown in **Fig. 5.7.2**. The first lesion shows an increase in Ld and DR over six months with no transparent surface layer (TSL) visible at the surface. CP-OCT images show a continual advance of the lesion in depth and area over time. In the second lesion example, a TSL is clearly visible at 3-months and after 6-months and the depth of the lesion has not appeared to increase significantly suggesting that it progressed from an active to arrested state (became arrested). The color images in **Fig. 5.7.2** show no changes in appearance between 0 and 6-months for either lesion.

Three parameters were calculated for each of the 42 lesions at each of the three time points from the CP-OCT data. The lesion depth in microns (Ld), the lesion reflectivity integrated over the lesion depth (DR) and the thickness of the transparent surface zone (TSL) in microns. The mean$\pm$s.d. for each measurement are plotted in **Fig. 5.7.3**. There were significant increases ($P<0.05$) in the mean Ld and DR over the 6-month period for the 42 lesions. This suggests that most of the 42 lesions remained active and progressed in severity over the 6-month period. There were large increases in the mean TSL thickness for each 3-month period indicating that several of

the lesions did indeed become arrested or remained arrested. At 6-months 14 of the 42 lesions manifested a distinct TSL indicating they were arrested. Six of the lesions had a TSL at month-0 and all 6 retained that surface zone over 6-months. The mean TSL thickness increased from 21±25(baseline month-0) to 115±51(month-6). Eight additional lesions formed new TSL's over 6-months and the TSL thickness increased significantly for the 6 arrested lesions from 49±12(month-0) to 150±43(month-6). Of the 14 lesions that had measurable TSLs at 6-months all 14 showed decreases in lesion severity (DR) from 0 to 6-months.

Analysis of the SWIR reflectance images at 0 and 6-months was more difficult than anticipated and only 48 of the 116 acquired videos were processed. Two parameters were calculated from the acquired time vs. intensity curves, the change in intensity with drying (DI) and the initial delay before the rise in reflectivity (DEL). The 48 SWIR videos were separated into two groups defined as active and arrested based on the absence or presence of a TSL on the lesion. Due to the low number of lesions with TSLs, month-0 and 6 SWIR reflectance images were pooled together to yield 8 arrested videos and 40 active videos. For the mean±s.d. DEL there was a large and significant difference ($P<0.05$), 16±8.9-sec vs 4.3±5.1-sec for active vs arrested lesions. For active lesions (DI) was higher, 18±11 vs 13±11 for active vs arrested lesions but the difference was not significant, ($P>0.05$).

Fig. 5.7.4A shows time-sequenced SWIR images of matched areas of the occlusal surface recorded during the 30 seconds of drying at 0 and 6-months. There is a very small lesion in the occlusal pit that was active at baseline and arrested at month-6 that can be seen in the CP-OCT images shown in **Figs. 5.7.4B** along with color pictures of the area imaged in the SWIR. Profiles of the SWIR reflectance intensity are shown in **Fig. 5.7.4C** extracted from the lesion area and a peripheral sound

area during drying. The "active" lesion (month 0) shows a large delay of more than 20-seconds before a rapid rise in reflectivity as expected for an active lesion. The arrested lesion (month 0) manifests almost no delay before a more gradual rise in reflectivity as expected for an arrested lesion. However, since the rise in reflectivity occurs very late for the month-0 curve it is unclear whether all the changes in that curve were captured in the 30-seconds that were recorded.

5.5 Discussion

This study was successful in recruiting a majority of test subjects with active lesions by choosing recently erupted primary teeth. Even though only a small number of those lesions that were initially active became arrested after 6 months with "lesion arrest" defined as the formation of a TSL measurable using CP-OCT, the number was sufficient to show a statistically significant increase ($P<0.0001$) in the TSL thickness over time. Comparison of this study consisting of mainly "active" lesions in which no TSL was present at baseline (36/42) with a previous study on permanent teeth where most lesions (62/63) had TSLs at baseline and there were no significant changes in lesion severity over 30-wks [51] provides further confirmation that the TSL thickness is a key objective indicator of lesion activity. Furthermore, the TSL thickness provides a measure of the lesion activity that can be made at a single time-point. The mean TSL thickness for the 63 lesions at month-6 from the previous study was 184 ± 56 compared to 115 ± 51 for this study. The thickness was significantly higher ($P<0.0001$, unpaired t-test) for the lesions on the permanent teeth in the previous study as would be expected for lesions that had a greater time to undergo remineralization. This is consistent with previous studies of age-related differences in lesion structure based on histopathology [117].

These two studies also show the poor reliability of visual/tactile indicators of lesion activity and severity such as color and texture. Active lesions were a recruitment criterion for both studies and out of the 111 primary and permanent teeth recruited for the two clinical studies only 37 were active according to CP-OCT imaging, 6 were sound and 69 were arrested and those 76 sites manifested no further change increase in severity over 6-months while the other suspected active lesions ether progressed in severity (n=28) or became arrested (n=7). Moreover, visual monitoring with ICDAS indicated no changes in any of the lesions over 6-months for either study further confirming the low sensitivity of conventional visual monitoring.

In this study, there was a significant increase of the lesion depth (Ld) and the integrated reflectivity (DR) over the 6-month period suggesting that most of the lesions did not become arrested and actually progressed in severity. *In vitro* studies suggest that DR should decrease if all of the lesions become arrested and undergo major remineralization [61, 122, 135]. As mineral is deposited into the lesion due to remineralization the overall reflectivity of the lesion decreases yielding a net decrease in DR. However, we observed TSL's in only 14 of the 42 lesions at 6-months indicating that only 1/3 of the lesions underwent enough remineralization to appear arrested. Therefore, the increases in DR and Ld are consistent with the majority of lesions remaining active during the duration of the study.

This was the first clinical study in which SWIR reflectance imaging was employed to assess lesion activity. Based on *in vitro* studies it was anticipated that (DI) the overall change in intensity would be significantly higher for active lesions versus arrested lesions [49, 56, 138, 139]. However, the time required for drying was much higher than encountered for *in vitro* studies and many of the active lesions did not sufficiently dry in 30-seconds [139]. This influenced the ability to observe

the full change in intensity for accurate calculation of (DI). For example, in **Fig. 5.7.4C** the rise in intensity did not occur until after 20-seconds so it is unlikely that the DI calculated from that curve is reliable. The dehydration curves were also much noisier than expected making curve fitting difficult. These problems can be addressed in future studies by further increasing the air pressure and by further optimization of the air flow geometry in the probe to better penetrate the occlusal fits and fissures. The delay in the onset of the intensity change (DEL) appeared to be a better indicator of lesion activity than DI for this study. This onset delay (DEL) was ignored in early *in vitro* studies and was only recently discovered to be an indicator of lesion activity [49, 56, 138, 139]. For active lesions there are exposed pores in the outer layer of the lesion, when those pores are filled with fluid they absorb the SWIR light lowering the reflectivity from the lesion. When the fluid is removed from the pores during drying the reflectivity rises. Arrested lesions have an outer highly mineralized TSL of low porosity with minimal fluid present between the lesion body and the surface so there is minimal delay before there is a rise in reflectivity during drying [139]. It appears that this onset delay (DEL) is a good indicator of lesion activity that can be easily measured *in vivo*. It is desirable to be able to extract multiple indicators of lesion activity from the SWIR reflectivity versus time curves during drying as has been possible in *in vitro* studies where the curves were fit to extract additional information about the rate of increase in the reflectivity [139], not just DEL and DI as was done in this study and we plan on further development of the SWIR reflectance imaging handpiece for more rapid dehydration of the lesions.

Both OCT and SWIR imaging was done in contact with the tooth surface too minimize motion artifacts. Even so, several scans had to be repeated due to excessive movement during scanning for both OCT and SWIR reflectance imaging. In the case of SWIR imaging many of the image frames had to be corrected due to slight movement during the 30 seconds.

This study was not intended to be a clinical trial of fluoride varnish, therefore a non-fluoride varnish control group was not used. Fluoride varnish was applied because it was the standard of care for patients of high caries risk and it was likely to increase the probability that more active lesions would undergo remineralization and become arrested.

5.6 Conclusion

This was the first clinical study to monitor changes in lesion structure and activity in primary teeth over time *in vivo* using CP-OCT and SWIR Imaging. The formation of a TSL at the surface of active lesions indicative of lesion arrest was observed using CP-OCT on multiple lesions. In addition, this was the first clinical study to use SWIR reflectance imaging to show differences in the dehydration dynamics between active and arrested lesions.

5.7 Tables and Figures

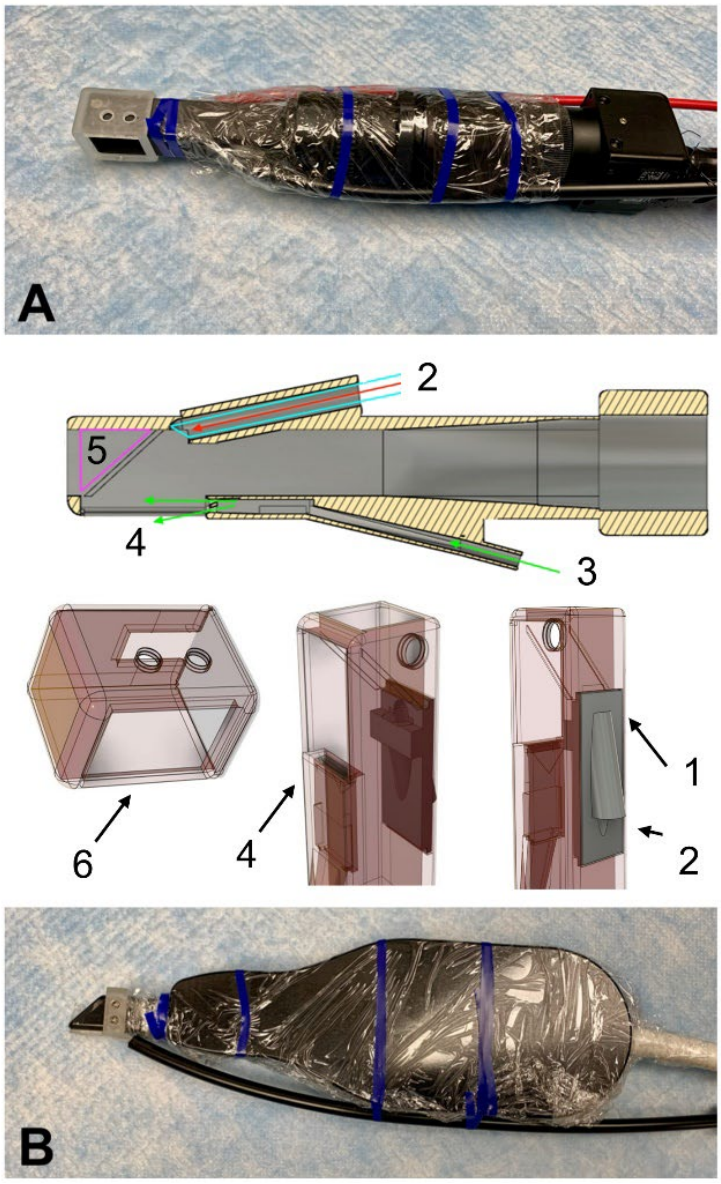

Figure 5.7.1. (A) Image of the fully assembled SWIR imaging handpiece that consists of three 3D printed autoclavable attachments, a 1 mm in diameter optical fiber for delivery of the SWIR light, an air nozzle and an assembly of two lenses, an adjustable iris that is attached to the miniature InGaAs camera. Labeled diagrams of the probe body and 2 additional 3D printed components are also shown, where (1) is a 3D attachment that snaps into the probe body and holds the optical fiber and the Teflon pug that is inserted into the opening at (2), air enters the nozzle at (3) and exits at (4). The mirror attaches at (5) and another 3D printed component fits over the end of the probe body and makes contact with the tooth surface and functions as a bite block (6). Images of the CP-OCT handpiece are shown in (B) with an attached 3D printed autoclavable appliance with air nozzle.

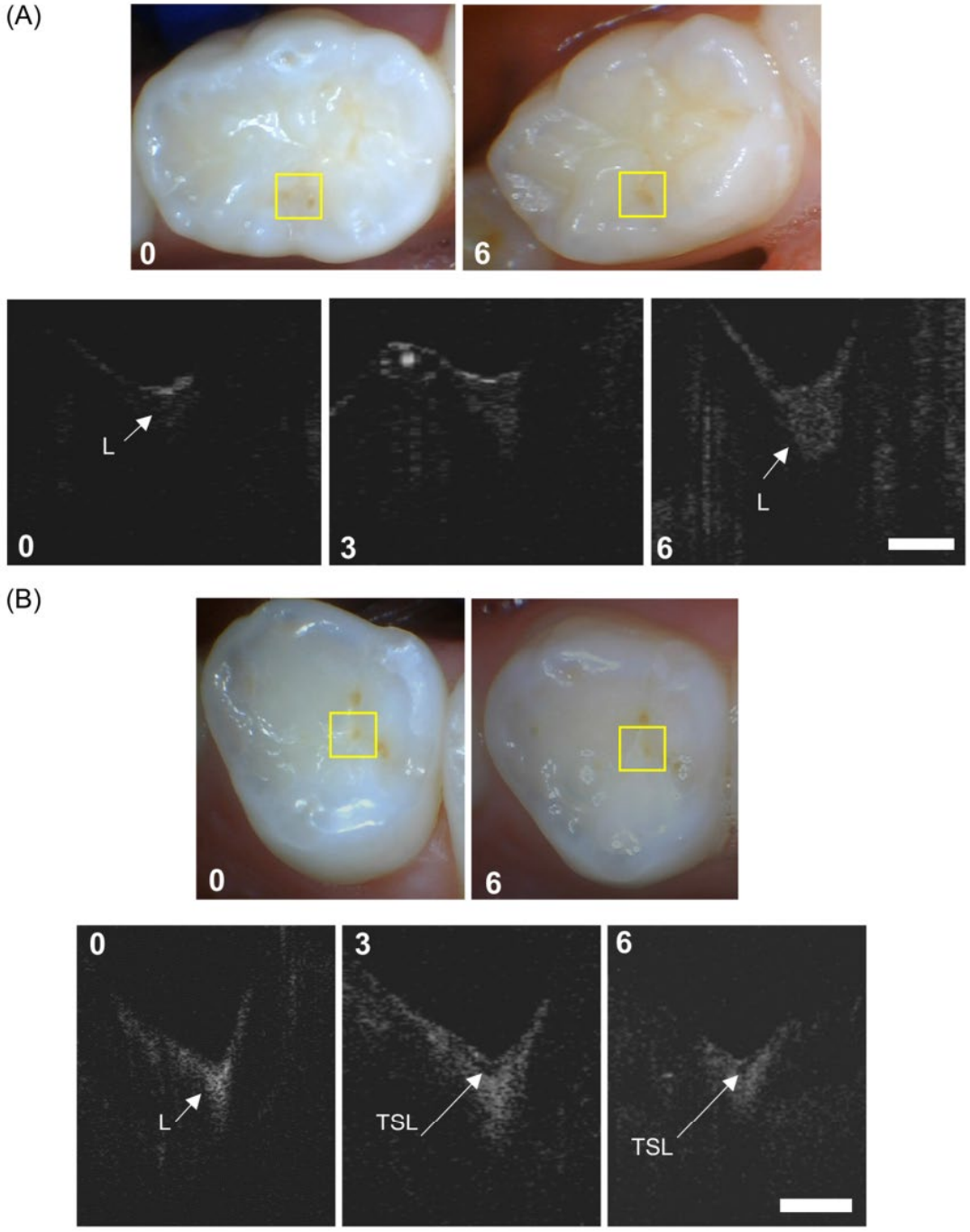

Figure 5.7.2. (A) Color and raw CP-OCT images of a suspected active lesion at 0, 3 and 6-months that remains active and progresses in severity. The position of the lesion in the color images is indicated by the yellow boxes. The lesion (L) is indicated in the CP-OCT b-scans at each time-point and the white bar represents a distance of 500-mm. No TSL was detected for this lesion. (B) Color and CP-OCT images of a suspected active lesion at 0, 3 and 6-months that appears to become arrested with the formation of a TSL at 3-months.

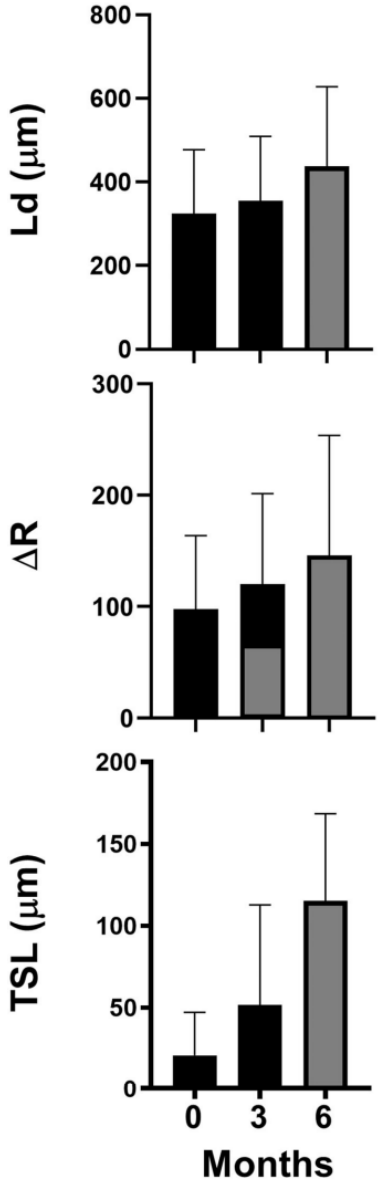

Figure 5.7.3. Plots of the measured mean± s.d. of the lesion depth (Ld) in microns, integrated reflectivity over the lesion depth (DR) in arbitrary units (n=42) and the transparent surface zone thickness (TSL) in microns (n=14) at 0, 3 and 6-months. Only the 14 lesions that had TSLs at 6-months are included for the TSL thickness. Bars containing the same color in each plot are statistically similar, RM-ANOVA with Tukey-Kramer multiple comparison test with (P>0.05).

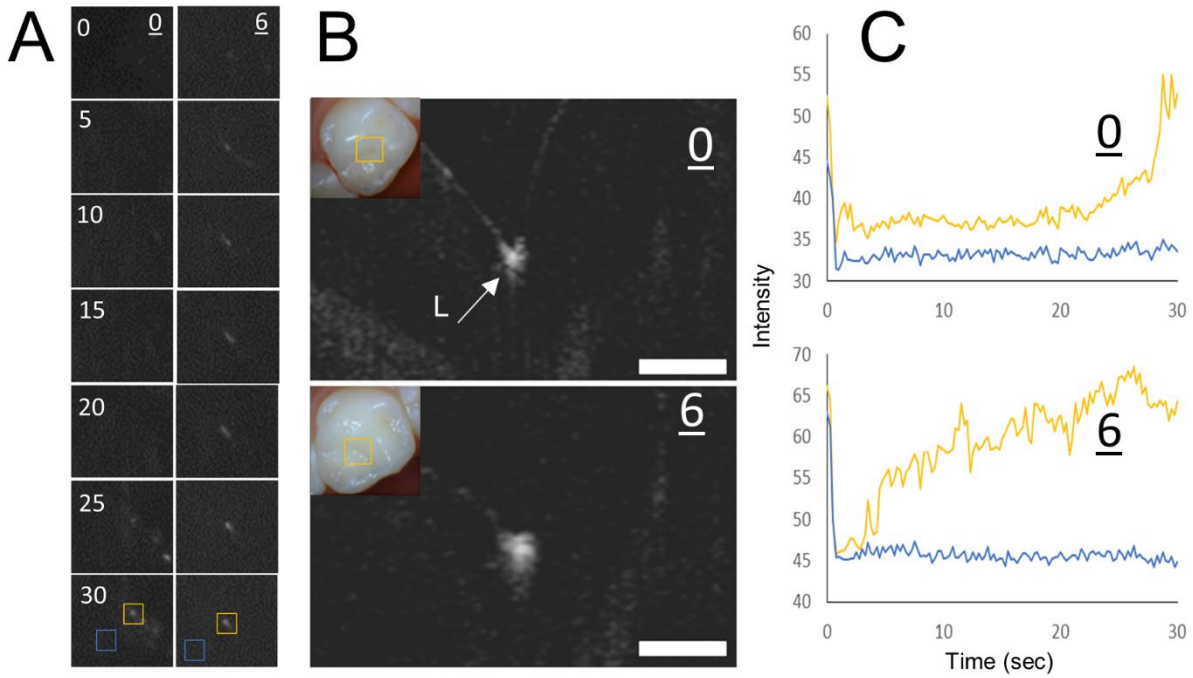

Figure 5.7.4. **SWIR reflectance and CP-OCT images of another suspected active lesion that appears to become arrested at 6-months**. (A) Time-sequence SWIR images of the lesion area from 0 to 30 seconds at 0 and 6-months are shown during drying. Lesion area is in yellow box and sound area is in the blue box. (B) CP-OCT scans at 0 and 6-months show a small pit and fissure lesion (L), the white bar represents 500-mm. Color images of the occlusal surface at 0 and 6-months are inset in each image and the lesion area monitored by SWIR is indicated by the yellow box. (C) The SWIR reflectance intensity is plotted between with time at 0 and 6-months at the lesion position shown by the small yellow boxes inset in the SWIR images at 30-seconds (yellow) and for adjacent sound areas (blue).

CHAPTER VI

Active Surveillance of Root Caries *in Vivo* with CP-OCT

6.1 Summary

Active surveillance of root caries lesions to monitor potential remineralization or decay progression is challenging for the clinician due to unreliable diagnostic information. Conventional visual and tactile methods for assessing lesion activity are not reliable and the clinician is often unable to determine if the lesion is progressing or has been arrested. An important marker of an arrested lesion is a highly mineralized transparent surface zone (TSL) that forms when mineral is deposited in the outer layer of the lesion. The purpose of this study was to determine if cross polarization optical coherence tomography (CP-OCT) could be used to detect changes in lesion severity and activity during active monitoring. Eighteen subjects with 22 suspected active root caries lesions were evaluated using CP-OCT at baseline, 3 and 6 months. All subjects were instructed to use a high fluoride dentifrice at baseline. Results showed that CP-OCT was able to discriminate active from arrested lesions by identifying the presence of a TSL on arrested lesions. Results also indicated the mean TSL thickness increased significantly ($P<0.05$) for 9 lesion areas. In addition, CP-OCT was able to show the progression of demineralization, erosion and changes in gingival contours in scanned areas. CP-OCT was valuable for monitoring the activity and severity of root caries lesions *in vivo*. CP-OCT can be used to assess the activity of root caries lesions at a single time point by detecting the presence of a TSL at the lesion surface indicative of lesion arrest.

6.2 Introduction

Root caries remains a clinical concern, especially in the elderly [90]. Management remains challenging because the clinical diagnosis of root caries is subjective and is based on visual and tactile parameters. In contrast to coronal caries, root caries lacks a valid diagnostic standard, such as radiography [140]. Investigators have not developed a reliable relationship between root caries

appearance and activity [53, 141]. Most experts agree that active root lesions are soft, yet tactile hardness assessments remain subjective and lack reliability [53]. Multifactorial root caries scoring systems have been developed with mixed success [142, 143]. The International Caries Detection and Assessment System (ICDAS) coordinating committee proposed a system for assessing lesion activity [17, 142]. Criteria include: color; texture (smooth, rough); appearance (shiny, dull); tactile (soft, leathery, hard); loss of anatomical contour; and proximity to the gingival margin [144, 145]. Histological analyses for lesion assessment such as microradiography require destruction of the tooth and are not suitable for use *in-vivo*. Optical coherence tomography (OCT) is a noninvasive technique for creating cross-sectional images of internal biological structure and is well suited for imaging coronal and root surfaces *in vivo* [59, 130, 146]. Polarization sensitivity has proven to be valuable for enhancing the contrast of demineralization, reducing the strong specular reflection from tooth surfaces and measuring birefringence [60, 132, 147]. Studies have demonstrated that CP-OCT can be used to quantify the loss of cementum and the severity of demineralization on root surfaces [73, 148]. OCT can be used to discriminate between non-carious cervical lesions and root caries *in-vivo* [149]. Importantly, CP-OCT can be used to monitor the formation of a highly mineralized transparent surface layer (TSL) on demineralized dentin after exposure to a remineralization solution [9, 73]. The optical changes associated with lesion dehydration have been investigated via thermal, fluorescence, and SWIR imaging for lesions on enamel surfaces [125-128, 150]. Thermal imaging during lesion dehydration has been used to measure the lesion permeability [9, 49, 101, 129]. Decreased thermal emission from the lesion surface is indicative of reduced permeability and drying rate that is consistent with an arrested lesion. During drying lesion areas will cool due to the loss of water from porous areas and from the collapsed and unsupported collagen matrix of the demineralized cementum and dentin. Arrested lesions have

mineral filling the pores at the lesion surface due to remineralization and the formation of a TSL inhibits water diffusion and permeability, resulting in less temperature change and shrinkage during drying. Lesions with a TSL have significantly lower thermal emission [3, 25, 32].

In a recent study, CP-OCT and thermal imaging were used to assess the activity of root caries lesions on 30 test subjects [129]. In that study CP-OCT was used to measure the lesion structure and the presence of TSL formation indicative of arrested lesions at a single time point. The activity of those lesions was confirmed with thermal imaging. The next step is to consider if CP-OCT can detect changes in lesion activity over time during active monitoring. The purpose of this study was to monitor root caries lesions over a period of 6 months to determine if CP-OCT could be used to detect changes in lesion severity and activity. Subjects with root caries lesions that were clinically diagnosed as active were prescribed a high fluoride dentifrice and monitored from baseline to 6 months.

6.3 Materials and Methods

6.3.1 Participant Recruitment and Procedures

Thirty test subjects at the UCSF comprehensive clinics were recruited for this study (UCSF-IRB 18-25927). This study was a single-site longitudinal observational clinical study. Test subjects were aged 18-90 and had one root caries lesion that was diagnosed as active based on visual and tactile assessment by an experienced clinician using the ICDAS II root caries lesion activity criteria [17]. Test subjects were prescribed and instructed to use a high flouride (5000 ppm) dentifrice, Prevident 5000 Plus (Colgate, NY). Test subjects were imaged at baseline, 3 and 6 months with CP-OCT after beginning brushing with high fluoride toothpaste. Color images were acquired at baseline and 6 months using a FocusDent MD740 (Vilnius, Lithuania)1280x960-pixel intraoral

camera. The sample size of 30 was based on an *in vitro* study of the remineralization of simulated dentin lesions, the mean transparent surface layer (TSL) thickness increased from 0 to 53.8±13.3 μm after 12 days of remineralization [9]. Therefore, based on an average SD of 6.65-μm for TSL thickness with a 2-sided significance level of 0.05, a study with 30 subjects would have a 90% power to detect an increase in TSL thickness of 5.7 μm.

6.3.2 Cross Polarization Optical Coherence Tomography (CP-OCT)

The cross-polarization OCT system used for this study was the Model IVS-3000-CP purchased from Santec (Komaki, Aichi, Japan). This system acquires only the cross-polarization image (CP-OCT), not simultaneous cross and co-polarization images (PS-OCT). This is a 3D system with a right-angle dental handpiece capable of acquiring complete tomographic images of a volume of 6x6x7-mm in approximately 3 seconds. This system has been used for multiple *in-vivo* caries imaging studies [7, 51, 134]. This system operates at a wavelength of 1321-nm with a bandwidth of 111-nm with a measured resolution in air of 11.4-μm.

An attachment with an internal air nozzle made of autoclavable Dental-SG resin was printed using a Formlabs 3D printer (Somerville, MA) and attached to the OCT scanning handpiece. Air at 10-psi was connected to the probe to prevent fogging of the mirror and to dry the tooth surface. Images were acquired after drying for 30 seconds. Images of the CP-OCT handpiece are shown with and without the 3D printed attachment in **Fig. 6.7.1**. The entire handpiece assembly was covered with polypropylene film for infection control prior to imaging as shown in **Fig. 6.7.1**. Entire (3D) CP-OCT cross polarization images of each lesion were acquired at each of the three timepoints and co-registered using Dragonfly from ORS (Montreal, Canada) software using the sum of squared differences method. Image processing was also applied using MATLAB (Natick, MA) with modifications from previous *in-vitro* studies to despeckle the images [8, 138]. Image segmentation

was first performed with 90% intensity thresholding, followed by application of a 3D median filter with a kernel size of 3 for noise reduction while preserving the potential transparent surface layer (TSL). Lesion areas were selected and a ruler was placed perpendicular to the surface of each lesion area. For quantitative measurement, the diameter of the ruler was modified to 100 micrometers to form a cylinder along the z-axis, and the intensity profile along the z-axis was chosen to display the average intensity of a slice of the cylinder along the ruler. Positive TSL detection was confirmed with two significant consecutive intensity peaks detected at the beginning of the ruler, and TSL thickness was measured as the distance between the two peaks. Lesion depth (Ld) was measured as the overall length of the ruler's non-zero intensity profile. To prepare for integrated reflectivity (ΔR) measurement, an intensity histogram of the cylindrical ruler was exported from Dragonfly, and analyzed with a custom-Matlab script to identify the median intensity over the lesion depth that was later used as a intensity normalization correction factor. Each OCT scan has a different intensity profile due to the variation in the angle and position of imaging and other environmental factors, so normalization was necessary for accurate ΔR comparison across all 3 co-registered images. ΔR was then calculated as the sum of the intensity over the lesion depth divided by the normalization correction factor.

6.4 Results

In this study, only 22 of the 30 test subjects initially recruited completed all three visits. The COVID-19 pandemic greatly interfered with the study. Test subject visits at UCSF for clinical studies considered nonessential for patient health were banned during part of the pandemic. Images from 18 of the test subjects were successfully co-registered, while data from 4 of the test subjects were discarded due to the inability to co-register the images at baseline, 3 and 6 months.. Four

subjects presented with both clinically appearing active and arrested caries on the same tooth based on the presence of a transparent surface zone (TSL), so that twenty two lesion areas were included for analysis from the 18 test subjects. Eight of the lesion sites were arrested at baseline as shown by a visible TSL and only one active lesion became arrested during the 6 months of the study according to CP-OCT. Therefore, nine of the 22 lesion sites had a measureable TSL at month 6 indicating those lesion areas were arrested. Interestingly, many of the arrested lesions showed an increase in the TSL thickness from baseline to 6 months.

All the lesions were initially classified as active lesions based on clinical assessment and the multiple ICDAS II lesion activity criteria. Of the 22 lesion sites analyzed 8 were dark and 14 were light colored at baseline and 10 appeared rough and 12 appeared smooth. Digital images of the lesions at baseline and 6 months were shown to two clinicians after completion of the study and they were asked to score the caries status and activity of the lesions at the two time points based on digital photographs. **Table 6.7.1** is a contingency table comparing the caries status (caries present or not present) and caries activity (active and arrested) assessed by visual examination of the images with CP-OCT assessment in which the presence of a TSL indicated the lesion was arrested while the presence of demineralization without a TSL indicated an active lesion. CP-OCT indicated that demineralization was present for all lesion sites confirming root caries presence.

The diagonal elements (bold) of the contingency table show the number of visual assessments that match CP-OCT analysis. At baseline, 9 of the 14 active lesions were visually classified correctly while none of the 8 arrested lesions were correctly visually classified as arrested. At month 6, only 5 of the 13 active lesions were visually classified correctly while none of the 9 arrested lesions

were correctly visually classified as arrested. The two lesions that were classified as arrested by the clinicians at month 6 were shown to be active in CP-OCT images at month 6.

An example of an arrested lesion with minimal change after 6 months is shown in the color and CP-OCT images of **Fig. 6.7.2**. In the color images the lesion area looks similar, however the exposed root surface appears to have decreased due to growth of the gingival margin. A surface rendering (3D) of the entire CP-OCT scan taken at baseline is also shown with the yellow line showing the position of the extracted CP-OCT b-scans. The CP-OCT scan at baseline shows the gingiva on the left and the exposed root surface on the right. The lesion appears with a lesion body of higher intensity covered by a thin transparent layer (dark zone) that indicates the TSL. The TSL has a very thin layer of higher intensity that represents reflectance from the tooth surface. The lesion does not appear to change in depth or severity after 6 months.

A second lesion that is active with advancing cavitation is shown in **Fig. 6.7.3**. In the color image a shadow is visible just above exposed lesion area at baseline and that area is no longer visible at month 6. It is hard to determine from the color images whether or not the lesion area is larger. The surface renderings of the CP-OCT scans that are shown at baseline and 6 months show that the area of caviation is larger and that the area near the top of the lesion has collapsed. The CP-OCT scan at baseline extracted at the position of the yellow line shows the gingiva on the left and a cavitated lesion area on the right along with the mostly transparent sound enamel. A small lesion area (LB) is visible just below the enamel demarcated by the orange arrows. That lesion area between the orange arrows becomes cavitated after 6 months in the lesion area. The depth lost was measured to be 151-µm from 0-3 months and 296-µm from 3-6 months.

A third representative lesion that appears initially active at baseline and appears to become arrested at month 6 is shown in **Fig. 6.7.4**. The color images show little change after 6 months. The CP-OCT b-scan at baseline extracted at the position of the yellow line in the CP-OCT surface rendering shows a highly reflective slightly cavitated active lesion located between the enamel and the gingiva. In this scan the gingiva is on the right and the enamel is on the left. The lesion also extends into the enamel above the exposed root surface. Between baseline and month 6 the reflectivity of the lesion body decreases from both the enamel and dentin lesion (exposed root) areas and a distinct TSL forms over the lesion.

A fourth lesion is shown in **Fig. 6.7.5**. Color images show a large area of the exposed root surface at baseline that becomes almost completely covered by inflamed gingiva after 6 months. CP-OCT surface renderings also shown at baseline and 6 months show dramatic hypertrophy of the gingival tissues. CP-OCT b-scans extracted at the position of the yellow line show that the tooth is covered by a crown and that there is an exposed cavitated area of the root surface located between the gingival (left) and the crown (CR) on the right located between the two orange areas. The CP-OCT scan also shows that there is some shallow demineralization on the exposed root surface, but it's localized and very shallow. The month 3 and 6 CP-OCT scans show that the gingiva expands to cover much of the exposed root surface and that the lesion is much smaller at month 6. The lesion depth, integrated reflectivity over the lesion depth (ΔR), and the thickness of the transparent surface zone if present (TSL) were measured from the co-registered CP-OCT scans. Values were calculated for 22 lesion areas from 18 teeth and the mean ± s.d. are plotted for all three values in **Fig. 6.7.6**. Both the mean lesion depth and mean DR increased slightly from baseline to month 6 but the changes were not significant ($P > 0.05$), n=22. The mean TSL thickness increased from

baseline to month 6 and the increase was significant ($P < 0.05$) for the nine lesion areas that showed measurable TSLs.

6.5 Discussion

The goal of this study was to demonstrate that CP-OCT could monitor changes in lesion activity and severity over time during active monitoring. We anticipated to see initially active lesions in the CP-OCT images with no TSLs at baseline transition to arrested lesions with TSLs at month 6. Unfortunately, only 1 of the 22 lesion sites exhibited that ideal behavior. It is disappointing that most of the lesion sites did not improve with the use of 1.1% NaF, however it is important to point out that this study was not a clinical trial on the remineralization performance of high fluoride dentifrices nor could we control the compliance and hygiene of the participants. CP-OCT was able to show changes in many of the lesions over time and this study demonstrated that those lesion sites that appeared initially arrested with the presence of a measurable TSL did not progress further in lesion severity. Therefore, the presence of a measurable TSL present on the lesion in CP-OCT images appears to be a key indicator that the lesion is arrested and did not progress during the six month study. CP-OCT detected the presence of a TSL in a single measurement so lesion activity could be assessed at a single time point *in vivo*. The use of the highly mineralized transparent surface zone as our "benchmark" for an arrested lesion surface is supported by several *in vitro* and *in vivo* studies and the histopathology of active vs arrested lesions [51, 61, 151]. Before the introduction of optical coherence tomography, a tooth had to be extracted, sectioned and imaged with polarized light microscopy or transverse microradiography to detect and measure the thickness of a transparent surface zone [117, 143]. Of those methods only OCT can be used clinically.

In this study, CP-OCT was also able to monitor changes in the dimensions of the gingival tissues. We did not anticipate that the gingiva in some patients would change so dramatically in 6 months. For example, in **Fig. 6.7.5** the gingival margin appears to advance more than a millimeter from baseline to 6 months to nearly cover the previously exposed root surface. Such changes are challenging for image registration since the gingival margin cannot be used as a fixed reference. Since active root lesions are soft, considerable erosion is expected and CP-OCT was able to show that at multiple sites the demineralized dentin was preferentially eroded/abraded away over time. The severity of demineralization can be quantified using CP-OCT by measurement of the lesion depth and the integrated reflectivity over the lesion depth (ΔR). However, this approach is problematic when considerable erosion is present as can be the case for root lesions. For example, the lesion site in **Fig. 6.7.3** shows large drops in lesion depth and ΔR after 6 months. This is not due to remineralization but because the softer areas of demineralization were likely abraded/ eroded away. The mean lesion depth and ΔR increased slightly over 6 months but neither increase was statistically significant. However, considering the influence of erosion discussed above it is likely that with the exception of the 9 lesions that manifested a TSL at 6 months most of the lesions progressed and increased in severity.

This study and our prior study [129] further demonstrate that not only is it difficult to visually assess the activity of root caries but it is also difficult to visually identify whether or not demineralization is present on the exposed root surfaces, or if the lesion is actually located on the root surface. The dentinal enamel junction (DEJ) and the cementum enamel junction (CEJ) are easy to identify in OCT images but are often very difficult to visually identify, particularly in lesion areas. For many of the lesions encountered in this study, the location of demineralization in OCT

images did not correspond to where it was anticipated based on lesion color and texture. Tactile assessments of root caries lesions are more reliable, however tactile assessments and aggressive probing with the explorer risks further damage to lesion areas and the use of the sharp explorer is discouraged. It is also important to note that OCT has limited access to subgingival lesion areas.

6.6 Conclusions

This was the first clinical study to show that CP-OCT can be used to monitor changes in lesion structure and activity over time during active monitoring. It demonstrates the ability of CP-OCT to identify and monitor the activity of root caries in adults and shows the limitations of diagnosis by visual inspection as compared to CP-OCT. CP-OCT imaging has great potential for lesion activity assessment in a single visit. In addition, CP-OCT was able to monitor erosion of the root surface, loss of the cementum layer, changes in the gingival tissues, and provide anatomic landmarks of the DEJ and CEJ. The therapeutic relevance of the study is that it shows that CP-OCT can be used to monitor the efficacy of chemical intervention and can potentially be used in clinical trials to establish the effectiveness of potential treatment options for root caries.

6.7 Tables and Figures

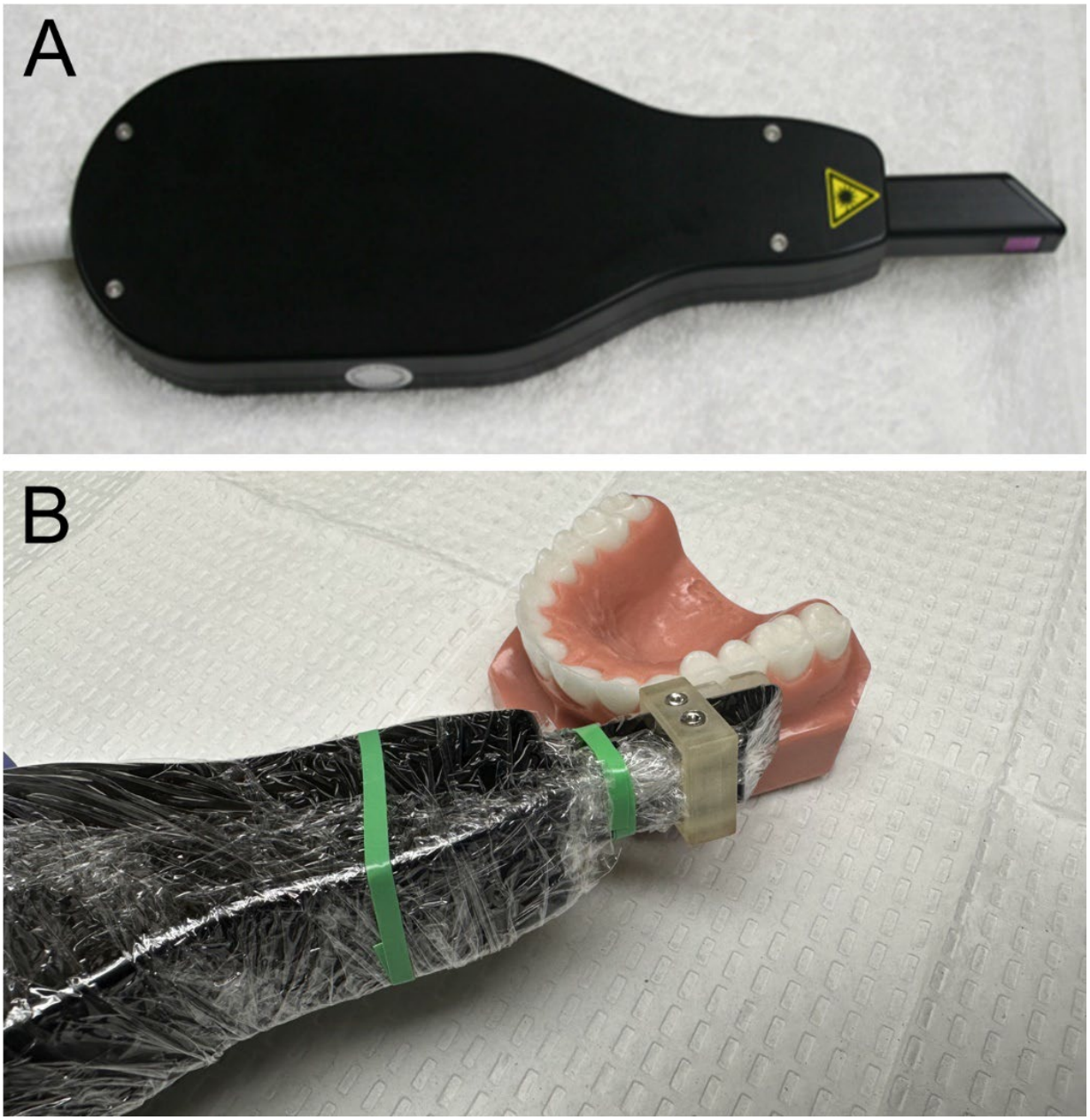

Figure 6.7.1. (A) CP-OCT handpiece used for these studies and (B) a closeup of the handpiece with the added 3D printed attachment and covered by polypropylene wrap for infection control.

Table 6.7.1. Contingency table comparing visual assessment of the digital images of the 22 lesion areas to the CP-OCT images at baseline and at 6 months.

		CP-OCT Baseline				**CP-OCT Month 6**			
		No Lesion	Active lesion	Arrested lesion	Total	No Lesion	Active lesion	Arrested lesion	Total
Visual	No Lesion	**0**	5	1	6	**0**	6	1	7
	Active Lesion	0	**9**	7	16	0	**5**	8	13
	Arrested Lesion	0	0	**0**	0	0	2	**0**	2
	Total	0	14	8	22	0	13	9	22

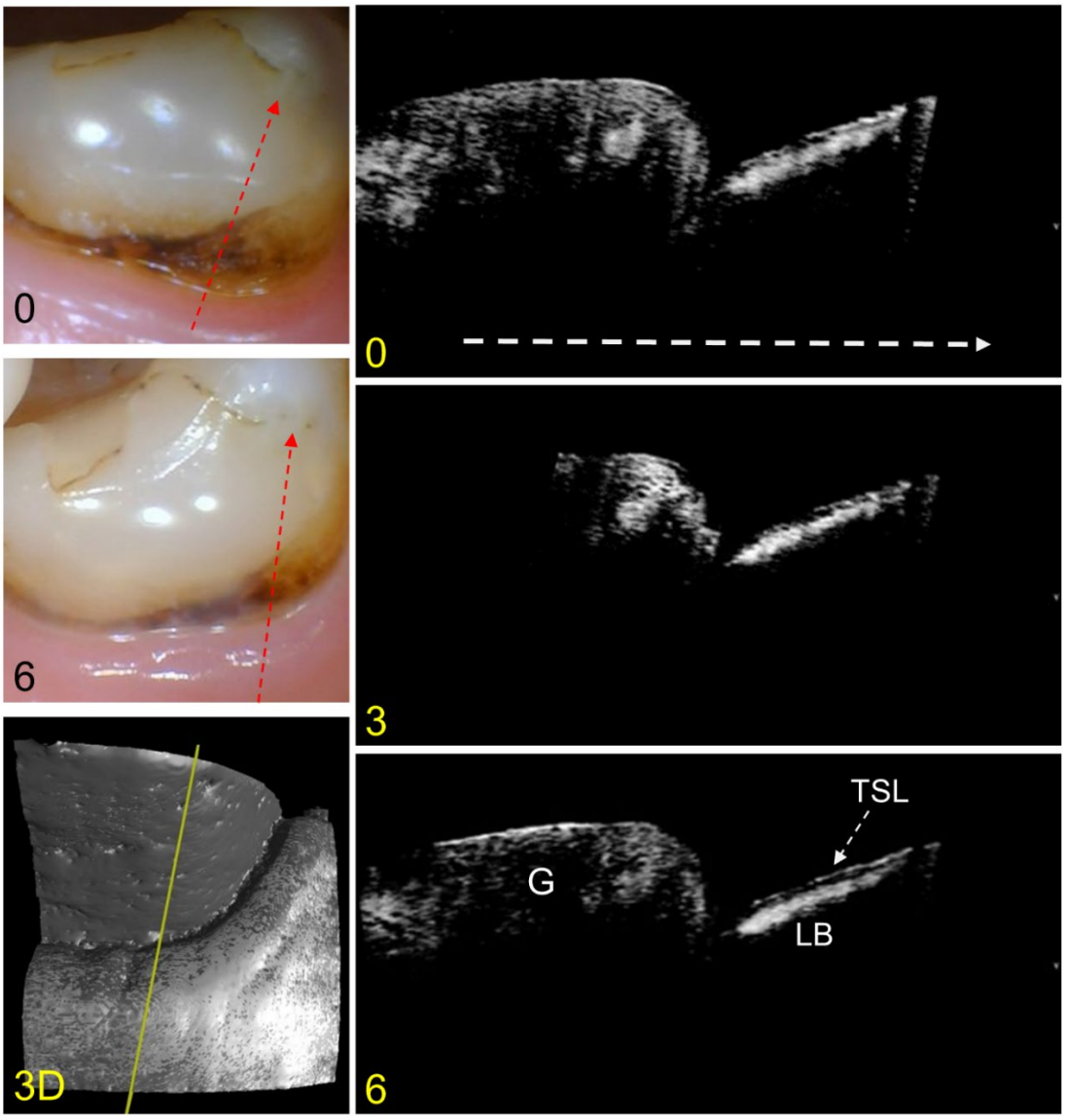

Figure 6.7.2. Color pictures at baseline and 6 months are shown for an arrested lesion. The dashed red lines show the likely position of the three CP-OCT b-scans shown at baseline, 3 and 6 months. The white dashed arrow in the OCT b-scan is directed from the root to the crown. A surface rendering (3D) of the entire CP-OCT scan taken at baseline is also shown with the yellow line showing the position of the extracted b-scans. The position of the gingiva (G) and the lesion body (LB) with the TSL located on top of the lesion are indicated. Little change has occurred for the lesion over 6 months.

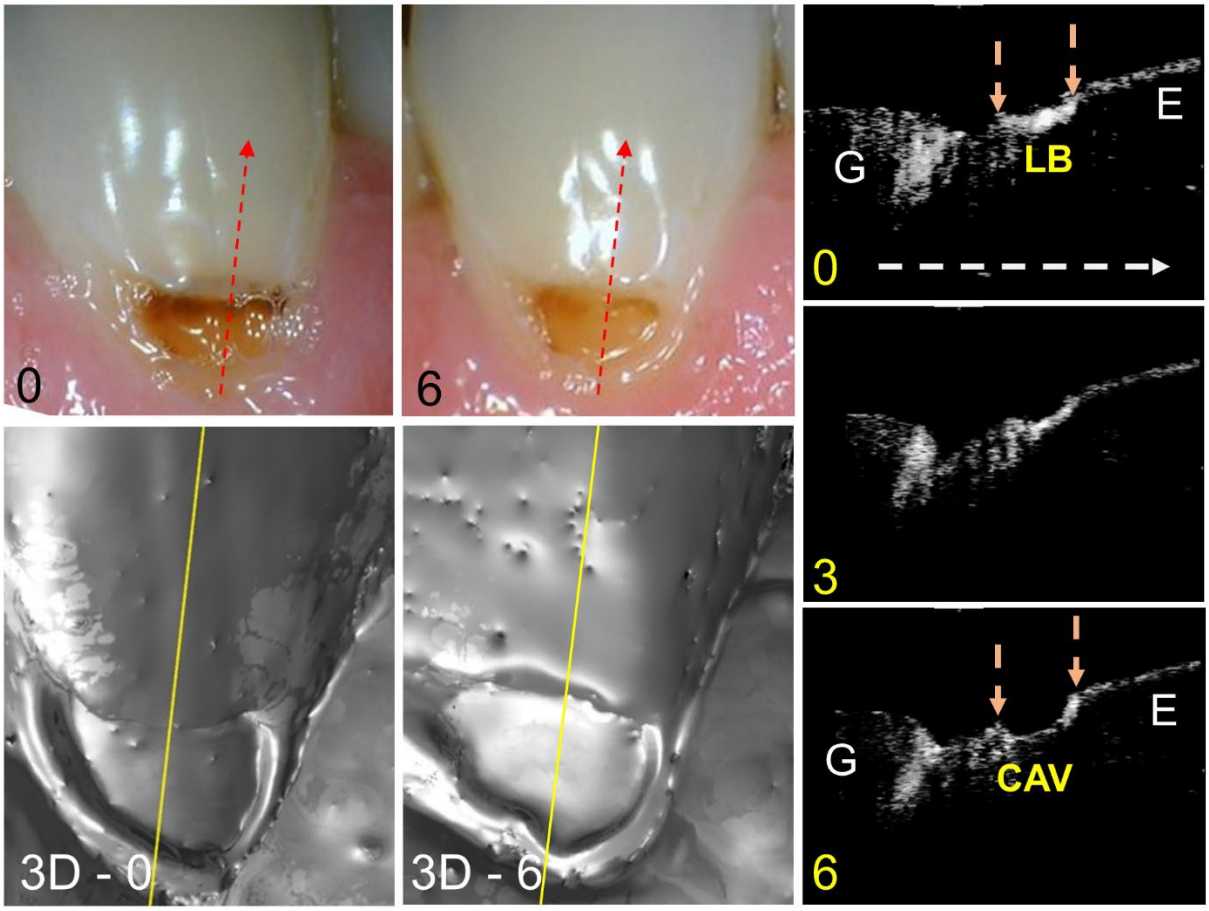

Figure 6.7.3. Color pictures at baseline and 6 months are shown for an active lesion with advancing cavitation. The dashed red lines show the likely position of the three CP-OCT b-scans shown at baseline, 3 and 6 months. The white dashed arrow in the OCT b-scan is directed from the root to the crown. Surface renderings (3D) of the entire CP-OCT scans taken at baseline and 6 months are also shown with the yellow lines showing the position of the extracted b-scans. The position of the gingiva (G) and enamel (E) along with the lesion body (LB) are indicated. After 6 months the demineralized area encompassing the lesion body between the two arrows has eroded leaving a cavitated region (CAV).

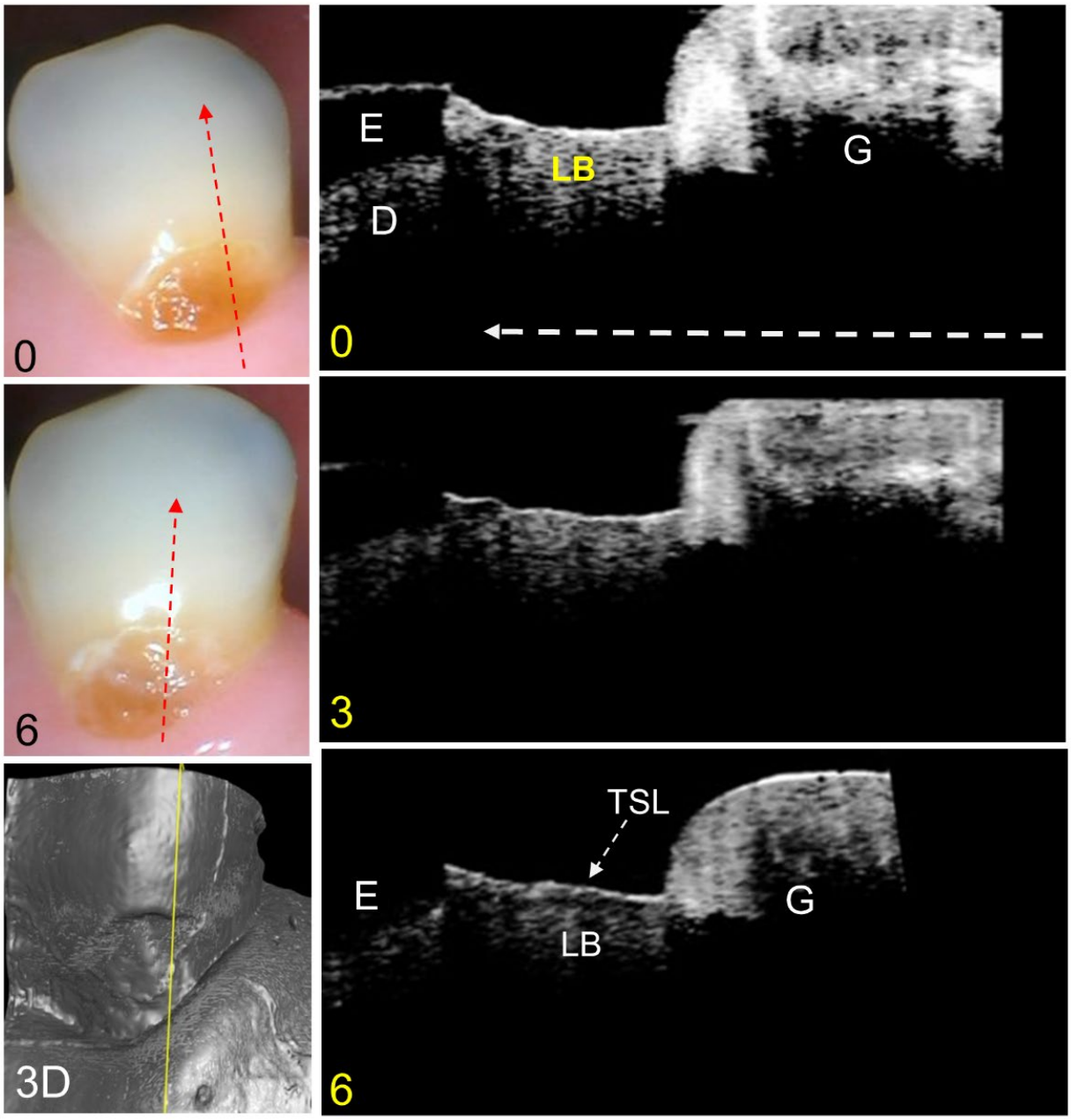

Figure 6.7.4. Color pictures at baseline and 6 months are shown for an active lesion that has undergone increasing remineralization and has a TSL after 6 months. The dashed red lines show the likely position of the three CP-OCT b-scans shown at baseline, 3 and 6 months. The white dashed arrow in the OCT b-scan is directed from the root to the crown. A surface rendering (3D) of the entire CP-OCT scan taken at 0 months is also shown with the yellow line showing the position of the extracted b-scans. The position of the gingiva (G), enamel (E) and underlying dentin (D) are shown and the lesion body (LB) is indicated. After 6 the intensity of reflectivity from the lesion body has decreased and a distinct TSL is visible at the lesion surface.

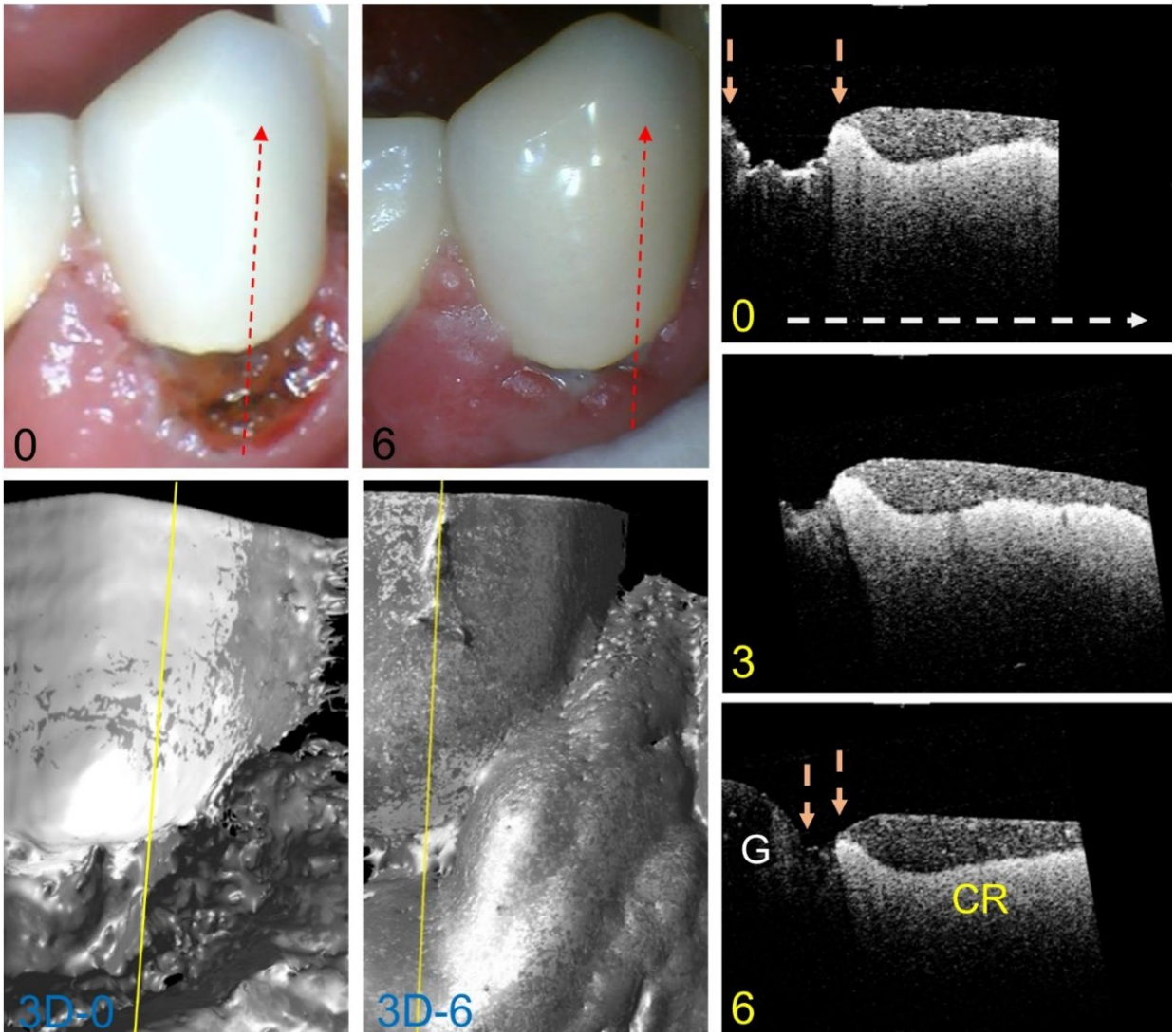

Figure 6.7.5. Color pictures at baseline and 6 months of an exposed root surface that becomes completely covered by inflamed gingiva after 6 months. The dashed red lines show the likely position of the three CP-OCT b-scans shown at baseline, 3 and 6 months. The white dashed arrow in the OCT b-scan is directed from the root to the crown. Surface renderings (3D) of the entire CP-OCT scans taken at baseline and 6 months are also shown with the yellow lines showing the position of the extracted b-scans. The position of the gingiva (G) and the attached crown (CR) are indicated. After 6 months the exposed root surface indicated by the position between the two arrows has contracted markedly and the 3D surface rendering show most of the root surface that was exposed at baseline is now covered by the expanded gingiva.

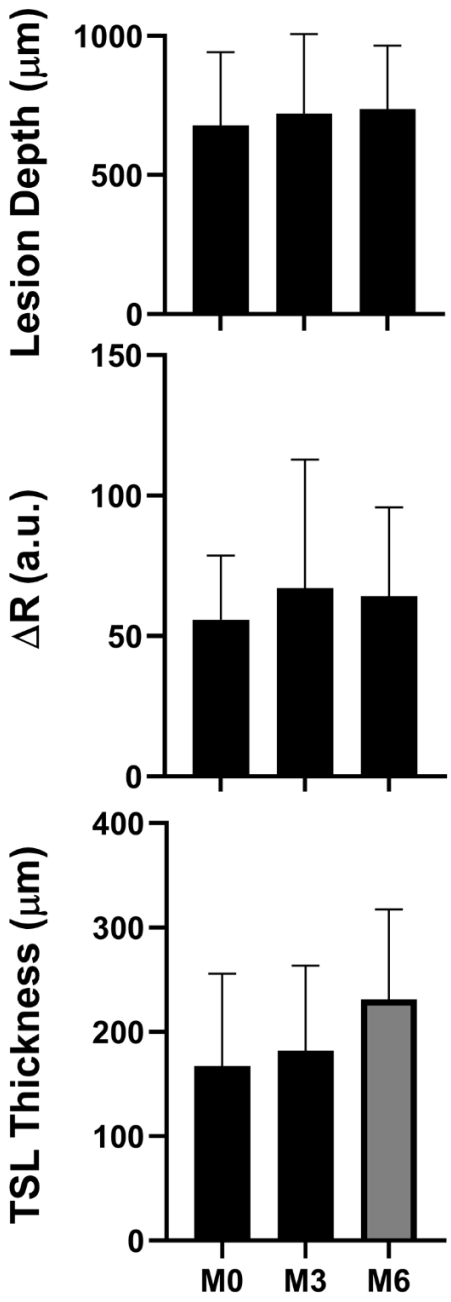

Figure 6.7.6. Bar graphs for mean ± s.d. for the CP-OCT measurements of the lesion depth, integrated reflectivity over the lesion depth (*Δ*R), and the TSL thickness. Bars of the same color are statistically similar (P >0.05). There were 22 samples for the lesion depth and *Δ*R and 9 samples that had measurable TSLs.

CHAPTER VII

Clinical SWIR and CP-OCT Imaging of Interproximal Lesions

7.1 Summary

Enamel is highly transparent at short wavelength infrared imaging (SWIR) wavelengths allowing the detection of dental decay without the need for ionizing radiation. The purpose of this study was to use SWIR imaging methods including cross polarization optical coherence tomography (CP-OCT), occlusal transillumination (SWIR-OT), proximal transillumination (SWIR-PT), and occlusal reflectance (SWIR-R) to image interproximal lesions *in vivo* and compare the sensitivity with radiography.

Participants (n=30) aged 18-80 each with a radiopositive interproximal lesion scheduled for restoration were enrolled in the study. Studies have shown that the opposing proximal surfaces across the contact will likely also have lesions. SWIR images were acquired of the adjoining teeth at each contact with an interproximal lesion scheduled for restoration. Lesion presence and depth were assessed on each side of the contact for radiography and each SWIR imaging method. Lesions on radiographs and in CP-OCT images were identified by a single examiner while lesions in SWIR images were identified by a contrast threshold via semi-automatic image segmentation.

All SWIR imaging methods had significantly higher sensitivity ($P<0.05$) than radiographs for the detection of interproximal lesions on the teeth opposite those restored. CP-OCT and SWIR-R imaging methods had significantly higher sensitivity than the other methods. SWIR imaging methods showed significantly higher lesion contrast than radiography.

SWIR imaging methods can be used to detect interproximal lesions on posterior teeth with higher diagnostic performance than radiographs. CP-OCT appears well suited as a potential gold standard for the detection of interproximal lesions and assessment of their severity *in vivo*.

7.2 Introduction

In the US, dental decay continues to be the leading cause of tooth loss even though caries progression is potentially preventable and reversible if detected early [90, 91]. New approaches are needed to detect lesions earlier than radiographs that are better suited for monitoring lesions over time. Imaging methods at wavelengths longer than 1000-nm (SWIR wavelengths) are highly promising due to the higher transparency of dental enamel [24, 47, 80-82, 102]. Lesions can be imaged using transillumination and reflectance from tooth occlusal, buccal and lingual surfaces [6, 24, 78, 79, 102]. Interproximal lesions, the lesions located at the proximal contact points in between teeth, can be imaged via all three imaging geometries: SWIR-OT, SWIR-PT, and SWIR-R imaging. SWIR-OT and SWIR-R have been combined into a single probe (SWIR-OTR) and tested *in vivo* [40, 100, 152].

Early lesions on proximal surfaces can be difficult to detect with radiography due to lack of physical access and the challenge of identifying the initial, subtle mineral loss of these lesions [1, 2]. Lesions are not typically visible on radiographs until decalcification has exceeded 30% [1, 2], while SWIR imaging methods are diagnostic with only 5% decalcification [111]. Radiographs markedly underestimate the depth and severity of interproximal lesions and clinicians generally assume that lesions penetrate much deeper than indicated in radiographs [13-15]. The first clinical SWIR study was carried out in 2010, when it was demonstrated that interproximal lesions that appeared on radiographs could also be detected *in vivo* using SWIR-OT and SWIR-PT imaging at 1310-nm with similar sensitivity [24]. Two later clinical studies showed that SWIR imaging methods have higher sensitivity than radiographs for the detection of dental caries, however those studies were limited to premolars that were scheduled for extraction [6, 153] for orthodontic reasons. Currently the only clinical infrared dental imaging systems that are commercially

available operate at shorter near-IR wavelengths at 830 and 780-nm [83-85, 87] where the enamel is less transparent [78]. The contrast between sound and demineralized enamel is markedly higher at wavelengths beyond 1400-nm [70, 88, 89] and stains do not interfere at wavelengths longer than 1200-nm [88]. In the latest clinical SWIR imaging study SWIR-OT and SWIR-R were combined in a single imaging device, that allowed simultaneous transillumination and reflectance measurements, SWIR-OTR [153].

Optical coherence tomography (OCT) which uses SWIR light at 1300-nm can also provide high resolution cross-sectional images of interproximal lesions from the occlusal surface. Lesions can be seen at depths of more than 3-mm [154-156].

In this SWIR imaging study, test subjects with at least one radiopositive interproximal lesion scheduled for restoration were recruited. This new clinical study includes more advanced lesions and other teeth in addition to premolars that are not subject to crowding. The adjacent proximal surface at the contact point must either have a radiopositive lesion that appears confined only to enamel or have no visible lesion. Studies have shown that interproximal lesions are likely present on both sides of the contact even if both are not visible in radiographs [157, 158]. The two teeth at each contact point were imaged using SWIR-OT, SWIR-PT, SWIR-R imaging, and CP-OCT. The lesion contrast and penetration depth were also estimated from each image. Intraoral color images were also taken before and after cavity preparation and any demineralization on the exposed surface opposite the preparation was noted. The purpose of this study was to show that SWIR imaging methods have superior sensitivity for the detection of interproximal lesions on posterior teeth.

7.3 Materials and Methods

7.3.1 Participant Recruitment and Procedures

Study participants (n=30) aged 18+ were recruited from the UCSF General Dentistry Clinic by the study investigators (UCSF IRB 19-27656). Informed consent was obtained from all subjects and/or their legal guardians. Participants were required to have one radiopositive interproximal lesion scheduled for restoration. Radiographs and treatment planning were carried out prior to recruitment by students and staff of the clinic independent of study investigators. Color images of the teeth on both sides of the contact were acquired before and after restoration using a FocusDent MD740 (Vilnius, Lithuania) Intraoral camera. Before restoration SWIR video was acquired using SWIR-PT from buccal and lingual views and SWIR-OTR over the occlusal surface. CP-OCT was used to acquire a 3D image 6x6-mm and 7-mm deep centered on each contact. Radiographical contrast was calculated using $(I_S-I_L)/I_S$ for each lesion area that was identified. I_L was measured as the mean intensity over the lesion area at each proximal contact and I_S was selected at a sound position either directly below or directly above I_L to ensure a similar enamel thickness. Lesions on radiographs and demineralization in color images of proximal surfaces were identified by a single clinical examiner.

7.3.2 SWIR Occlusal reflectance and transillumination (SWIR-OTR)

Details regarding the fabrication of the dual occlusal transillumination and reflectance SWIR-OTR handpiece has been described previously [40]. An image of the handpiece is shown in **Fig.7.7.1A**. The SWIR images were captured using a 640x480 pixel micro-SWIR focal plane array (FPA) from Sensors Unlimited (Princeton, NJ), Model SU640CSX measuring only 32x32x28-mm. Two planoconvex antireflection coated lenses of 60 and 100-mm focal length along with an adjustable

aperture were placed between the handpiece and the InGaAs FPA to provide a field of view of 11-mm^2 at the focus plane. A low-OH optical fiber of 1-mm diameter was used to deliver light from a 1604-nm superluminescent diode (SLD), Model ESL1620-2111 from Exalos (Schlieren, Switzerland) for reflectance with an output of 17-mW and a bandwidth of 46-nm. The intensity delivered to the tooth was 5-mW. The 1600-nm light passes through a polarizing beam splitting cube before incidence on the tooth and a linear polarizer was placed before the FPA to achieve cross-polarization for glare reduction. The transillumination light was delivered through two 0.4-mm diameter low-OH optical fibers. A 1314-nm (BW) SLD, Model DL-CS3452A-FP from Denselight (Singapore) with an output of 48-mW and a bandwidth of 33-nm was used as the source for transillumination. A 50/50 beamsplitter was used to deliver light to each arm for transillumination. The output intensity of each arm was set at 10-mW before entering the Teflon plugs located at the end of each arm.

Image processing of the acquired images was performed by custom scripts written using MATLAB from Mathworks (Natick, MA). A semi-automatic image segmentation technique was used to detect interproximal lesions. Raw SWIR images were first converted into contrast maps by applying the following transformation to every pixel in the image: $(I_t - I_s)/I_t$ for reflectance, and $(I_s - I_t)/I_s$ for transillumination. I_s was manually selected to the average intensity of sound enamel adjacent to the interproximal contact. I_t was the target pixel receiving the transformation. In a previous clinical study contrast was significantly higher ($P<0.05$) between sound and interproximal lesion areas for SWIR imaging methods but not for radiography [153]. Therefore, contrast thresholds can be set for lesion detection for SWIR imaging methods but not for conventional radiography. A contrast of 0.1 is a reliable threshold for positive detection of interproximal lesion with reflectance and transillumination SWIR imaging [153]. Pixels with

contrast lower than 0.1 were removed to generate a binary mask showing every pixel with contrast higher than 0.1. Isolated areas of the mask adjoining the proximal contacts were designated as proximal lesion areas. This approach avoids high intensity areas caused by specular reflection (SWIR-R) or direct light that doesn't pass through tooth structure (SWIR-PT and SWIR-OT). Specular reflection is easy to identify since it depends on angle of incidence and vanishes as the handpiece is rotated. Segmented lesions areas were isolated for depth and contrast measurements. Successful segmentation of an interproximal lesion with this technique was recorded as a positive detection. Failed segmentation of a lesion was considered a negative detection. If the detection was positive, lesion area (in pixels), mean contrast, and lesion depth were then automatically calculated following the semi-automatic lesion segmentation. Examples of lesion areas after segmentation are shown in **Fig. 7.7.2** for SWIR-R, OT & PT.

7.3.3 SWIR Proximal transillumination (SWIR-PT)

An image of the SWIR-PT handpiece is shown in **Fig. 7.7.1B**, it is similar to the device described previously [152]. Images were captured using another SU640CSX micro-SWIR FPA. Two planoconvex antireflection coated lenses of 75 and 100-mm focal length along with an adjustable aperture were placed between the handpiece and the InGaAs FPA to provide a field of view of 9x14-mm^2 at the focus plane. The transillumination light is delivered through a 0.4-mm diameter low-OH optical fiber. A 1330-nm superluminescent diode (SLD) from Covega (Jessip, MD) with an output of 26-mW and a bandwidth of 36-nm was used as the light source for transillumination. The output intensity was set at 10-mW before entering the Teflon scattering rod.

7.3.4 Cross Polarization Optical Coherence Tomography (CP-OCT)

The cross-polarization OCT system used for this study was the Model IVS-3000-CP from Santec (Komaki, Aichi, Japan). It operates at a wavelength of 1321-nm with a bandwidth of 111-nm (11.4-µm axial-resolution) and can acquire complete tomographic images 6x6x7-mm in approximately 3-seconds. An image of the CP-OCT handpiece is shown in **Fig. 7.7.1C**. It has been used for multiple *in vivo* caries imaging studies [7, 51, 134]. An appliance made of autoclavable Dental SG resin printed using a 3D printer, Formlabs 2 (Somerville, MA) was placed on the distal end of the OCT scanning handpiece and the handpiece was covered with polyethylene film for infection control. Air at 10-psi was connected to the appliance to prevent fogging of the imaging window during image acquisition.

Images were filtered with a median filter of kernel size 3 to reduce speckle noise and imported into Dragonfly from ORS software (Montreal, CA) for co-registration and analysis. Lesion depth was measured by applying a cylindrical ruler starting perpendicularly to the interproximal lesion surface. The scale of the ruler was customized to be the average intensity of the image inside a 100-mm disk surrounding the central axis of the ruler. Lesion depth was measured as the difference between the two lowest intensities along the ruler.

7.3.5 Lesion Detection Rates, Lesion Contrast and Lesion Depth Calculations

Radiography, CP-OCT, and visual inspection of opposing sites after restoration are all methods that have a high specificity for the detection of caries lesions. Therefore, the detection of any lesions by these methods was considered a true positive for the assessment of the lesion detection rates. A recent *in vitro* OCT study using n=36 extracted teeth with 45 proximal lesions using histology as a gold standard showed that OCT had similar values of specificity and higher

sensitivity and diagnostic accuracy to digital radiography [159]. According to these methods every surface was considered a positive lesion site for a total of n=58 lesions.

Lesion detection rates were compared with radiography using Fishers' exact test. Repeated measures ANOVA was used to compare the lesion contrast and lesion depth by removing all samples with missing values yielding a sample size of n=26 for contrast and n=24 for lesion depth. In addition, a mixed effects multiple comparisons model was employed that allows missing values. The results were the same for both methods. Prism statistical software from GraphPad Software, Inc., (La Jolla, CA) was used for the calculations. Significance level was set at $P<0.05$.

7.4 Results

Lesion detection rates are tabulated in **Table 7.7.1** for all the lesions and lesions only located on the restored and opposing surfaces. The detection rates for all the lesions (n=58), restored (n=29) and opposing surfaces (n=29) were all calculated as the fraction of the surfaces on which a lesion was detected for each method, and they are tabulated in **Table 7.7.1**. Even though half the lesion sites were selected based on their appearance on radiographs and scheduled for restoration, detection rates for the SWIR methods were all significantly higher than for radiography. SWIR-R and SWIR-PT were both significantly higher than other methods. Radiography detection rates for the surfaces opposing those restored provides a less biased comparison and the detection rates were much lower 0.38 versus 0.62 for all the lesions. In contrast the detection rates for the opposing surfaces with each of the SWIR methods was similar to the detection rates for all the lesions. All the SWIR detection rates were significantly higher than radiography. Also listed are mean lesion contrast values for radiography and SWIR-R,OT&PT and lesion depths for CP-OCT, and SWIR-R,OT&PT. The mean lesion contrast for the three SWIR methods SWIR-R,OT&PT

was significantly higher than radiographs, nearly twice as high. Higher lesion depths were measured for OCT and SWIR-OT compared to radiography, but the difference was not significant. The lesion depths measured for SWIR-PT were significantly lower than for the other methods including radiography.

Images acquired from the contact area in which the lesion on the opposing proximal surface was not visible in the radiograph are shown in **Fig. 7.7.3**. In **Fig. 7.7.3B** the radiograph shows a large lesion penetrating well into dentin on tooth#12 while there is no lesion visible on the opposing surface of tooth#13. The color image acquired after the restoration (**Fig. 7.7.3C**) shows some discoloration indicative of demineralization on tooth#13, but the severity of the lesion cannot be determined. The CP-OCT image in **Fig. 7.7.3D** shows strong reflections below the tooth surface at the position of the red and yellow arrows clearly indicating that lesions are present on both tooth#12 and tooth#13. The SWIR-R image shown in **Figs. 7.7.3E** acquired with the dual SWIR-OTR imaging probe shows lesions on both surfaces while SWIR-OT shows only one of the lesions. The SWIR-PT images acquired from buccal and lingual views are shown in **Figs. 7.7.3G&H** and the buccal view shows both lesions.

Images acquired from another contact area are shown in **Fig. 7.7.4**. For this example, lesions were identified in radiography on both sides of the contact. The color image acquired after the restoration (**Fig. 7.7.4C**) shows demineralization and staining on tooth#5. The CP-OCT image in **Fig. 7.7.4D** shows strong reflections below the tooth surface at the position of the red and yellow arrows clearly indicating that lesions are present on both tooth#4 and tooth#5. The SWIR-R and SWIR-OT images shown in **Figs. 7.7.4E&F** acquired with the dual SWIR-OTR imaging probe both show the lesions present on both surfaces. The SWIR-PT images acquired from buccal and

lingual views are shown in **Figs. 7.7.4G&H**. Lesions are visible in both the buccal and lingual views.

7.5 Discussion

In this study radiography and SWIR imaging methods were used to image the proximal contacts at which an interproximal lesion was scheduled for restoration. It is known that if a lesion develops on one side of the contact another lesion will likely also develop on the opposing tooth [157, 158] and lesions were identified on all of the opposing surfaces. No gold standards exist for the detection of caries lesions that can be used *in vivo*, however three of the methods, radiography, OCT, and visual examination of the exposed proximal surface after restoration have high specificity for caries detection and were used to identify surfaces as true positives. It is important to note that visual examination only shows that demineralization is present on the surface and gives no indication regarding the depth of lesion penetration, while both radiography and OCT show the depth penetration. Based on positives from any one of these three methods we found that all 58 of the proximal surfaces had lesions.

Comparison of lesion detection rates for the n=29 surfaces opposite to those restored gives the best unbiased measure for lesion detection and all the SWIR methods were significantly higher than radiography with SWIR-R & PT having the highest performance. SWIR methods also yield much higher lesion contrast than radiography. High lesion contrast is particularly important for the implementation of auto-segmentation image analysis algorithms and machine learning. SWIR-OT & R and OCT provided similar lesion depth measurements to radiography which is important for lesion diagnosis. SWIR-PT provided high lesion contrast and high lesion detection rates. However, it greatly underestimated the lesion depths. In addition, imaging with SWIR-PT is more

cumbersome than the other methods requiring two measurements per contact, buccal and lingual as opposed to a single measurement. Moreover, SWIR-PT can only be used as a stand-alone probe and is not useful for the detection of occlusal lesions. In contrast, SWIR-R & OT can be combined into a single multispectral SWIR-OTR probe that can be used for the detection of lesions on both proximal and occlusal surfaces and is more practical for caries screening.

CP-OCT performed extremely well for the detection of proximal lesions from tooth occlusal surfaces showing clear easily identifiable increases in intensity below the surface. Features in the images such as the subsurface rise in intensity and the reflectivity along the length of the lesion cannot be confused with false positives, nor can they be confused with increased reflectivity from the dentino-enamel junction (DEJ) due to the position and angle of the DEJ near tooth proximal surfaces. CP-OCT did miss a few of the lesions that appeared clearly on radiographs, however it appears that those lesions were located beyond the imaging range of the CP-OCT system. The scanning range of the system used was 7-mm in air which is greatly reduced by the high refractive index of enamel (1.6) to 4.4-mm. Other systems have been investigated *in vitro* with scanning ranges up to 10-mm that would be capable of reaching deeper lesions [159]. CP-OCT is a good candidate as a surrogate gold standard for interproximal lesions due to the potential high sensitivity and specificity. It is also well suited for automated image analysis and machine learning.

SWIR imaging devices operating beyond 1000-nm are not commercially available for dental imaging because of past restrictions due to military applications and high cost, however that is expected to change soon. In the past few years, costs have decreased markedly due to increased competition and production and there is a reduction in export restrictions for InGaAs devices. In addition, new SWIR imaging devices that use alternative semiconductor materials to InGaAs are

under development for large imaging arrays using colloidal quantum dots that have improved sensitivity over InGaAs at longer SWIR wavelengths [160].

7.6 Conclusions

SWIR imaging methods have significantly higher ($P<0.05$) sensitivity for the detection of Class II interproximal lesions than radiographic and visual methods. CP-OCT appears well suited as a potential gold standard for the detection of interproximal lesions and assessment of their severity *in vivo*.

7.7 Tables and Figures

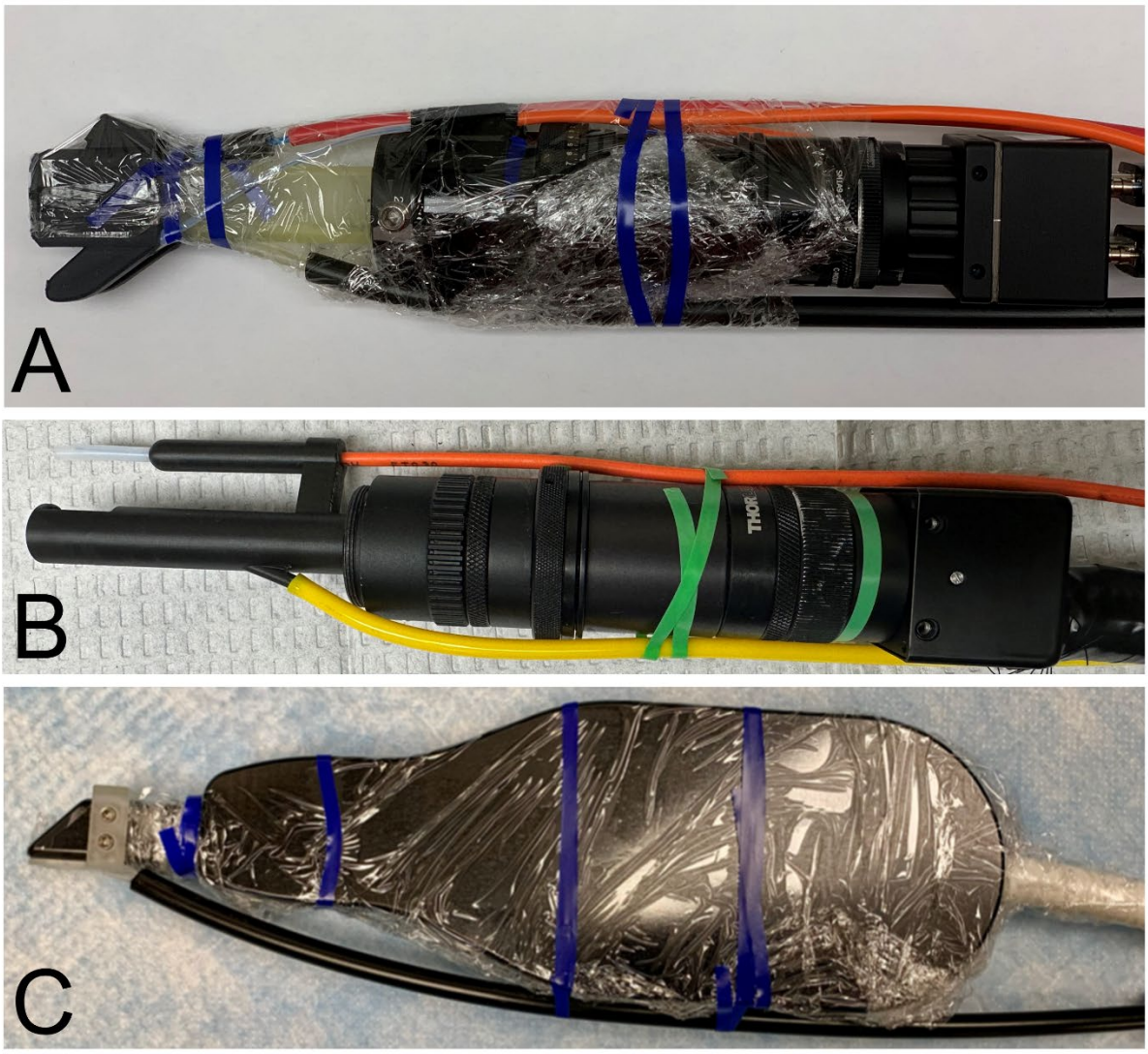

Figure 7.7.1. The three SWIR imaging devices used in this clinical study: (A) Dual SWIR-OTR clinical handpiece wrapped for infection control ready for clinical imaging, (B) SWIR-PT clinical handpiece and, (C) CP-OCT handpiece wrapped for infection control.

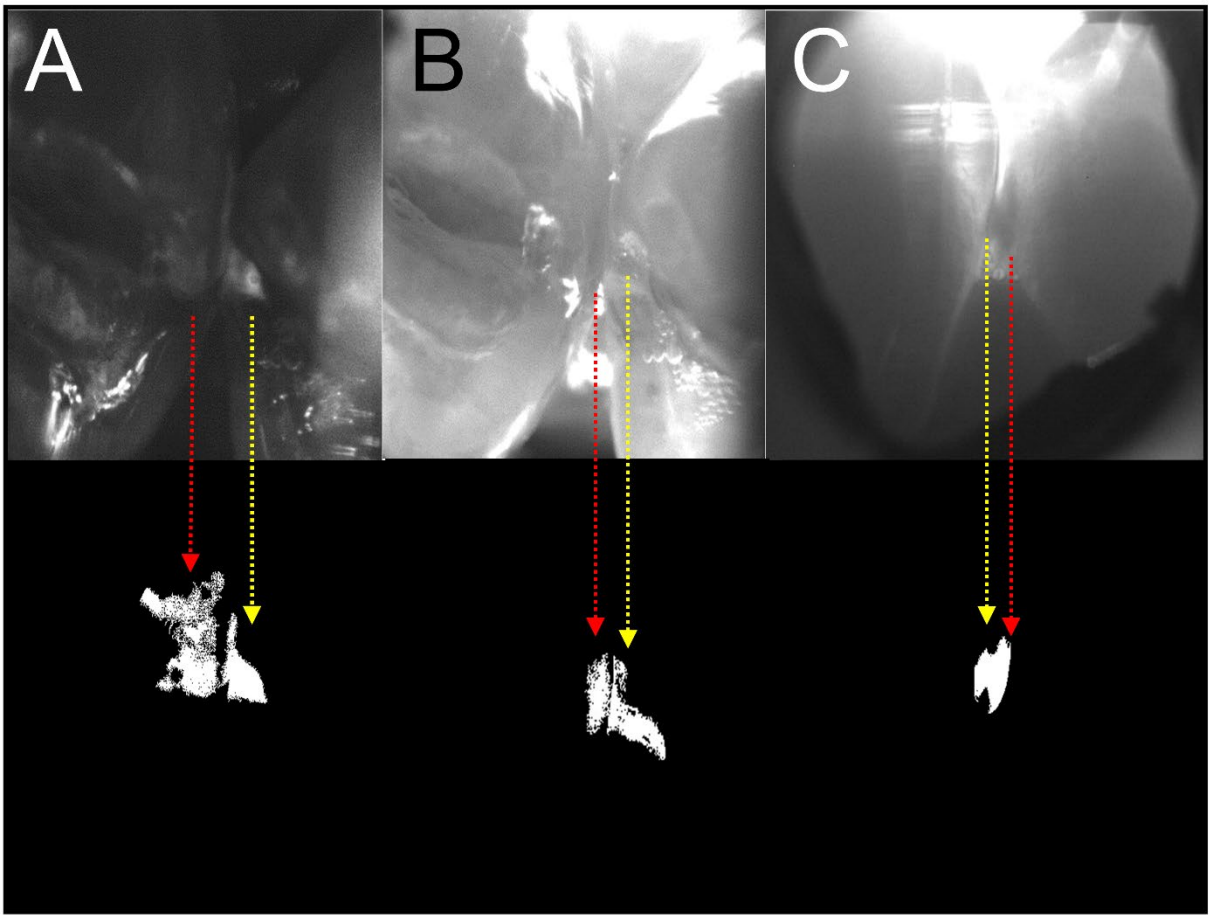

Figure 7.7.2. Segmented images showing extracted lesions areas from (A) SWIR-R, (B) SWIR-OT, and (C) SWIR-PT.

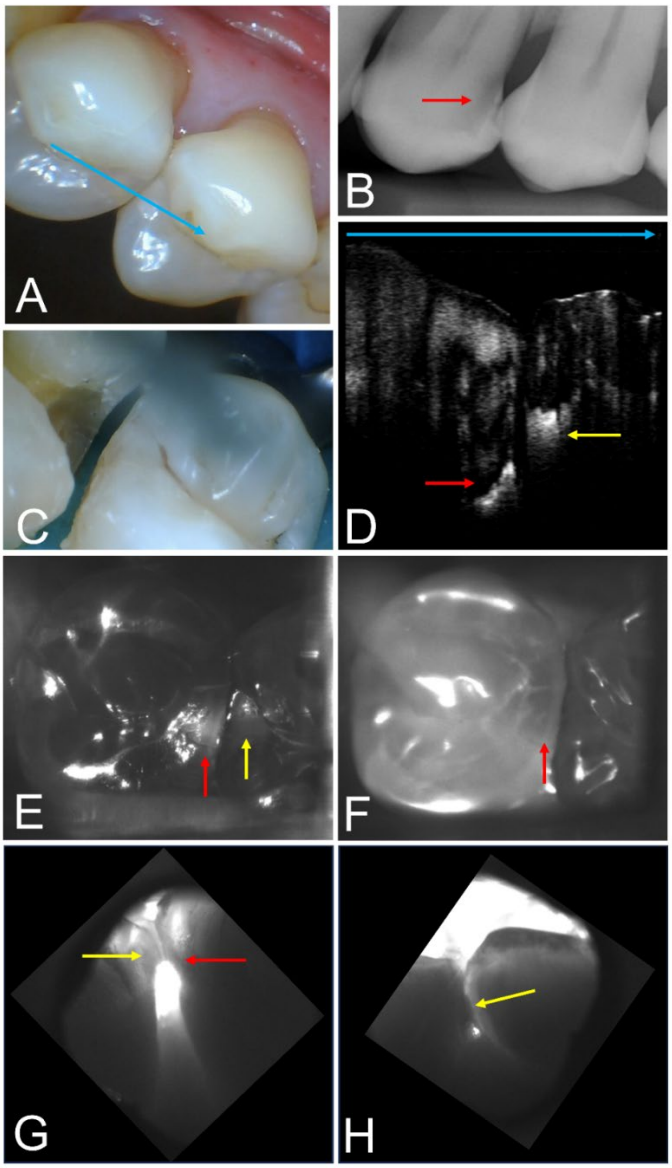

Figure 7.7.3. (A) Color image of the contact between tooth #12 and tooth #13, no lesions are visible. (B) Radiograph shows a large proximal lesion (red arrow) on tooth#12 at the distal contact that was scheduled for restoration. No lesion is visible on the opposing mesial contact of tooth #13. (C) After the cavity preparation decalcification is now visible on the mesial contact of tooth#13. (D) A CP-OCT b-scan image taken from the occlusal surface above the contact along the path of the blue arrow shown in (A) shows both proximal lesions that appear with increased subsurface reflectivity at the positions indicated by the red and yellow arrows. The CP-OCT scan shows the intensity with depth and lateral position with white high intensity and black low intensity. (E) SWIR-R occlusal reflectance shows lesions on both surfaces (red and yellow arrows) while (F) SWIR-OT only shows the lesion that was restored. (G) SWIR-PT image taken from the buccal side shows both proximal lesions across the contact while the (H) SWIR-PT image taken from the lingual shows only the lesion on tooth #13.

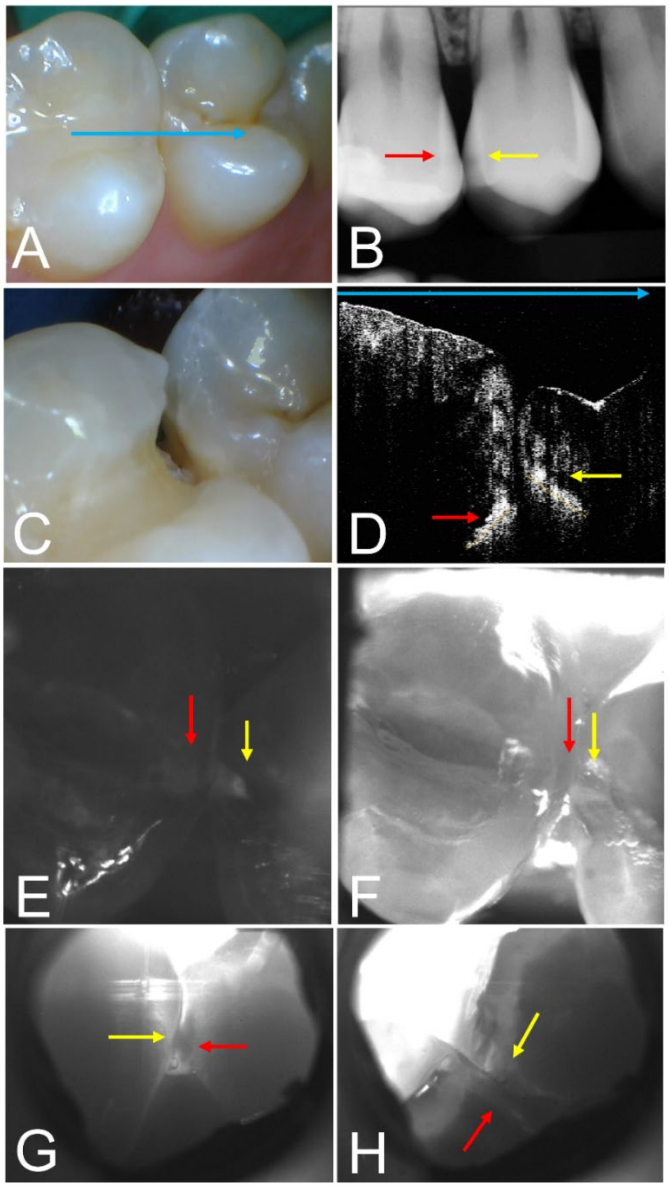

Figure 7.7.4. (A) Color image of the contact between tooth #4 and tooth #5, no lesions are visible. (B) Radiograph shows a lesion (red arrow) on tooth#4 at the distal contact that was scheduled for restoration and on the opposite contact on tooth#5 (yellow arrow). (C) After the cavity preparation decalcification is visible on the mesial contact of tooth#5. (D) A CP-OCT b-scan image taken from the occlusal surface above the contact along the path of the blue arrow shown in (A) shows both proximal lesions that appear with increased subsurface reflectivity at the positions indicated by the red and yellow arrows. The CP-OCT scan shows the intensity with depth and lateral position with white high intensity and black low intensity. (E) SWIR-R and (F) SWIR-OT images show lesions on both surfaces (red and yellow arrows). SWIR-PT images taken from the (G) buccal and (H) lingual sides show both proximal lesions across the contact.

Table 7.7.1. The respective lesion detection rates for all the lesions and lesions only located on the restored and opposing surfaces. The mean(standard deviation) of the lesion contrast and the lesion depth for all detected lesions. Columns with the same letter are statistically similar (P>0.05).

	Radiograph	**OCT**	**Visual (before)**	**Visual (after)**	**SWIR-R**	**SWIR-OT**	**SWIR-PT**
Detection Rate (All)	0.62 [a]	0.79 [a,b]	0.05 [c]	-	0.91 [b]	0.74 [a,b]	0.9 [b]
Res Surface	1(0.93) [a]	0.83 [a]	0.10 [c]	-	0.9 [a,b]	0.76 [b]	0.93 [a,b]
Op Surface	0.38 [a]	0.76 [b]	0 [c]	0.86 [b]	0.93 [b]	0.72 [b]	0.86 [b]
Lesion Contrast	0.13(0.064) [a]	-	-	-	0.22(0.063) [b]	0.20(0.010) [b]	0.27(0.013) [c]
Lesion Depth (um)	851(422) [a]	1069(363) [a]	-	-	830(379) [a]	1049(514) [a]	289(189) [b]

CHAPTER VIII

Conclusions

8.1 Summary

This dissertation introduces a novel multimodal imaging approach that combines Short Wave Infrared (SWIR) reflectance imaging with occlusal transillumination to improve the detection and assessment of dental caries. This dual-display approach reduces false positives, leading to enhancements in diagnostic accuracy, specificity, and non-invasive lesion severity assessment. Additionally, integrating Optical Coherence Tomography (OCT) with advanced computer vision techniques allows for high-resolution, cross-sectional imaging, enabling detailed analysis of lesion remineralization status and caries progression. These advancements facilitate earlier caries detection and continuous monitoring, promoting more effective, conservative treatments. Moreover, the use of non-ionizing SWIR imaging permits more frequent, safe monitoring of dental health, potentially reducing the need for surgical interventions and supporting a shift towards more conservative dentistry and minimally invasive practices.

8.2 Future Perspective

While the dual-mode SWIR probe has shown effectiveness in enhancing diagnostic accuracy, there are still challenges to address for further improvement. For example, the occlusal transillumination (SWIR-OT) mode occasionally produces negative contrast on lesions due to light bleeding, potentially reflecting off the mirror before entering the tooth. To mitigate this, refining the transillumination arms for closer contact could be beneficial, although the 3D printing resin used, Formlabs Flexible Resin V1, is not biocompatible. In late 2023, Formlabs released a biocompatible Flexible BioMed Resin with greater tensile strength, which could allow for a tighter fit, potentially enhancing SWIR-OT performance. Additionally, the efficiency of the built-in air nozzle in the reflectance probe mentioned in Chapter V needs improvement. A 2023 study by Ng et al. [161]

showed that a narrower air nozzle could improve dehydration efficiency, yet still required 60 seconds of continuous dehydration to distinguish between active and arrested lesions. Future work is essential to optimize dehydration dynamics for clinical application of SWIR dehydration imaging. Moreover, despite the success of SWIR imaging and OCT in detecting in vivo interproximal lesions, assessing their activity remains a challenge due to their inaccessible location between teeth. Addressing this would have significant clinical implications, as many interproximal lesions, hidden from direct view, cannot be assessed by conventional color and texture analysis.

Looking forward, the field of dental imaging is poised on the brink of significant technological advances. SWIR imaging has proven more effective in detecting and assessing dental decay than traditional bitewing radiographs. Despite the high cost of SWIR imaging components, industrial efforts are progressing to reduce these costs. For example, over the past decade, Sony's InGaAs sensors (IMX990 ~ 993) were the only commercial SWIR camera sensors available, capable of producing images up to 3.21 megapixels, albeit at a premium price. Recently, SWIR Vision Systems has developed quantum-dot based sensors that offer even higher resolutions at lower costs, competing with Sony’s offerings. As continuous research explores SWIR imaging applications in fields like agriculture, healthcare, automotive, and the military, demand is expected to drive component costs down, making the technology more affordable and accessible. Additionally, the computer vision algorithms discussed in Chapters IV and VII of this dissertation highlight the potential for automated caries detection and severity evaluation. These algorithms could be enhanced with artificial intelligence to improve image analysis, offering real-time diagnostics and personalized treatment plans. With ongoing education about the efficacy of SWIR dental imaging, this technology is set to become a standard in routine caries screening, transitioning dentistry from a surgery-focused approach to a new era of preventive care.

REFERENCES

1. White, S.C. and M.J. Pharoah, *Oral Radiology: Principles and Interpretation*. 2014, St. Louis: Mosby.
2. Yang, J. and V. Dutra, *Utility of radiology, laser fluorescence, and transillumination.* Dent Clin North Am, 2005. **49**(4): p. 739-52, vi.
3. Jones, R., et al., *Near-infrared transillumination at 1310-nm for the imaging of early dental decay.* Optics Express, 2003. **11**(18): p. 2259-65.
4. Simon, J.C., et al., *Multispectral near-IR reflectance imaging of simulated early occlusal lesions: variation of lesion contrast with lesion depth and severity.* Lasers Surg Med, 2014. **46**(3): p. 203-15.
5. Simon, J.C., et al. *Multispectral near-infrared reflectance and transillumination imaging of occlusal carious lesions: variations in lesion contrast with lesion depth*. in *Lasers in Dentistry XXIV*. 2018.
6. Simon, J.C., et al., *Near-IR Transillumination and Reflectance Imaging at 1300-nm and 1500-1700-nm for in vivo Caries Detection.* Lasers Surg Med, 2016. **48**(6): p. 828-836.
7. Simon, J.C., et al., *Near-IR and CP-OCT imaging of suspected occlusal caries lesions.* Lasers Surg Med, 2017. **49**(3): p. 215-224.
8. Yang, V.B. and D. Fried, *Measurement of the shrinkage of natural and simulated lesions on root surfaces with CP-OCT.* J Dent, 2019. **90**(11): p. 103213.
9. Lee, R.C., C.L. Darling, and D. Fried, *Activity assessment of root caries lesions with thermal and near-infrared imaging methods.* Journal Biophotonics, 2016. **10**(3): p. 433-445.

10. Kaste, L.M., et al., *Coronal caries in the primary and permanent dentition of children and adolescents 1-17 years of age: United States, 1988-1991.* J Dent Res, 1996. **75**: p. 631-641.

11. Winn, D.M., et al., *Coronal and root caries in the dentition of adults in the United States, 1988-1991.* J Dent Res, 1996. **75**: p. 642-651.

12. Chauncey, H.H., R.L. Glass, and J.E. Alman, *Dental caries, principal cause of tooth extraction in a sample of US male adults.* Caries Res, 1989. **23**: p. 200-205.

13. Kooistra, S., et al., *Radiographic versus clinical extension of Class II carious lesions using an F-speed film.* Oper Dent, 2005. **30**(6): p. 719-26.

14. Jessee, S.A., S.R. Makins, and W.A. Bretz, *Accuracy of proximal caries depth determination using two intraoral film speeds.* Gen Dent, 1999. **47**(1): p. 88-93.

15. Bin-Shuwaish, M., et al., *Estimation of clinical axial extension of Class II caries lesions with ultraspeed and digital radiographs: an in-vivo study.* Oper Dent, 2008. **33**(6): p. 613-21.

16. Pitts, N., *"ICDAS"--an international system for caries detection and assessment being developed to facilitate caries epidemiology, research and appropriate clinical management.* Community Dent Health, 2004. **21**(3): p. 193-8.

17. Ismail, A.I., et al., *The International Caries Detection and Assessment System (ICDAS): an integrated system for measuring dental caries.* Community Dent Oral Epidemiol, 2007. **35**(3): p. 170-8.

18. Topping, G.V. and N.B. Pitts, *Clinical visual caries detection.* Monogr Oral Sci, 2009. **21**: p. 15-41.

19. Carvalho, R.N., et al., *Accuracy of visual and image-based ICDAS criteria compared with a micro-CT gold standard for caries detection on occlusal surfaces.* Braz Oral Res, 2018. **32**: p. e60.

20. NIH, *Diagnosis and Management of Dental Caries throughout Life*. 2001, NIH Consensus Statement. p. 1-24.

21. Featherstone, J.D.B., *Prevention and reversal of dental caries:role of low level fluoride.* Community Dent Oral Epidemiol, 1999. **27**: p. 31-40.

22. Chan, K.H. and D. Fried, *Multispectral cross-polarization reflectance measurements suggest high contrast of demineralization on tooth surfaces at wavelengths beyond 1300-nm due to reduced light scattering in sound enamel* J Biomed Opt, 2018. **23**(6): p. 060501.

23. Bühler, C.M., P. Ngaotheppitak, and D. Fried. *Imaging of occlusal dental caries (decay) with near-IR light at 1310-nm*. in *Lasers in Dentistry XI*. 2005. San, Jose, CA: SPIE.

24. Staninec, M., et al., *In vivo near-IR imaging of approximal dental decay at 1,310 nm.* Lasers in Surgery and Medicine, 2010. **42**(4): p. 292-8.

25. Fried, W.A., et al., *High contrast reflectance imaging of enamel demineralization and remineralization at 1950-nm for the assessment of lesion activity.* Lasers Surg Med, 2021. **53**(7): p. 968-977.

26. Pandya, M. and T.G.H. Diekwisch, *Enamel biomimetics-fiction or future of dentistry.* Int J Oral Sci, 2019. **11**(1): p. 8.

27. Simon, J.C., et al. *Transillumination and reflectance probes for near-IR imaging of dental caries*. in *Lasers in Dentistry XX*. 2014. Proc SPIE

28. Fried, D., et al., *Nature of light scattering in dental enamel and dentin at visible and near-infrared wavelengths.* Applied optics, 1995. **34**(7): p. 1278-85.

29. Jones, R.S. and D. Fried. *Attenuation of 1310-nm and 1550-nm Laser Light through Sound Dental Enamel*. in *Lasers in Dentistry VIII*. 2002. San Jose: Proc SPIE.

30. Hale, G.M. and M.R. Querry, *Optical constants of water in the 200-nm to 200-µm wavelength region.* Appl. Optics, 1973. **12**: p. 555-563.

31. Chung, S., et al. *Near infrared imaging of teeth at wavelengths between 1200 and 1600 nm*. in *Lasers in Dentistry XVII*. 2011. SPIE.

32. Kleter, G.A., *Discoloration of dental carious lesions (a review).* Arch. Oral. Bio. , 1998. **43**: p. 629-632.

33. Sarna, T. and R.C. Sealy, *Photoinduced oxygen consumption in melanin systems. Action spectra and quantum yields for eumelanin and synthetic melanin.* Photochem. Photobiol. , 1984. **39**: p. 69-74.

34. Fu, D., et al., *Two-color, two-photon, and excited-state absorption microscopy.* J Biomed Opt, 2007. **12**(5): p. 054004.

35. Nead, K.T., et al., *Lower abdominal and pelvic radiation and testicular germ cell tumor risk.* PLoS One, 2020. **15**(11): p. e0239321.

36. Han, M.A. and J.H. Kim, *Diagnostic X-Ray Exposure and Thyroid Cancer Risk: Systematic Review and Meta-Analysis.* Thyroid, 2018. **28**(2): p. 220-228.

37. Simon, J.C., et al. *Near-infrared imaging of natural secondary caries*. in *Lasers in Dentistry XXI* 2015. Proc SPIE

38. Walsh, T., et al., *Imaging modalities to inform the detection and diagnosis of early caries.* Cochrane Database Syst Rev, 2021. **3**(3): p. CD014545.

39. Dayo, A.F., et al., *Radiology of Dental Caries.* Dent Clin North Am, 2021. **65**(3): p. 427-445.

40. Zhu, Y., et al., *Dual short wavelength infrared transillumination/reflectance mode imaging for caries detection.* J Biomed Opt, 2021. **26**(4): p. 043004.

41. Abdelaziz, M., *Detection, Diagnosis, and Monitoring of Early Caries: The Future of Individualized Dental Care.* Diagnostics (Basel), 2023. **13**(24).

42. Heck, K., et al., *Proximal Caries Detection Using Short-Wave Infrared Transillumination at Wavelengths of 1050, 1200 and 1300 nm in Permanent Posterior Human Teeth.* Diagnostics, 2023. **13**(20): p. 3257.

43. Zhu, Y., et al. *A dual handheld SWIR transillumination/reflectance probe for imaging lesions on tooth occlusal and proximal surfaces*. in *Lasers in Dentistry XXVI*. 2018.

44. Ekstrand, K.R., et al., *Lesion activity assessment.* Monographs in oral science, 2009. **21**: p. 63-90.

45. Wyne, A.H. and E.E. Guile, *Caries activity indicators. A review.* Indian J Dent Res, 1993. **4**(2): p. 39-46.

46. Pitts, N.B. and D.T. Zero. *White Paper on Dental Caries Prevention and Management: A summary of the current evidence and the key issues in controlling this preventable disease*. 2016.

47. Hirasuna, K., D. Fried, and C.L. Darling, *Near-IR imaging of developmental defects in dental enamel.* J. Biomed. Opt., 2008. **13**(4): p. 044011:1-7.

48. Lee, R.C., A.T. Jang, and D. Fried. *Near-infrared imaging of enamel hypomineralization due to developmental defects*. in *Lasers in Dentistry XXIII*. 2017.

49. Lee, R.C., C.L. Darling, and D. Fried, *Assessment of remineralization via measurement of dehydration rates with thermal and near-IR reflectance imaging.* J Dent, 2015. **43**: p. 1032-1042.

50. Chang, N.N., et al., *Analysis of the transparent surface zone formed at the surfaces of arrested enamel caries lesions with tomographic imaging methods.* JADA Foundational Science, 2023. **in press**.

51. Chan, K.H., et al., *Clinical monitoring of smooth surface enamel lesions using CP-OCT during nonsurgical intervention.* Lasers Surg Med, 2016. **48**(10): p. 915-923.

52. Fried, D., et al. *Clinical Monitoring of Early Caries Lesions using Cross Polarization Optical Coherence Tomography*. in *Lasers in Dentistry XIX*. 2013. Proc SPIE.

53. Banting, D.W., *Diagnosis and prediction of root caries.* Adv Dent Res, 1993. **7**(2): p. 80-6.

54. Hellyer, P., et al., *Root caries in older people attending a general practice in East Sussex.* Brit Dent J 1990. **169**: p. 201-206.

55. Lee, R.C., C.L. Darling, and D. Fried. *Assessment of remineralized dentin lesions with thermal and near-infrared reflectance imaging*. in *Laser in Dentistry XXII*. 2016. Proc. SPIE.

56. Chang, N.N., J.M. Jew, and D. Fried. *Lesion dehydration rate changes with the surface layer thickness during enamel remineralization*. in *Lasers in Dentistry XXIV*. 2018.

57. Chang, N.N., M. Abdelaziz, and D. Fried, *The Relationship of Dehydration Rate and Transparent Surface Layer Thickness for Coronal Lesions on Extracted Teeth.* Proc SPIE Int Soc Opt Eng, 2019. **10857**.

58. Colston, B.W., et al., *Dental OCT.* Optics Express, 1998. **3**(3): p. 230-238.

59. Feldchtein, F.I., et al., *In vivo OCT imaging of hard and soft tissue of the oral cavity.* Optics Express, 1998. **3**(3): p. 239-251.

60. Wang, X.J., et al., *Characterization of Dentin and Enamel by use of Optical Coherence Tomography.* Appl. Opt., 1999. **38**(10): p. 586-590.

61. Kang, H., C.L. Darling, and D. Fried, *Nondestructive monitoring of the repair of enamel artificial lesions by an acidic remineralization model using polarization-sensitive optical coherence tomography.* Dent Mater, 2012. **28**(5): p. 488-94.

62. Le, M.H., C.L. Darling, and D. Fried, *Automated analysis of lesion depth and integrated reflectivity in PS-OCT scans of tooth demineralization.* Lasers Surg Med, 2010. **42**(1): p. 62-8.

63. Yang, V.B. and D. Fried. *An appliance for monitoring the shrinkage of root caries with OCT*. in *Lasers in Dentistry XXV*. 2019.

64. Chang, N.N., et al. *SWIR, thermal and CP-OCT imaging probes for the in vivo assessment of the activity of root caries lesions*. in *Lasers in Dentistry XXVI*. 2020.

65. Peers, A., et al., *Validity and reproducibility of clinical examination, fibre-optic transillumination, and bite-wing radiology for the diagnossis of small approximal carious lesions.* Caries Res., 1993. **27**: p. 307-311.

66. Pine, C.M. and J.J. ten Bosch, *Dynamics of and diagnostic methods for detecting small carious lesions.* Caries Res, 1996. **30**(6): p. 381-8.

67. Purdell-Lewis, D.J. and T. Pot, *A comparison of radiographic and fibre-optic diagnoses of approximal caries lesions.* J Dent, 1974. **2**(4): p. 143-8.

68. Vaarkamp, J., et al., *The real performance of bitewing radiography and fiber-optic transillumination in approximal caries diagnosis.* J Dent Res, 2000. **79**(10): p. 1747-51.

69. Stephen, K.W., et al., *Comparison of fibre optic transillumination with clinical and radiographic caries diagnosis.* Community Dent Oral Epidemiol, 1987. **15**(2): p. 90-4.

70. Chung, S., et al., *Multispectral near-IR reflectance and transillumination imaging of teeth* Biomed Opt Express, 2011. **2**(10): p. 2804-2814.

71. Gomez, J., *Detection and diagnosis of the early caries lesion.* BMC Oral Health, 2015. **15 Suppl 1**(Suppl 1): p. S3.

72. Simon, J.C., C.L. Darling, and D. Fried. *A system for simultaneous near-infrared reflectance and transillumination imaging of occlusal carious lesions*. in *Lasers in Dentistry XXI*. 2016. Proc. SPIE

73. Manesh, S.K., C.L. Darling, and D. Fried, *Polarization-sensitive optical coherence tomography for the nondestructive assessment of the remineralization of dentin.* Journal of Biomedical Optics, 2009. **14**(4): p. 044002.

74. Manesh, S.K., C.L. Darling, and D. Fried, *Nondestructive assessment of dentin demineralization using polarization-sensitive optical coherence tomography after exposure to fluoride and laser irradiation.* J Biomed Mater Res B Appl Biomater, 2009. **90**(2): p. 802-12.

75. Chan, K.H., et al., *Use of 2D images of depth and integrated reflectivity to represent the severity of demineralization in cross-polarization optical coherence tomography.* J Biophotonics, 2015. **8**(1-2): p. 36-45

76. Lee, R.C., et al., *Infrared methods for assessment of the activity of natural enamel caries lesions.* IEEE Journal of Selected Topics in Quantum Electronics, 2016. **22**(3): p. 6803609.

77. Tressel, J., et al., *Caries inhibition of simulated active caries lesions with CO2 laser irradiation and fluoride.* Proc SPIE Int Soc Opt Eng, 2022. **11942**.

78. Jones, G., R.S. Jones, and D. Fried. *Transillumination of interproximal caries lesions with 830-nm light*. in *Lasers in Dentistry X*. 2004. San Jose: SPIE.

79. Jones, R.S., et al., *Near-IR Transillumination at 1310-nm for the Imaging of Early Dental Caries.* Optics Express, 2003. **11**(18): p. 2259-2265.

80. Fried, D., et al., *Early Caries Imaging and Monitoring with Near-IR Light.* Dental Clinics of North America - Incipient and Hidden Caries, 2005. **49**(4): p. 771-794.

81. Karlsson, L., et al., *Near-infrared transillumination of teeth: measurement of a system performance.* Journal of Biomedical Optics, 2010. **15**(3): p. 036001-8.

82. Lee, C., et al., *Nondestructive assessment of the severity of occlusal caries lesions with near-infrared imaging at 1310 nm.* Journal of Biomedical Optics, 2010. **15**(4): p. 047011.

83. Kuhnisch, J., et al., *In vivo validation of near-infrared light transillumination for interproximal dentin caries detection.* Clin Oral Investig, 2015. **20**(4): p. 821-829.

84. Sochtig, F., R. Hickel, and J. Kuhnisch, *Caries detection and diagnostics with near-infrared light transillumination: clinical experiences.* Quintessence Int, 2014. **45**(6): p. 531-8.

85. Abdelaziz, M. and I. Krejci, *DIAGNOcam--a Near Infrared Digital Imaging Transillumination (NIDIT) technology.* Int J Esthet Dent, 2015. **10**(1): p. 158-65.

86. Abdelaziz, M., I. Krejci, and D. Fried, *Enhancing the detection of proximal cavities on near infrared transillumination images with Indocyanine Green (ICG) as a contrast medium: In vitro proof of concept studies.* J Dent, 2019. **91**: p. 103222.

87. Abdelaziz, M., et al., *Near infrared transillumination compared with radiography to detect and monitor proximal caries: A clinical retrospective study.* J Dent, 2018. **70**: p. 40-45.

88. Ng, C., et al., *Near-infrared imaging of demineralization on the occlusal surfaces of teeth without the interference of stains.* J Biomed Optics, 2019. **24**(3): p. 036002.

89. Fried, W.A., et al., *High Contrast Reflectance Imaging of Simulated Lesions on Tooth Occlusal Surfaces at Near-IR Wavelengths.* Lasers Surg Med, 2013. **45**(8): p. 533-541.

90. Dye, B.A., et al., *Dental Caries and Tooth Loss in Adults in the United States, 2011–2012*, in *NCHS Data Brief, #197*, N.C.f.H. Statistics, Editor. 2015.

91. Dye, B.A., et al., *Trends in oral health status, United States, 1988-1994 and 1999-2004.* Vital Health Stat 11. 2007;(248):1-92., 2007. **248**: p. 1-92.

92. Makhija, S.K., et al., *Characteristics, detection methods and treatment of questionable occlusal carious lesions: findings from the national dental practice-based research network.* Caries Res, 2014. **48**(3): p. 200-7.

93. Makhija, S.K., et al., *Twenty-month follow-up of occlusal caries lesions deemed questionable at baseline: findings from the National Dental Practice-Based Research Network.* J Am Dent Assoc, 2014. **145**(11): p. 1112-8.

94. Makhija, S.K., et al., *The prevalence of questionable occlusal caries: findings from the Dental Practice-Based Research Network.* J Am Dent Assoc, 2012. **143**(12): p. 1343-50.

95. Lee, C., C.L. Darling, and D. Fried. *In vitro near-infrared imaging of occlusal dental caries using a germanium enhanced CMOS camera*. in *Lasers in Dentistry XVI*. 2010. Proc. SPIE

96. Salsone, S., et al., *Histological validation of near-infrared reflectance multispectral imaging technique for caries detection and quantification.* J Biomed Opt, 2012. **17**(7): p. 076009.

97. Zakian, C., I. Pretty, and R. Ellwood, *Near-infrared hyperspectral imaging of teeth for dental caries detection.* Journal of Biomedical Optics, 2009. **14**(6): p. 064047-7.

98. Tom, H., et al., *Near-infrared imaging of demineralization under sealants.* J Biomed Opt, 2014. **19**(7): p. 77003.

99. Simon, J.C., et al., *Near-infrared imaging of secondary caries lesions around composite restorations at wavelengths from 1300-1700-nm.* Dent Mater, 2016. **32**(4): p. 587-95.

100. Simon, J.C., C.L. Darling, and D. Fried. *Assessment of cavitation in artificial approximal dental lesions with near-IR imaging*. in *Lasers in Dentistry XXIII*. 2017.

101. Lee, R.C., et al., *Infrared methods for assessment of the activity of natural enamel caries lesions.* IEEE Journal of Selected Topics in Quantum Electronics, 2014. **22**(3): p. 6803609.

102. Buhler, C., P. Ngaotheppitak, and D. Fried, *Imaging of occlusal dental caries (decay) with near-IR light at 1310-nm.* Optics Express, 2005. **13**(2): p. 573-82.

103. Simon, J.C., et al., *Near-IR and CP-OCT imaging of suspected occlusal caries lesions* Lasers Surg Med, 2017. **49**(3): p. 215-224.

104. Staninec, M., et al., *Nondestructive Clinical Assessment of Occlusal Caries Lesions using Near-IR Imaging Methods.* Lasers in Surgery and Medicine, 2011. **43**(10): p. 951-959

105. van Gemert, M., A.J. Welch, and W. Star, *One-dimensional transport Theory*, in *Optical-Thermal Response of Laser-Irradiated Tissue*, A.J. Welch and M. van Gemert, Editors. 2011, Springer.

106. Zhu, Y., et al., *Dual short wavelength infrared transillumination/reflectance mode imaging for caries detection.* J Biomed Opt, 2021. **26**(4).

107. Zhu, Y., et al. *Compact in vivo handheld dual SWIR transillumination/reflectance imaging system for the detection of proximal and occlusal lesions*. in *Photonic Therapeutics and Diagnostics in Dentistry, Head and Neck Surgery, and Otolaryngology*. 2021.

108. Yang, V.B., et al., *Cross-polarization reflectance imaging of root caries and dental calculus at wavelengths from 400-2350-nm.* J Biophotonics, 2018. **11**( ): p. e201800113.

109. Kashirtsev, F., et al., *High contrast imaging of dental fluorosis in the short wavelength infrared (SWIR)* Journal of Biophotonics, 2021. **in press**: p. .

110. Makhija, S.K., et al., *Dentists' decision strategies for suspicious occlusal caries lesions in a National Dental PBRN study.* J Dent, 2018. **69**: p. 83-87.

111. Darling, C.L., G.D. Huynh, and D. Fried, *Light Scattering Properties of Natural and Artificially Demineralized Dental Enamel at 1310-nm.* J. Biomed. Optics, 2006. **11**(3): p. 034023

112. Zhu, Y. and D. Fried. *Evaluating interproximal and occlusal lesion severity with a dual SWIR transillumination/reflectance probe*. in *Lasers in Dentistry XXVIII*. 2022.

113. Zhu, Y. and D. Fried, *Measurement of the Depth of Lesions on Proximal Surfaces with SWIR Multispectral Transillumination and Reflectance Imaging.* Diagnostics (Basel), 2022. **12**(3).

114. Casalegno, F., et al., *Caries Detection with Near-Infrared Transillumination Using Deep Learning.* J Dent Res, 2019. **98**(11): p. 1227-1233.

115. Fejerskov, O., B. Nyvad, and E. Kidd, eds. *Dental Caries: The Disease and its Clinical Management*. 2015, Wiley Blackwell.

116. ten Cate, J.M. and J. Arends, *Remineralization of artificial enamel lesions in vitro.* Caries Res, 1977. **11**(5): p. 277-86.

117. Kidd, E.A., *The histopathology of enamel caries in young and old permanent teeth.* British dental journal, 1983. **155**(6): p. 196-8.

118. Penning, C., et al., *Validity of probing for fissure caries diagnosis.* Caries Res, 1992. **26**: p. 445-449.

119. Angmar-Mansson, B.E., S. al-Khateeb, and S. Tranaeus, *Caries diagnosis.* J Dent Educ, 1998. **62**(10): p. 771-80.

120. Hume, W.R. *Need for change in dental caries diagnosis*. in *Early Detection of dental caries*. 1996. Indianapolis: Indiana University.

121. Kidd, E.A.M., D.N.J. Ricketts, and N.B. Pitts, *Occlusal caries diagnosis: a changing challenge for clinicians and epidemiologists.* J Dent Res, 1993. **21**: p. 3232-331.

122. Jones, R.S. and D. Fried, *Remineralization of enamel caries can decrease optical reflectivity.* J Dent Res, 2006. **85**(9): p. 804-8.

123. Stookey, G.K., *Quantitative light fluorescence: a technology for early monitoring of the caries process.* Dent Clin North Am, 2005. **49**(4): p. 753-70, vi.

124. Ando, M., G.K. Stookey, and D.T. Zero, *Ability of quantitative light-induced fluorescence (QLF) to assess the activity of white spot lesions during dehydration.* Am J Dent, 2006. **19**(1): p. 15-8.

125. Ando, M., et al., *Pilot clinical study to assess caries lesion activity using quantitative light-induced fluorescence during dehydration.* J Biomed Opt, 2017. **22**(3): p. 35005.

126. Kaneko, K., K. Matsuyama, and S. Nakashima. *Quantification of Early Carious Enamel Lesions by using an Infrared Camera*. in *Early detection of Dental caries II*. 1999. Indianapolis, IN: Indiana University.

127. Zakian, C.M., et al., *Occlusal caries detection by using thermal imaging.* Journal of Dentistry, 2010. **38**(10): p. 788-795.

128. Usenik, P., et al., *Near-infrared hyperspectral imaging of water evaporation dynamics for early detection of incipient caries.* J Dent, 2014. **42**(10): p. 1242-7.

129. Yang, V., et al., *Thermal Imaging of Root Caries In Vivo.* J Dent Res, 2020. **99**(13): p. 1502-1508.

130. Colston, B., et al., *Imaging of hard and soft tissue structure in the oral cavity by optical coherence tomography.* Applied Optics, 1998. **37**(19): p. 3582-3585.

131. Jones, R.S., et al., *Imaging artificial caries on the occlusal surfaces with polarization-sensitive optical coherence tomography.* Caries research, 2006. **40**(2): p. 81-89.

132. Fried, D., et al., *Early detection of dental caries and lesion progression with polarization sensitive optical coherence tomography.* J. Biomed. Optics, 2002. **7**(4): p. 618-627.

133. Louie, T., et al., *Clinical assessment of early tooth demineralization using polarization sensitive optical coherence tomography.* Lasers in Surg. Med., 2010. **42**: p. 738-745.

134. Nee, A., et al., *Longitudinal monitoring of demineralization peripheral to orthodontic brackets using cross polarization optical coherence tomography.* J Dent, 2014. **42**(5): p. 547-555.

135. Jones, R.S., et al., *Remineralization of in vitro dental caries assessed with polarization-sensitive optical coherence tomography.* Journal of Biomedical Optics, 2006. **11**(1): p. 014016.

136. Liu, H., et al. *Infrared imaging confirms the role of the transparent surface zone in arresting dental caries*. in *Photonic Therapeutics and Diagnostics in Dentistry, Head and Neck Surgery, and Otolaryngology*. 2021.

137. Fried, W.A., et al., *A SWIR imaging handpiece for the clinical assessment of lesion activity via dehydration. Preclinical Assessment.* Proc SPIE Int Soc Opt Eng, 2020. **11217**.

138. Lee, R.C., et al., *Automated assessment of the remineralization of artificial enamel lesions with polarization-sensitive optical coherence tomography.* Biomed Opt Express, 2014. **5**(9): p. 2950-62.

139. Tressel, J., M. Abdelaziz, and D. Fried, *Dynamic SWIR Imaging near the 1950 nm water absorption band for caries lesion diagnosis* J Biomedical Opt 2021. **26**(5): p. 056006.

140. Banting, D.W., *Diagnosis of Root Caries*, in *NIH Diagnosis and Management of Dental Caries throughout Life*. 2001, NIH Consensus Statement. p. 1-24.

141. Schaeken, M., H. Keltjens, and J. Van der Hoeven, *Effects of fluoride and chlorhexidine on the microflora of dental root surfaces and progression of root-surface caries.* J Dent Res, 1991. **70**: p. 150-153.

142. Ekstrand, K., S. Martignon, and P. Holm-Pedersen, *Development and evaluation of two root caries controlling programmes for home-based frail people older than 75 years.* Gerodontology, 2008. **25**(2): p. 67-75.

143. Fejerskov, O., et al., *Active and inactive root surface caries lesions in a selected group of 60- to 80-year-old Danes.* Caries Res, 1991. **25**(5): p. 385-91.

144. Lynch, E. and D. Beighton, *A comparison of primary root caries lesions classified according to colour.* Caries Res, 1994. **28**(4): p. 233-9.

145. Pitts, N., ed. *Detection, Assessment, Diagnosis and Monitoring of Caries*. Monographs in Oral Science, ed. A.L.a.G.M. Whitforn. Vol. 21. 2009, Karger: Basel.

146. Bouma, B.E. and G.J. Tearney, *Handbook of Optical Coherence Tomography*. 2002/08/21 ed. 2002, New York, NY: Marcel Dekker.

147. Baumgartner, A., et al., *Polarization-sensitive optical optical coherence tomography of dental structures.* Caries Res., 2000. **34**: p. 59-69.

148. Lee, C., C. Darling, and D. Fried, *Polarization Sensitive Optical Coherence Tomographic Imaging of Artificial Demineralization on Exposed Surfaces of Tooth Roots.* Dent. Mat., 2009. **25**(6): p. 721-728.

149. Wada, I., et al., *Clinical assessment of non carious cervical lesion using swept-source optical coherence tomography.* J Biophotonics, 2015. **8**(10): p. 846-54.

150. Ando, M., N. Sharp, and D. Adams. *Pulse thermography for quantitative nondestructive evaluation of sound, de-mineralized and re-mineralized enamel*. in *Health Monitoring of Structural and Biological Systems*. 2012. *Proc SPIE*.

151. Jones, R.S. and D. Fried, *Remineralization of enamel caries can decrease optical reflectivity.* Journal of dental research, 2006. **85**(9): p. 804-8.

152. Zhu, Y. and D. Fried, *Measurement of the Depth of Lesions on Proximal Surfaces with SWIR Multispectral Transillumination and Reflectance Imaging.* Diagnostics (Basel), 2022. **12**(3): p. 597.

153. Zhu, Y., et al., *Diagnostic Performance of Multispectral SWIR Transillumination and Reflectance Imaging for Caries Detection.* Diagnostics (Basel), 2023. **13**(17): p. 2824.

154. Ngaotheppitak, P., et al., *PS-OCT of Occlusal and Interproximal Caries Lesions viewed from Occlusal Surfaces.* Lasers in Dentistry XII, 2006. **6137**(L): p. 1-9.

155. Katkar, R.A., et al., *Optical Coherence Tomography.* Dent Clin North Am, 2018. **62**(3): p. 421-434.

156. Fried, D., *Optical Coherence Tomography for Imaging Dental Caries*, in *Detection and Assessment of Dental Caries: A Clinical Guide*, A. Zandona and C. Longbottom, Editors. 2019, Springer: Switzerland. p. 199-208.

157. Bimstein, E., et al., *Distribution of caries in different tooth surfaces in 7-year-old children.* Caries Res, 1981. **15**(4): p. 324-30.

158. Mejare, I., et al., *Influence of approximal caries in primary molars on caries rate for the mesial surface of the first permanent molar in swedish children from 6 to 12 years of age.* Caries Res, 2001. **35**(3): p. 178-85.

159. Shimada, Y., et al., *3D imaging of proximal caries in posterior teeth using optical coherence tomography.* Sci Rep, 2020. **10**(1): p. 15754.

160. Gregory C, et al. *Colloidal Quantum Dot Photodetectors for Large Format NIR, SWIR, and eSWIR Imaging Arrays*. Whitepaper, 2023.

161. Ng, M., et al., *Time-resolved SWIR imaging for the assessment of the activity of occlusal caries lesions.* J Biophotonics, 2023. **16**(10): p. e202300165.

Publishing Agreement

It is the policy of the University to encourage open access and broad distribution of all theses, dissertations, and manuscripts. The Graduate Division will facilitate the distribution of UCSF theses, dissertations, and manuscripts to the UCSF Library for open access and distribution. UCSF will make such theses, dissertations, and manuscripts accessible to the public and will take reasonable steps to preserve these works in perpetuity.

I hereby grant the non-exclusive, perpetual right to The Regents of the University of California to reproduce, publicly display, distribute, preserve, and publish copies of my thesis, dissertation, or manuscript in any form or media, now existing or later derived, including access online for teaching, research, and public service purposes.

DocuSigned by:
Yilina Zhu
CCA1F7ED43E54F6...
Author Signature

4/30/2024
Date